Since January 2020 Elsevier has created a COVID-19 resource centre with free information in English and Mandarin on the novel coronavirus COVID-19. The COVID-19 resource centre is hosted on Elsevier Connect, the company's public news and information website.

Progress in Materials Science 58 (2013) 1173–1243

Contents lists available at SciVerse ScienceDirect

Progress in Materials Science

journal homepage: www.elsevier.com/locate/pmatsci

Electro-spinning/netting: A strategy for the fabrication of three-dimensional polymer nano-fiber/nets

Xianfeng Wang [a,b,c], Bin Ding [a,b,*], Gang Sun [b], Moran Wang [d,*], Jianyong Yu [b,*]

[a] State Key Laboratory for Modification of Chemical Fibers and Polymer Materials, College of Materials Science and Engineering, Donghua University, Shanghai 201620, China
[b] Nanomaterials Research Center, Modern Textile Institute, Donghua University, Shanghai 200051, China
[c] College of Textiles, Donghua University, Shanghai 201620, China
[d] Department of Engineering Mechanics and CNMM, School of Aerospace, Tsinghua University, Beijing 100084, China

ARTICLE INFO

Article history:
Received 23 April 2011
Received in revised form 14 November 2011
Accepted 9 May 2013
Available online 26 May 2013

ABSTRACT

Since 2006, a rapid development has been achieved in a subject area, so called electro-spinning/netting (ESN), which comprises the conventional electrospinning process and a unique electro-netting process. Electro-netting overcomes the bottleneck problem of electrospinning technique and provides a versatile method for generating spider-web-like nano-nets with ultrafine fiber diameter less than 20 nm. Nano-nets, supported by the conventional electrospun nanofibers in the nano-fiber/nets (NFN) membranes, exhibit numerous attractive characteristics such as extremely small diameter, high porosity, and Steiner tree network geometry, which make NFN membranes optimal candidates for many significant applications. The progress made during the last few years in the field of ESN is highlighted in this review, with particular emphasis on results obtained in the author's research units. After a brief description of the development of the electrospinning and ESN techniques, several fundamental properties of NFN nanomaterials are addressed. Subsequently, the used polymers and the state-of-the-art strategies for the controllable fabrication of NFN membranes are highlighted in terms of the ESN process. Additionally, we highlight some potential applications associated with the remarkable features of NFN nanostructure. Our discussion is concluded with some personal perspectives on the future development in which this wonderful technique could be pursued.

* Corresponding authors. Address: State Key Laboratory for Modification of Chemical Fibers and Polymer Materials, College of Materials Science and Engineering, Donghua University, Shanghai 201620, China (B. Ding), Department of Engineering Mechanics and CNMM, School of Aerospace, Tsinghua University, Beijing 100084, China (M. Wang).
E-mail addresses: binding@dhu.edu.cn (B. Ding), mrwang@tsinghua.edu.cn (M. Wang), yujy@dhu.edu.cn (J. Yu).

0079-6425/$ - see front matter © 2013 Elsevier Ltd. All rights reserved.
http://dx.doi.org/10.1016/j.pmatsci.2013.05.001

Contents

1. Introduction

Nanostructured materials, as the forefront of the hottest fundamental materials nowadays, provide one of the greatest potentials for improving performance and extended capabilities of products in a number of industrial sectors, which are gradually accessing into our daily life [1–4]. As one of the most important nanomaterials, one-dimensional (1D) nanoscale materials have steadily attracted growing interest in the past decades because of their unique shape, fundamental properties, and potential applications in many different areas [5–7]. A variety of advanced techniques have already been developed to fabricate 1D nanostructures in the form of fibers, wires, rods, belts, tubes, and spirals from various materials [8–15]. Nanofibers represent one of the most important 1D nanostructures standing at the leading edge of nanoscience and nanotechnology [16]. In comparison with other methods of fiber fabrication such as template synthesis, drawing, and phase-separation, electrohydrodynamics (EHD) techniques [17–20] (e.g. electrospinning) have emerged as straightforward approaches to the fabrication of nanofibers with high specific surface areas, high porosities, and controllable compositions for a wide range of applications [21–26].

Electro-spinning/netting (ESN), as a recently developed advanced EHD technique, may be considered as a variant of electrospinning process [27–30]. Both of these techniques involve the use of a high voltage to induce the formation of a liquid jet. In addition to the formation of liquid jet, the ESN process also comprises an electro-netting process, which defined as the phase separation-induced splitting of a small charged droplet in a high electric field [31,32]. Therefore, the ESN technique allows one-step fabrication of three-dimensional (3D) nano-fiber/nets (NFN) that are consisted of common electrospun nanofibers and unique ultrafine nano-nets. To be more precise, in 3D NFN membranes, the conventional electrospun nanofibers act as a support for the soap-bubble-like structured or spider-web-like nano-nets comprising interlinked 1D nanowires [33,34]. NFN membranes possess the general properties and functions of conventional electrospun nanofibers as well as the fascinating features (e.g. extremely small diameter, high porosity, Steiner tree network geometry, controllable coverage rate) that distinguish themselves from their counterparts [27–29]. Taking advantage of these intriguing characters, NFN materials are of huge interest for use in various applications. Take for example the extremely small diameter, a large number of new opportunities could be realized by down-sizing currently existing structures to the nanometre scale [1,35]. The most typical examples can be seen in filtration, where "smaller" has always meant a greater performance and even promising as filters to intercept nano-sized viruses. Moreover, NFN membranes are probably one of the safest nanomaterials currently used, since they are unlikely to become airborne and penetrate the body because of their fiber length and net area [36].

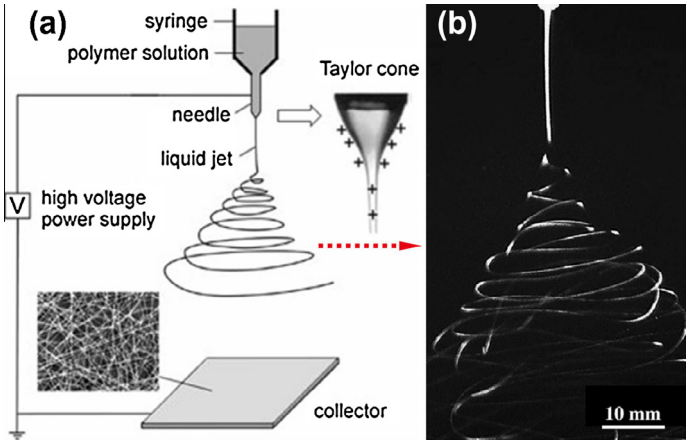

Fig. 1. (a) Schematic illustration of the basic setup for electrospinning. Reprinted with permission from [45]. © 2004 WILEY-VCH Verlag GmbH & Co. (b) Photograph of typical electrospinning jets captured by a high-speed video showing the bending instability of the jet. Reprinted with permission from [110]. © 2007 Elsevier B.V.

There is no doubt that ESN NFN nanomaterials has risen as a shining star in the horizon on the path of the scientists' searching for new materials for future environment, energy and healthcare applications. In the past few years, significant progresses have been made in terms of our fundamental understanding of the ESN process, the controllable fabrication of NFN membranes based on various polymers as well as the exploitation of their applications [27–30,33,34]. In this article, we will provide a comprehensive review of the state-of-the-art research activities related to ESN NFN nanostructures, including their fabrication, novel properties studies and potential applications. We begin with a brief introduction of electrospinning technique, description of their history and modern development, followed by the description of historical background of ESN technique and three prevailing formation mechanisms of NFN materials. Several fundamental properties of NFN nanomaterials such as extremely small diameter, high porosity, Steiner tree network geometry, controllable coverage rate, and controllable density are also discussed. These properties have generated tremendous interest among material researchers. Subsequently, we introduce the polymers and polymer composites that can be ESN into NFN structures. The following chapter fully illustrates the strategies for the controllable fabrication of NFN membranes based on various parameters (solution, processing, and ambient). Then, we highlight a range of applications associated with 3D NFN nanomaterials in various areas. Finally, we draw conclusions regarding the research activities of this new technique and the prospects of future research directions.

2. Electrospinning and electro-spinning/netting (ESN)

2.1. Electrospinning technique

2.1.1. History of electrospinning

Electrospinning, also known as electrostatic spinning, is a powerful, rather simple and highly versatile technique which allows fabricating micro- and nanoscale fibers from process solutions or melts using an electrically forced fluid jet (Fig. 1) [37–40]. The diverse properties of these fibers, based on various physical, chemical, or biological behavior, mean they are of interest for a multitude of applications ranging from filtration, wound dressing, drug delivery, tissue engineering, living membranes, sensors, and so on [36,41–44]. Electrospinning is considered as a variant of the electrostatic spraying process (i.e. the behavior of electrically driven liquid jets) [45] whose history can be traced back to more than 260 years ago when Bose used high electric potentials to generate aerosols from fluid drops in 1745 [46]. The maximum amount of charge which is required to overcome the surface tension of a droplet was calculated in 1882 by Rayleigh [47]. Subsequently, the first devices to spray liquids through the application of an electrical charge were patented by Morton and Cooley at the beginning of the 20th century [48,49], and electrospinning as a physical phenomenon and an application to produce tiny fibers was first suggested. From 1934 to 1944, Formhals published a series of US patents, describing an experimental setup for the production of polymer filaments using an electrostatic force [50]. In 1969, Taylor determined that an angle of 49.3° is required to balance the surface tension of the polymer with the electrostatic forces [51]. Later on, focus shifted to study the structural morphology of nanofibers based on a wide variety of polymeric systems [52].

Despite these early discoveries, electrospinning was nearly forgotten until the late 1990s. Electrospinning technique has regained substantial attention triggered by a surging interest in nanotechnology, as ultrafine fibers or fibrous structures of various polymers with diameters down to submicrons or nanometers can be easily fabricated with this process [44,53]. Several research groups (e.g. Reneker group and Wendorff group) revived interest in this process, have shown that a wide variety of polymeric nanofibers can be obtained via electrospinning [54–59]. A lot of review papers have been published recently which provide an insight into the most prominent aspects of electrospinning [35,41,44,45,60]. Additionally, the popularity of electrospinning has increased sharply as clearly reflected from the fact that more than 200 universities and research institutes in the world have engaged themselves in investigating various aspects of the electrospinning process. Several companies (e.g. eSpin Technologies, NanoTechnics, and KATO Tech) are actively seeking to reap the benefits from the advantages offered by electrospinning, while companies such as Donaldson Company and Freudenberg have utilized this technique to prepare air filtration products [44,61].

2.1.2. Modern electrospinning technology

The preparation of nanofibers using electrospinning method has attracted worldwide attention due to its versatile maneuverability of producing controlled fiber structures, porosity, orientations and dimensions. Generally, electrospun fibers are collected as nonwoven membranes with randomly arranged structures, which have greatly limited their applications in electronic devices or biomedical applications [62–64]. In order to fully realize the potential of electrospun fibers, it is important to fabricate fibrous assemblies with controllable structures. Recently, many groups have demonstrated that electrospun nanofibers could be collected as uniaxially aligned arrays by using specially designed collectors [65–68]. For instance, Li et al. [65] reported that nanofibers could be uniaxially aligned by introducing insulating gaps into conductive collectors. Matthews and co-workers [66] demonstrated that aligned fibers could be fabricated by using a high-speed rotating roller; the mandrel rotation speed and fiber orientation strongly influence the properties of the electrospun nanofibers. Moreover, it was possible to obtain various patterned architectures of the electrospun nanofibers by varying the design of electrode pattern [69,70]. One of the most interesting features associated with this approach is that this technique enables direct integration of nanofibers with controllable configurations into an electrode system, which will greatly facilitate the production of nanofiber-based devices [70].

Besides aligned and patterned fibers, recent demonstrations from a number of literatures indicate that electrospinning technique is also able to fabricate nanofibers with porous [71–73], ribbon-like [74], helical [75,76], necklace-like [77,78], firecracker shape [79], rice-grain shape [80], multi-channel tubular [81], multi-core cable-like [82], tube-in-tube [83], nanowire-in-microtube [84], core–shell [58,85] and hollow [86] structures. Additionally, this technique has become particularly significant when combining other remarkable features, such as tremendous surface-to-volume ratio and pore sizes of nanofibers, with unique physical, chemical, and mechanical functions provided by adding other components with ease and control [87].

Given the versatility of preparing various structured fibrous membranes based on different materials, electrospinning have been identified for use in different fields ranging from healthcare, biotechnology, and environmental engineering to defense and security, and energy generation [37,44,53,88,89]. To fulfill these applications, several techniques such as multi-jet electrospinning [90,91], tip-less electrospinning [92], electroblowing [36,93] and edge electrospinning [94] have been developed to overcome the problem of low mass throughput. Moreover, the electrospinning tip has also been modified to fabricate either side-by-side or coaxial multicomponent fibers and tubes [95]. Not surprisingly, the enhanced mass throughputs certainly will render electrospun nanomaterials commercially viable products.

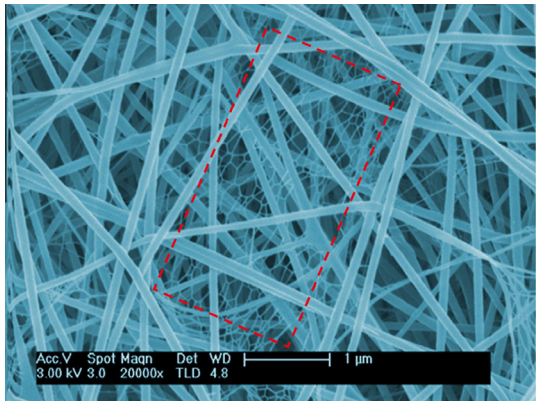

Fig. 2. SEM image of PA-6 NFN membranes discovered by Ding in 2004 [99]. A handle of "fishnet-like nanowebs" were highlighted by the red rectangle.

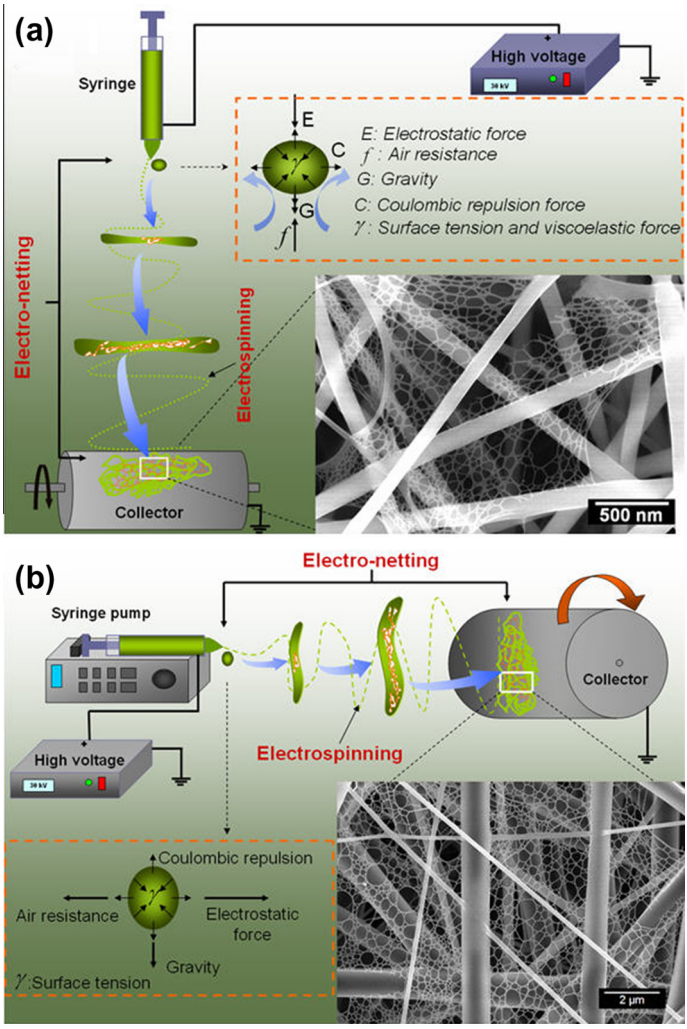

Fig. 3. Schematic diagram of setup of electro-spinning/netting apparatus (a) typical vertical setup (reprinted with permission from [108]. © 2011 Elsevier B.V.) and (b) horizontal set up of electrospinning apparatus (reprinted with permission from [32]. © 2011 Royal Society of Chemistry). The insets show drawings of the forces acting on the charged droplet and typical FE-SEM images of NFN membranes.

Notwithstanding the ability to generating micro- and nanoscale fibers of electrospinning which offer great potential in different fields, enormous researches in the past 10 years have indicated that the large average diameter (100–500 nm) of common electrospun fibers prevented their further applications in ultrafiltration, ultrasensitive sensors, catalyst, etc. [96]. Simultaneously, recent studies have shown that properties such as surface area and porosity become more significant when the fiber diameter falls below 20 nm [97]. Therefore, a current major challenge is to develop robust strategies for manufacturing large-scale and extremely small nanofibers (<50 nm). Various approaches, such as decreasing the polymer concentration [40], elevating the solution temperature [98], and increasing the net charge density of the solution [54], have been utilized to reduce the diameter of electrospun nanofibers. However, these methods typically produce nonuniform fibers with poorly defined structures and the objective of reducing fiber diameter down to 50 nm was rarely achieved.

2.2. ESN: advanced nanotechnology

2.2.1. Origin of ESN

In 2004, when Ding and coworkers found a unique scanning electron microscopy (SEM) image of electrospun polyamide-6 (PA-6) fibrous membranes in which existing a handle of "fishnet-like nanowebs" (supported by common electrospun nanofibers and comprised interlinked 1D ultrathin nanowires; highlighted with red rectangle) (Fig. 2) [99], they did not realize that they had discovered a material that caught much attention a few years later [100–102]. While they were excited about the discovery that might lead to a smaller, cheaper substitute for existing electrospun fibers, they were puzzled by the cause of this fascinating material and cautious about the future applications. Until 2006 when surprisingly partly split polyacrylic acid (PAA) nanowebs were observed, Ding and coworkers preliminarily mastered the principles of structure control for nanowebs and proposed a possible formation mechanism of this versatile structure (Section 2.2.3.1). The preliminary results were reported in the journal of "*Nanotechnology*" in which they introduced the concept of "electro-netting" [33]. Electro-netting accompanies the electrospinning process and allows one-step fabrication of ultrathin nano-nets (i.e. nanowebs) in large quantities and with uniform size. Here, the term of "nano-nets" was used to replace the older term "nanowebs" that was unsuitable in the representation of this 2D net-like structure, because a 3D electrospun fibrous structure can also be called "nanowebs" [32,103,104]. The research object of electro-netting process is small charged droplets other than electrospinning jets. Additionally, nano-nets were primitively regarded as a by-product caused by a high electric field that induces instability of suspended charged droplets during electrospinning rather than formed from the breaking jets [33]. Since then, the research on nano-nets including the exploitation of spinnable polymers, morphology control, functionalizing nano-nets and exploring the applications of nano-nets has grown exponentially [34,105–108].

The term "electro-spinning/netting", abbreviated as ESN, represents the combination of "electrospinning" and "electro-netting", while the "nano-fiber/nets", abbreviated as NFN, represents the combination of nanofibers and nano-nets [27].

2.2.2. Basic setup

Fig. 3 shows schematic diagrams illustrating the basic setup for ESN process. Currently, there are two standard ESN setups, vertical (Fig. 3a) and horizontal (Fig. 3b). Like traditional electrospinning setup, an ESN system also consists of three major components: a high voltage power supply, a spinneret (a metallic needle) and a grounded collecting plate (usually a metal screen, plate, or rotating roller) and utilizes a high voltage source to inject charge of a certain polarity into a polymer solution or melt, which is then accelerated towards a collector of opposite polarity [45,109,110]. Direct current (DC) power supplies are usually used for ESN although the use of alternating current (AC) potentials is also feasible. In contrast to electrospinning, the ESN process usually needs a higher voltage to enhance the instability of the Taylor cone [33]. With the use of syringe pump, the solution can be fed through the spinneret at a constant and controllable rate.

2.2.3. Formation mechanism of nano-fiber/nets (NFN)

The development of ESN technology attracted the scientists who became eager to learn as much as they could understand the formation mechanism of NFN membranes. The knowledge on this issue turned out indispensable to select the spinnable polymer, control the manufacturing process, and regulate the final structure of resultant fibrous membranes. However, it is worth noting that the formation mechanism of the NFN structures is complicated and consensus on the formation mechanism has not been reached [105]. One puzzling question is this: What happens to the charged polymer jets and droplets during their running in such small distance between needle and collector? More rigorous experimental and theoretical work need to be addressed to reveal the secrets behind this process. Nevertheless, we are pleased to see that more and more researchers involve themselves in this domain and propose several mechanisms to explain the formation of the NFN structure [33,34,111–113]. In this section, we will review current four predominant formation mechanisms of NFN structure which include phase separation of charged droplets, ions initiated splitting up of the electrospun fibers, intermolecular hydrogen bonding, and intertwining among branching jets.

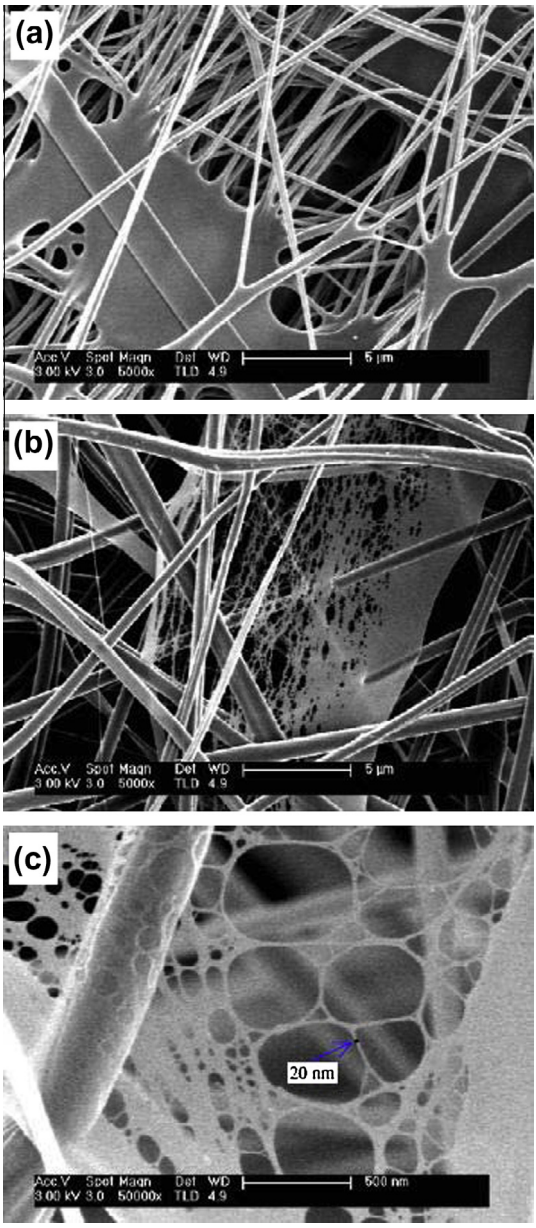

Fig. 4. SEM images of PAA fibrous membranes formed in PAA solution combined with (a) H_2O and (b) ethanol at a concentration of 6 wt%, voltage of 30 kV, spinning distance of 15 cm and humidity of 20%. (c) High magnification SEM image taken from the sample shown in (b). Reprinted with permission from [33]. © 2006 IOP Publishing Ltd.

2.2.3.1. Phase separation of charged droplets. The mechanism of phase separation of charged droplets generated during ESN was proposed based on the experimental observation of defect PAA films (Fig. 4a) and partly split PAA nano-nets (Fig. 4b and c). Based on the observation described above, Ding et al. [33] attributed the formation of nano-nets to the phase separation of charged droplets generated during electrospinning. They suggest that under a high electric force, the charged droplets deform

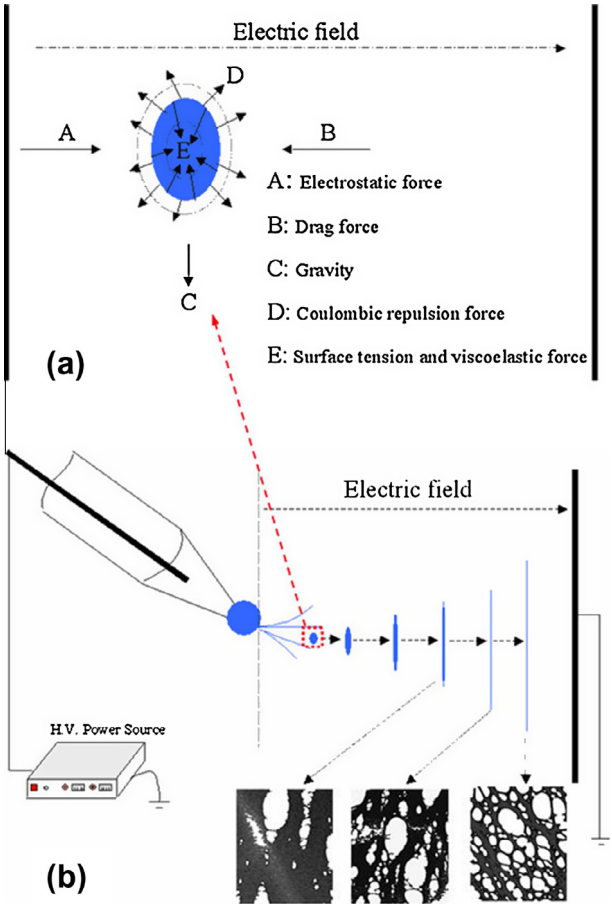

Fig. 5. (a) Forces acting on the charged droplet. (b) Schematic diagram illustrating the possible mechanism of nano-nets formation during ESN process. Reprinted with permission from [33]. © 2006 IOP Publishing Ltd.

significantly to a thin liquid film, which undergoes rapid phase separation with the solvent rich domains to transform into pores. The forces, including electrostatic force, drag force, gravity, Coulombic repulsion force, surface tension and viscoelastic force, act on the charged droplet when it flights with a high speed in the electric field as shown in Fig. 5a. The electrostatic force carries the charged droplet from capillary tip to collector. The drag force between the surrounding air and the charged droplet is the main cause that deforms the droplets into films. The Coulombic repulsion force tried to expand the droplet. The surface tension and viscoelastic forces led the contraction of charged droplet [114]. The electric field could be increased by increasing the applied voltage within a constant distance. Consequently, the electrostatic and Coulombic repulsion forces of charged droplet were reinforced with increasing of electric field. The increased electrostatic force further accelerated the moving of charged droplet, which led to an increased drag force. The distortion and expansion of charged droplet (i.e. from spherical-like to spindle-like) in the electric field during electrospraying was reported by Grimm and Beauchamp [115]. The further expansion could happen when the electric field increased further to form thin films from droplets with the effect of increased Coulombic repulsion and drag forces. Moreover, the increased radial charge repulsion force also has a tendency to expand the charged films. As a result, the deformation of charged droplet was strongly affected by the electric field [99].

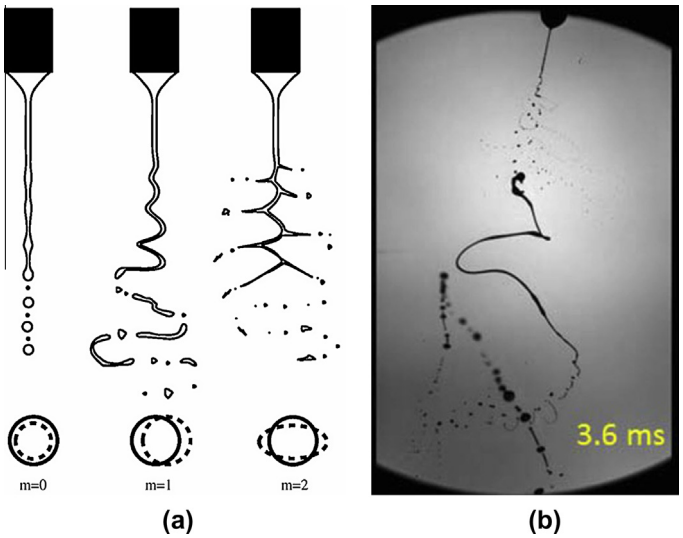

Fig. 6. (a) Three jet break-up modes, the axisymmetric varicose break-up ($m = 0$), the lateral kink break-up ($m = 1$), and the ramified jet break-up ($m = 2$) (reprinted with permission from [119]. © 2000 Elsevier B.V.). (b) High-speed camera images of unstable cone-jet mode (reprinted with permission from [123]. © 2011 Elsevier B.V.).

Fig. 5b shows the schematic diagram illustration of the possible formation mechanism of nano-net during ESN. As shown in this figure, the defect films or nano-nets could be regarded as a by-product caused by a high electric field induced instability of suspended charged droplets during electrospinning [40]. The microsized charged droplets [116] could be generated together with the common electrospun fibers from the capillary tip with a high instability. During the flight of charged droplet from tip to collector, the microsized droplet was distorted and expanded into a thin film due to the comprehensive effects of the forces acting on it [31]. The splitting of thin film into nano-net was ascribed to the rapid phase separation between polymer and solvent and to the fast evaporation of solvent at lower humidity. The fast phase separation led the spinodal or binodal types of phase morphologies within the fibers, and the solvent rich regions in the thin film were transformed into pores [33,57]. As the electrospun fibers and nano-nets were formed at the same time, the 2D nano-nets stacked into 3D fibrous mats in a layer-by-layer structure as well as 1D electrospun fibers. The improved formation frequency and area density of nano-nets could be achieved by increasing the instability of droplet at the electrospinning tip, such as increasing the applied voltage [33,117].

Actually, the break-up of a jet and the formation of small charged droplets is a very old and interesting problem and the research can be date back to the EHD atomization process [118–120]. In EHD atomization in the cone-jet mode a highly charged jet emerges at the apex of the liquid cone. Due to its charge, the liquid is still accelerating, while breaking up into a number of primary or main droplets and a number of secondary droplets and satellites [121,122]. In order to model the jet break-up process with analytical relations, Hartman et al. presented a physical numerical model to describe the harmonic perturbations on the jet surface based on a cylindrical coordinate system [119]:

$$r_s = r_{jet} + \alpha_0 e^{(\omega t + jm\theta - jkz)}, \quad k = \frac{2\pi}{\lambda}, \tag{1}$$

where r is the radial component (m), θ is the angular component (rad), z is the axial component (m), r_s is the radius of the surface (m), r_{jet} is the radius of the unperturbed jet, ω is the growth rate of the perturbation (s^{-1}), t is time (s), α_0 is the amplitude of the perturbation at $t = 0$ (m), m is a constant, k is the wave number of the perturbation (m^{-1}), and λ is the wavelength of the perturbation (m).

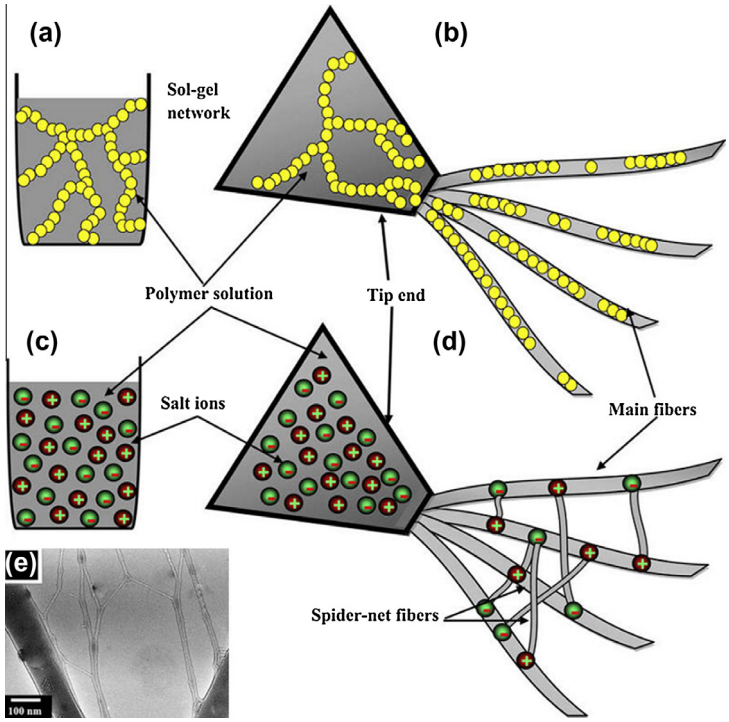

Fig. 7. Schematic illustration showing the nature of sol–gel/polymer solution (a) and (b) mechanism of the corresponding electrospinning process. (c) A conceptual image showing the sol–gel formation for a polymer solution which consists of an inorganic salt; the corresponding behavior of this solution during the electrospinning process is demonstrated in panel (d). (e) TEM images of nylon 6 with NaCl (1.5 wt%). Reprinted with permission from [34]. © 2009 Elsevier B.V.

Depending on the value of m, three modes of jet break-up have been proposed (Fig. 6a). If $m = 0$, the jet break-up is independent of the angular component θ, which is also called varicose instability. If $m = 1$, then the radius of the jet depends on angle θ, which represents the whipping motion of the jet. This kind of lateral instability is also called kink instability. If $m = 2$, then the jet is no longer circular. This mode can only occur if the jet is highly charged (e.g. the ESN process). If the surface charge is above a certain threshold value, then the electric stresses can overcome the surface tension. These electric stresses will transform the shape of the jet. The ramified jet is an extreme example of a jet in which this kind of perturbations occur [119]. Additionally, the formation of small charged droplets has also been demonstrated by Kim et al. [123] through a high-speed camera (Fig. 6b).

2.2.3.2. Ions initiated splitting up of the electrospun fibers. In addition to the phase separation of charged droplets, a recent study by Kim et al. [34] demonstrated that nano-nets can be prepared by adding strong ionic salts to the polar polymer solutions, such as PA-6/formic acid. They believed that nano-nets are formed by the joints between many fibers and the possible joints occur at the apex of Taylor cone. To explain the differences between electrospinning of sol–gel and salt/polymer solution, they suggested a conceptual illustration to explain the mechanism of forming the nano-nets (Fig. 7). In case of electrospinning sol–gel solution (Fig. 7b), the ionically-balanced sol–gel particles formed from the hydrolyzing and polycondensation of the utilized precursor was embed into the produced polymeric nanofibers, and therefore no nano-nets was observed. On the other hand, the ions randomly spread in the salt/polymer solution and might attach on the polymer chains (Fig. 7c). Fig. 7d presents the corresponding behavior of this solution during the electrospinning process. The different charged electric poles generated in the nanofibers could lead to formation of the joints, which finally shaped the

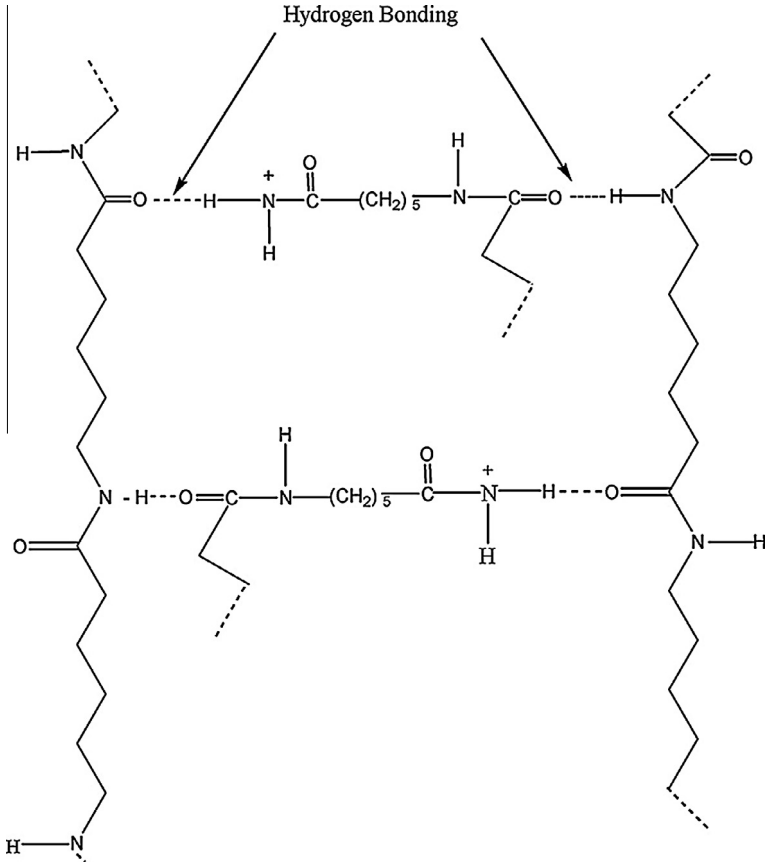

Fig. 8. Schematic illustration of possible hydrogen bond formation mechanism between nano-nets and main PA-6 nanofibers. Reprinted with permission from [125]. © 2010 Elsevier B.V.

observed nano-nets within the nanofibrous membranes. To precisely confirm the proposed synthesizing hypothesis, they showed us a transmission electron microscope (TEM) image that was obtained by placing a TEM grid very close to the tip end for very short time (Fig. 7e). According to the TEM image, they put forward that the joints do not only synthesized among the main nanofibers but also among pre-formed joints. In a further investigation, they attributed these joints to the splitting up of sub-nanofibers from the main fibers induced by the increased ionic strength [124].

2.2.3.3. Intermolecular hydrogen bonding. Based on the investigation of PA-6 and methoxy poly (ethylene glycol) (MPEG) oligomer/PA-6 NFN membranes, Kim and coworkers proposed the hydrogen bonds formation mechanism [107,125]. As shown in Fig. 8 which presents the possible hydrogen bond formation mechanism between nano-nets and main PA-6 nanofibers. In presence of high applied voltage during electrospinning, the protonated amide group of ionic molecule can effectively connect with oxygen atom of PA-6 molecule in main fiber and oxygen atom of ionic molecule can combine with hydrogen atom of amide of main fiber as usual, both of which can form the interconnected spider-web-like NFN membranes (Fig. 8) [125]. Similarly, they also featured the formation of network with the help of possible hydrogen bond formation mechanism between active group of MPEG and NH or C=O group of PA-6 molecules when interpreted the formation of MPEG oligomer/PA-6 NFN membranes [107].

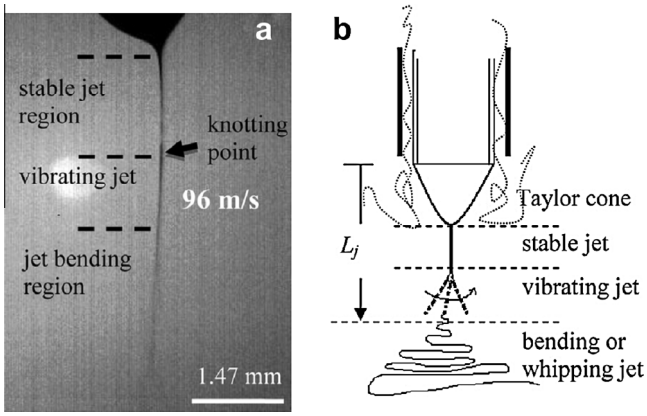

Fig. 9. (a) High-speed-camera image to observe the jet morphology during electrospinning of the nylon 6 solution. Three regions are identified as stable straight jet, laterally vibrating jet, and the bending jet undergoing the bending instability. Note the presence of a knotting point, below which a vigorous lateral vibration is seen. The speed of lateral movement is ca. 95 m/s, estimated by successive high-speed-camera images. (b) Schematics for the morphology of Taylor cone and electrified jet. The dotted black lines in the vibrating jet region show the rapid lateral vibration, indicating the initial formation of thin solid layer. Reprinted with permission from [111]. © 2011 Elsevier B.V.

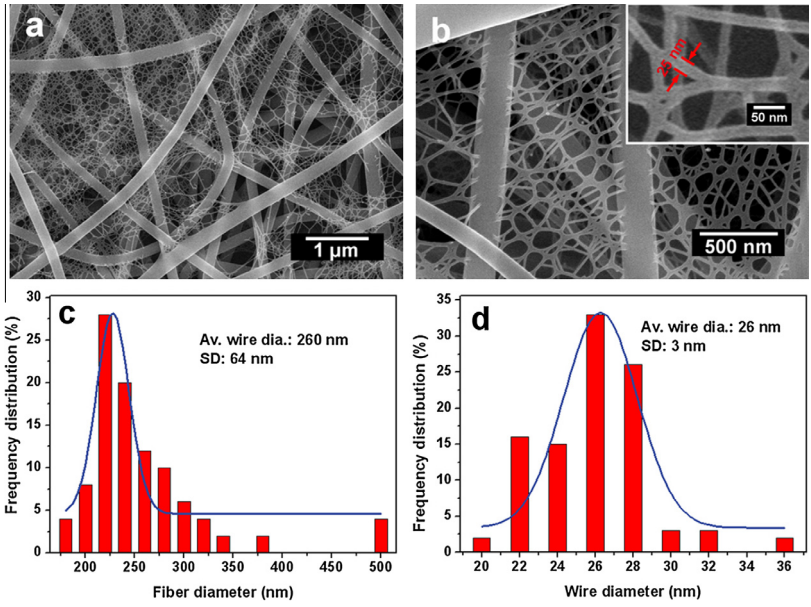

Fig. 10. (a and b) FE-SEM images of PA-6 NFN membranes formed with voltages of 20 kV. Histograms showing the (c) nanofiber and (d) nanowire diameter distributions of the membranes. Reprinted with permission from [27]. © 2011 Royal Society of Chemistry.

2.2.3.4. Intertwine among branching jets. Recently, another plausible formation mechanism of nanonets has been proposed by Tsou et al. [111]. Based on their argument, there were enormous tiny subsidiary jets and these jets underwent the whipping process as well as the main whipping jet. When many subsidiary jets with high ejecting speeds were intertwined in the chaotic whipping region, the short contact time between them diminished their mutual repulsive intrinsics. Formation of a

jet network became feasible after solvent removal, giving rise to nano-nets with connected nanofibrils. In other words, the formation of nano-nets is associated with the complex interaction between these subsidiary jets. The remaining challenge is that the diameter of subsidiary jets is too small to be seen using a high-speed camera with a frame rate of 2000 s^{-1} (Fig. 9a). The difficulty of clearly tracing a whipping jet with the proposed subsidiary jets is due to the high electric field experienced by this high conductive jet with a short L_j (the distance between the needle end to the initiation of jet bending is denoted as L_j) (Fig. 9b).

3. Fundamental properties of NFN membranes

NFN possess the general properties and functions of conventional electrospun nanofibers and other 1D nanostructures fabricated using different techniques, as well as the impressive feature characters (e.g. extremely small diameter, high porosity, Steiner tree network geometry, controllable coverage rate) that distinguish themselves from their counterparts, the properties donated by the polymer phase, and the 2D net-like geometry. These unique properties enable NFN membranes to have received a great deal of attention and been extensively investigated for wide applications. This chapter will highlight some remarkable features of NFN membranes mainly correlated with their existing nanostructures.

3.1. Extremely small diameter

Achieving new properties through reducing the dimensions of a material is one major principle of nanotechnology [35]. For instance, in semiconductor particles or films, a decrease in the diameter is often linked to new optoelectronic functions (quantum effects), and in magnetic materials, superparamagnetism appear [126]. Recently, growing attempts were reported to regulate the diameter or arrangement of electrospun fibers to achieve the designed functions [127–131]. One attractive property of nanofibers associated with decreased diameter is the increased surface area, which in turn, has immediate repercussions on ultrasensitive sensors and other significant applications [31,131]. NFN membranes are consisted of conventional electrospun nanofibers and nano-nets, in which the electrospun nanofibers acted as a support for the nano-nets comprising interlinked 1D ultrathin nanowires. One of the most interesting aspects of the NFN membranes is that it contains enormous interlinked ultrathin nanowires. Fig. 10a and b presents the typical field emission scanning electron microscopy (FE-SEM) images of PA-6 NFN membranes, indicating that the resultant nanofibers were randomly

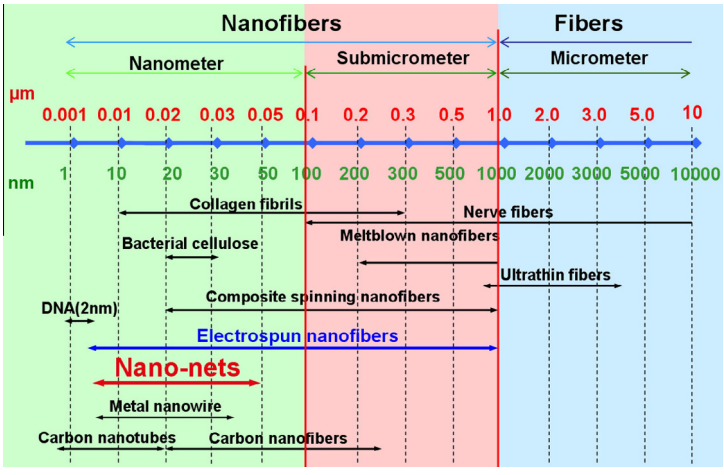

Fig. 11. Comparison of the diameters of nano-nets to those of biological and technological objects.

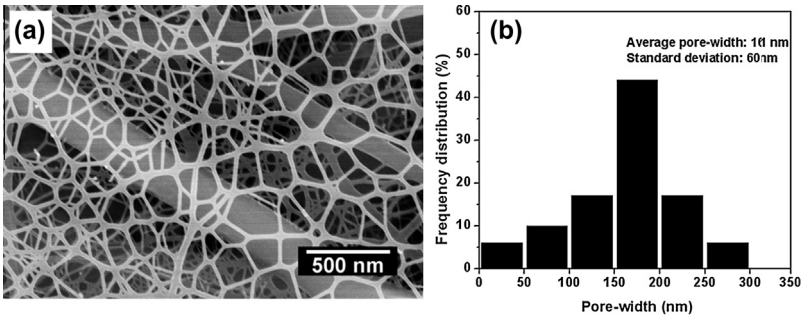

Fig. 12. (a) FE-SEM images of PAA/NaCl NFN membranes formed with a voltage of 30 kV, RH of 25%. (b) Histogram showing the pore-width distribution of nano-nets shown in (a). Reprinted with permission from [31]. © 2011 Royal Society of Chemistry.

oriented as 3D porous membranes. As shown in Fig. 10d, the major distribution region (over 95%) of nanowire diameters is in the range of 20–30 nm with an average diameter of 26 nm, which is one order of magnitude less than that of common electrospun nanofibers (Fig. 10c). Additionally, nano-nets promote the surface area of PA-6 NFN membranes as evident from a high Brunauer–Emmett–Teller (BET) surface area of 19.77 m^2/g compared to that of 12 m^2/g for even porous PA-6 fibers [27]. Fig. 11 shows the comparison of the diameters of nano-nets to those of biological and technological objects. It can be seen that the scale of nano-nets is particularly relevant for biological systems, because the dimensions of proteins and viruses fall in this size range. In comparison with the relatively wide range of electrospun nanofibers, nano-nets just span a narrow range from 5 to 50 nm.

3.2. High porosity and complex porous structure

As well known, the microstructure plays the key role on the transport properties of porous materials [132]. NFN membranes possess complex porous structures that mainly include the high density of pores formed because of entanglement of nanofibers and the enormous pores distributed among

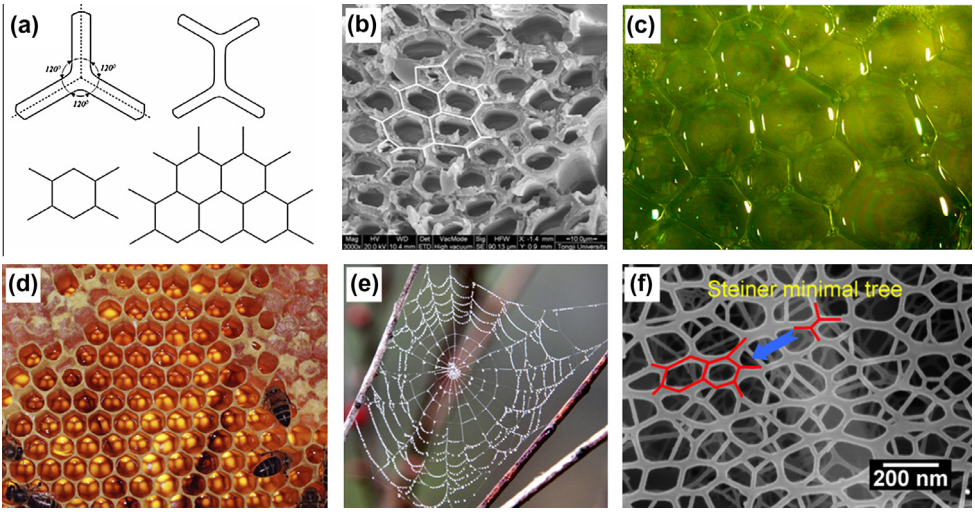

Fig. 13. (a) Template of a nanochannel network constructed by symmetric Y-branched nanochannel. Reprinted with permission from [134]. © 2006 IOP Publishing Ltd. Several biological organisms that exhibit Steiner minimal tree networks: (b) cell walls of sisal (Reprinted with permission from [135]. © 2010 Springer-Verlag.), (c) soap bubbles (Reprinted with permission from [32]. © 2011 Royal Society of Chemistry.), (d) honeycombs, (e) spider webs (Reprinted with permission from [108]. © 2011 Elsevier B.V.) and (f) nano-nets.

nano-nets (Fig. 12a). The pores among the conventional electrospun nanofibers are relatively large in size and all pores are fully interconnected to form a 3D network. In contrast, the enormous pores formed in the nano-nets present more regular geometric structures with pore-width distribution ranged from several nanometer to hundreds nanometer, which is much less than that of pores among electrospun nanofibers (Fig. 12a). For example, the region of pore-width distribution of typical PAA/NaCl nano-nets (Fig. 12b) ranged from 10 to 300 nm [31]. The complex porous structures contribute two impressive advances for NFN membranes: (1) the further enhanced specific surface area of the membranes that may improve the surface activity and hence gas sensitivity. (2) Porous structure may facilitate the air current transport in membranes and effectively reduce the air resistance when used as filters. Therefore, the combination of these two kinds of pores and thus formed complex porous structure makes NFN membranes possess the great potential application in ultrasensitive sensors and filtration system for the removal of particles or viruses with a size to nanometer ranges [27,105].

3.3. Unique geometric characteristic with Steiner tree networks

The general problem of finding Steiner minimal tree on a set of points is a very old and interesting problem and one which has been of considerable interest in network design and operations research [133]. Yin et al. [134] proposed the geometric conservation laws and proved that the mechanically stable equilibrium network of biomembrane nanotubes or super carbon nanotubes (CNTs) is geometrically equivalent to a Steiner minimal tree. This law provides the geometric fundamental for the mechanics of biomembrane nanotube networks and super CNT networks. To construct a Steiner minimal tree, simple geometric regulations were required, i.e. the angle between two neighboring branches should be 120° and the radii of the three branches should be equal (Fig. 13a). Recently, Li et al. [135] further confirmed that Steiner net-work is the geometric foundation for the mechanics of sisal fibers (Fig. 13b). Besides the sisal fibers, nature also abounds with other mysterious biological organisms that exhibit Steiner minimal tree networks, such as soap bubbles (Fig. 13c) [32], honeycombs (Fig. 13d) and spider webs (Fig. 13e) [108]. More exciting, we found that nano-nets present a clear geometric characteristic with ideal and weighted Steiner networks, in which three neighboring nanowires form a three-way junction with angular symmetry and topological invariability (Fig. 13f) [31,32]. Learning from nature gives us much inspiration to explain some mysterious phenomena. Thus from pure geometric viewpoint, we can answer an important question that why do the nano-nets "tend to" be Steiner geometry? The answer is very simple: once the jets or droplets phase are separated along with the Steiner geometry, an optimization phase separation mode (i.e. the "materials needed for architectures" are minimal) is selected. Minimal materials and maximum spaces are irresistibly attractive for the phase separation of the droplets. Additionally, another possible reason may be ascribed to the minimal energy principle, which is of universality in nature [135], and is valid for

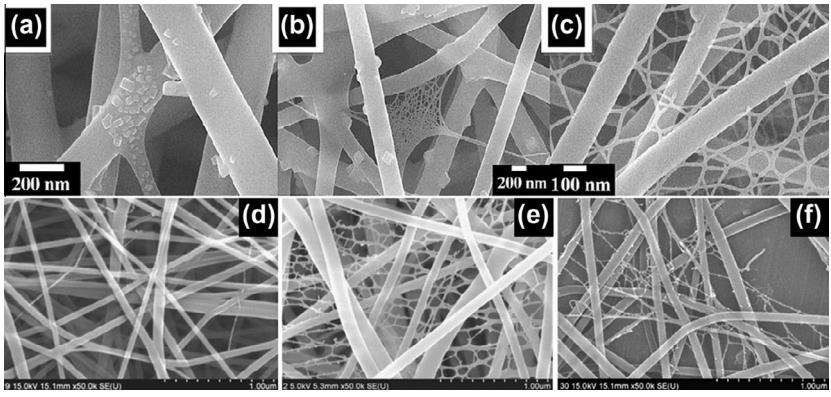

Fig. 14. FE SEM images of PVA/NaCl NFN membranes obtained from the solutions with different mixing times: (a) 0.5, (b) 3 and (c) 24 h. Reprinted with permission from [34]. © 2009 Elsevier B.V. FE-SEM images of PA-6 NFN membranes produced with the applied voltages of (d) 17 kV, (e) 22 kV and (f) 25 kV. Reprinted with permission from [136]. © 2010 Elsevier B.V.

the formation process of nano-nets. In another word, nano-nets tend to complete their phase separation processes by minimal energies. This means that a network with minimal energy is also a network with minimal length. Then it can be concluded that the formation of nano-nets is dominated by Steiner geometry.

3.4. Controllable coverage rate

Another important characteristic of NFN membranes is its controllable coverage rate, which is defined as the area ratio of nano-nets to the whole membranes. For accuracy, 10 SEM images with low magnification were randomly selected when we calculated the coverage rate. The coverage rate of nano-nets in 3D NFN nanostructures is of special interest since it may offer new functions or significant improvement of their filtration performance. This is for many cases the primary motivation to fabricate nano-nets with large and uniform area. ESN process represents a simple and straightforward method that can prepare nano-nets with controlled structures. Large coverage scale of nano-nets was easily accessible by regulating the voltage [136], adding salts in the polymer solutions (salt content and stirring time of salt/polymer solution) [34], changing the polymer concentration or solvent components [111,137], etc. For example, Kim et al. [34] reported the fabrication of NFN membranes by adding strong ionic salts to the polar polymer solutions and found that the stirring time had strong influence on the coverage rate of nano-nets (Fig. 14a–c). As shown in Fig. 14a, no nano-nets can be observed, however the salt nanoparticles are apparently attaching to the nanofibers. Actually, the main reason behind this is that the utilized stirring time (0.5 h) is not enough to completely dissolve the salt in the polymer solution, which means that the stirring time is not enough to liberate ions on the solution. With relatively little long time (3 h) the nano-nets start to appear but also some salt nanoparticles are present (Fig. 14b). However, with long stirring time (i.e. 1 day), larger coverage rate nano-nets were formed within the main electrospun nanofibrous membranes and no salt nanoparticles could be observed (Fig. 14c). Recently, Nirmala et al. [136] demonstrated the role of applied voltage for the coverage rate of PA-6 nano-nets (Fig. 14d–f). There were no nano-nets when the applied voltage was 17 kV (Fig. 14d). As the applied voltage was increased to 22 kV, it was clearly visible that the formation of large-scale nano-nets was strongly bound in between the main fibers (Fig. 14e). However, at too high-applied voltage, the formation of nano-nets was reduced and somewhat loosely bound to the main fibers (Fig. 14f). At lower applied voltage (e,g, 17 kV), the electrospinning jet was too stable to form microsized droplets and thus no obvious nano-nets were formed. The larger area density of the nano-nets at higher applied voltage (e.g. 22 kV) may be resulted from the improved formation probability of microsized droplets due to the increased instability of the Taylor cone. Further increasing the voltage can generate larger electrostatic forces on the droplets, which may stretch the jets fully for the favorable formation of completely split nano-nets (i.e. nano-nets were widespread in the fibrous membranes). Therefore, the applied voltage plays an important role in controlling the coverage rate of nano-nets.

3.5. Controllable density

The last but not the least interesting aspect of NFN membranes is their controllable density, which include the following two aspects: (1) arranged density of nano-nets in a plane and (2) stacking density of multi-layered nano-nets. Controllable density of nano-nets in NFN membranes makes it attractive candidate for various significant applications, such as filters and reinforcement materials for composites. Therefore, a few researchers have made efforts to regulate the density of nano-nets [27,33,138]. For instance, an enhanced density of nano-nets has been demonstrated by increasing content of chitosan (CS) in CS/PA-6 composite NFN membranes [138]. Recent studies have also shown that the controllable density of nano-nets could be achieved by changing the ESN parameters (i.e. solution, processing and ambient parameters) [27,33], which will be discussed in the following section (Section 5). On the other hand, stacking density of multi-layered nano-nets can be easily realized by appropriately prolonging the ESN time. It is worthy to mention that not the higher stacking density the better, there should be an optimal value that from the following two points to consider: (1) higher stacking density of NFN membranes on the collector will certainly affect the electric field between

Table 1
Different polymers used in ESN, solution properties and their applications.

Polymers	Chemical formula	Solvents	Perspective applications	Reference
PA-6	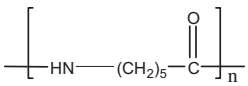	Formic acid	Filter; Protective clothing; Sensors	[27,33,34,136, 142,143]
PAA	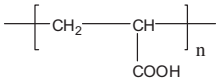	H_2O, Ethanol/ H_2O, Ethanol/ H_2O/formic acid	Sensors	[31–33,106]
PVA	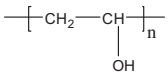	H_2O	Filter; Sensors	[34,99]
PU	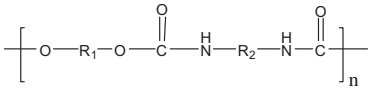	DMF, DMF/THF	Protective clothing; Tissue template Wound healing; Filter	[30,34,113]
PTT	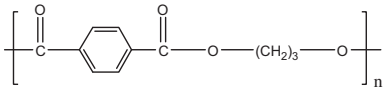	TFA/MC	Fueled academia	[174]
CS	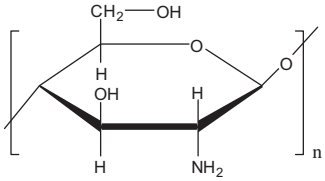	Acetic acid/H_2O	Tissue engineering scaffold; wound healing	[198]
Gelatin	–	Formic acid, acetic acid	Scaffold for wound healing	[108]
Silk	–	Formic acid/ SWCNT	Scaffold for tissue engineering	[112,199]
PEO/CNC	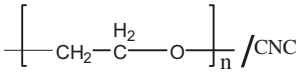	H_2O	Biomaterial scaffolds	[177]
MPEG/PA-6	–	Formic acid/ acetic acid	Scaffold for tissue engineering, drug delivery	[107]
Lecithin/PA-6	–	Formic acid	Scaffold for tissue engineering	[139]
PAA/PA-6	–	Formic acid	Sensors	[156]
CS/PA-6	–	Formic acid	Scaffold for tissue engineering	[138,149]
PANI/PA-6	–	Formic acid	Sensors; Conductive fiber	[28]

PA-6: polyamide-6, PAA: polyacrylic acid, PVA: polyvinil alcohol, PU: polyurethane, PTT: poly(trimethylene terephthalate), CS: chitosan, PEO: polyethylene oxide, CNC: cellulose nanocrystal, MPEG: methoxy poly(ethylene glycol), PANI: polyaniline, DMF: N,N-dimethylformamide, THF: Tetrahydrofuran, TFA: trifluoroacetic acid, MC: methylene chloride, SWCNT: single wall carbon nanotube.

the tip and collector and thus influence the morphology of subsequently deposited fibers; (2) higher stacking density of NFN membranes will increase the air resistance in filtration applications.

4. Polymers used in ESN

ESN has been applied to several natural and synthetic polymers, including polymers soluble and spinnable from water, biocompatible and biodegradable polymers, polymer blends and polymers into which nanoparticles, salts, surfactants and other functional materials have been incorporated. Similar

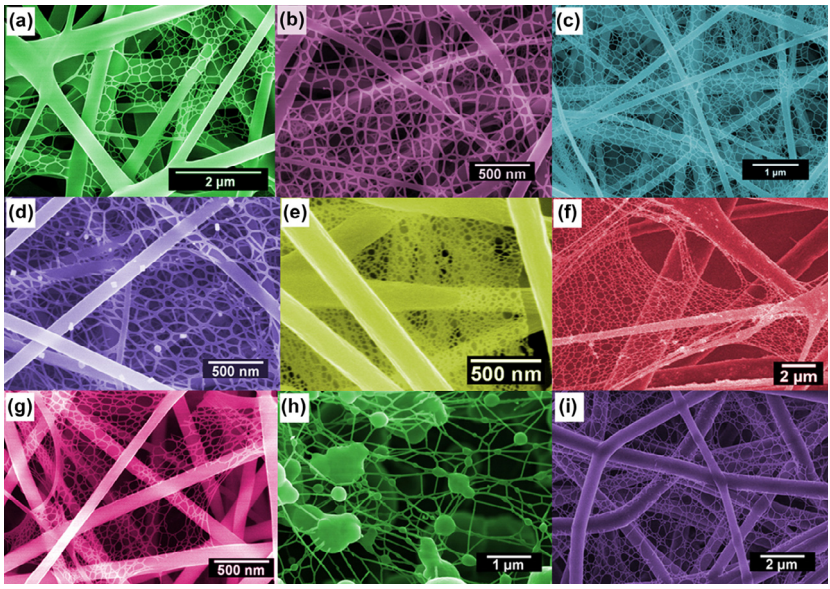

Fig. 15. Several typical NFN membranes based on different polymer systems fabricated in our laboratory. (a) PAA (reprinted with permission from [106]. © 2010 IOP Publishing Ltd.); (b) PA-6 (reprinted with permission from [27]. © 2011 Royal Society of Chemistry); (c) PANI/PA-6 (reprinted with permission from [28]. © 2011 Royal Society of Chemistry); (d) PA-66; (e) PVA/ZnO (reprinted with permission from [164]. © 2008 Elsevier B.V.); (f) PVA/SiO_2 [99]; (g) Gelatin, Reprinted with permission from [108]. © 2011 Elsevier Ltd.; (h) CS; (i) PU (reprinted with permission from [30]. © 2011 WILEY-VCH Verlag GmbH & Co.).

to electrospinning technique, the formation of NFN membranes via ESN also requires the materials to be fabricated to display electric conductivities in a limited range of values, specific viscous/visco-elastic properties as well as specific surface energies as obvious both from theoretical considerations and from experimental findings [41]. Although a broad range of polymers have been electrospun into micro- or nanofibers, it is worth noting that not all of those spinnable polymers can be ESN into NFN structured membranes. A comprehensive summary of polymers that have been successfully ESN into NFN structures to-date is listed in Table 1 for a quick and cursory review. Also given in the table are the chemical formulas of these polymers, solvents that have been used and proposed or perspective applications of the corresponding fibrous membranes. Fig. 15 shows the typical morphologies of NFN membranes based on different polymer systems, such as PAA, PA-6, polyamide-66 (PA-66), poly(-vinyl alcohol) (PVA), gelatin, CS, and polyurethane (PU), which have been synthesized in our laboratory. In this chapter, we present some typical recently developed processes for the synthesis of NFN nanomaterials based on various polymers and their structural characterizations. Additionally, spinnable polymers as supporter for functional materials have shown a great potential for various important applications. In the past few years, researchers have made successful attempts for functional material-polymer composite NFN membranes [27,28,139]. Their functionalization can offer exceptional properties in composites and applications in the field of energy, environment and biomedical. This section will also review these composite NFN membranes, illustrating their fabrication and discussing their intrinsic fundamentals.

4.1. Polyamide-6 (PA-6) based NFN membranes

4.1.1. PA-6

PA-6 is a polymorphic, biocompatible and synthetic polymeric material which has good mechanical and physical properties [140]. This polymer can be easily ESN with a controlled manner for fabricating NFN membranes. This PA-6 nanostructure exhibits several interesting morphological characteristics, for example, a high surface area to mass or volume ratio, high porosity, vast possibilities for surface

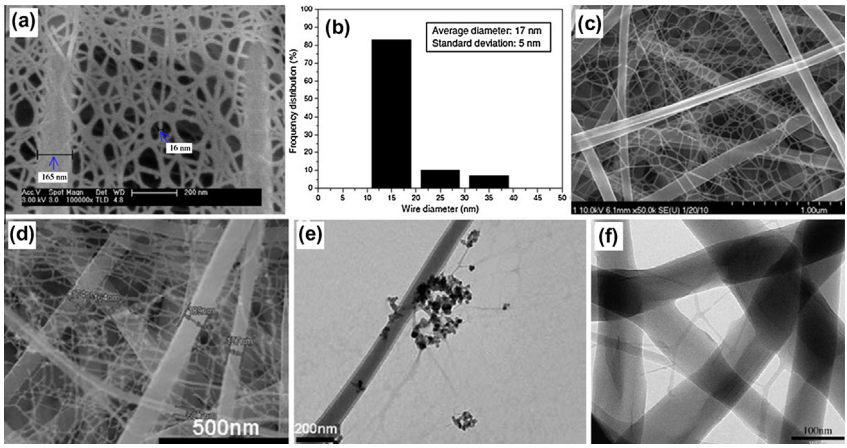

Fig. 16. FE-SEM images of (a) PA-6 [33], (c) PA-6 containing solvent degrade solution and (d) PA-6/TiO_2 NFN membranes. (b) Histogram showing the diameter distribution of nanowires shown in (a). TEM images of (e) PA-6/TiO_2 and (f) O-MMT/PA-6 nanocomposite NFN membranes. (a and b) Reprinted with permission from [33]. © 2006 IOP Publishing Ltd. (c) Reprinted with permission from [141]. © 2011 Elsevier B.V. (d and e) Reprinted with permission from [143]. © 2011 Elsevier B.V. (f) Reprinted with permission from [142]. © 2006 Elsevier B.V.

functionalization. These advantages render PA-6 NFN membranes good candidates for a wide variety of applications, including filters, composite reinforcements, drug carriers, and tissue-engineered scaffolds. At present, the most widely studied polymer for preparing NFN structured nanomaterials is PA-6, with demonstrated lots of literatures. Ding et al. [33] firstly demonstrated the fabrication of fishnet-like PA-6 NFN membranes (Fig. 16a) and they reported that the formation of such kind of morphology was due to the phase separation of charged droplets. The nanowire diameter distribution of PA-6 nano-nets shown in Fig. 16b exhibited that the major distribution region (over 80%) of nanowire diameters was 10–20 nm with an average diameter of 17 nm. The standard deviation of the wire diameters in nano-nets was 5 nm. PA-6 polymeric NFN membranes containing nano-net morphology have also been synthesized by the addition of metallic salt [34]. Nirmala et al. [136] investigated the formation of nano-nets in PA-6 NFN membranes as a function of applied voltage ranging from 15 to 25 kV. A large amount of sub-nanofibers (<50 nm in diameter) in the form of spider-web-like structures were achieved by increasing the amount of solvent degraded polymer solution in the freshly prepared PA-6 solution (Fig. 16c) [141]. Organically modified montmorillonite (O-MMT)/PA-6 nanocomposite NFN membranes (Fig. 16f) were also prepared by Li et al. [142]. The O-MMT layers were well exfoliated inside the nanocomposite fibers and were oriented along the fiber direction, which enhanced Young's modulus and ultimate tensile strength of the composite membranes. Recent study have also revealed that the incorporation of TiO_2 nanoparticles into the PA-6 solutions can form more spider-web-like nano-nets (Fig. 16d and e), which can lead to a remarkable increase in the number of reactive sites with a corresponding improvement in hydrophilicity, photocatalytic and antimicrobial activity [143].

4.1.2. Methoxy poly(ethylene glycol) (MPEG) oligomer/PA-6

The composite nanofibrous membranes have unique physical and chemical properties and therefore, research interest in the formation of polymer composite NFN membranes has caught more attentions. Kim and coworkers [107] reported the preparation of a composite MPEG/PA-6 by ESN the blend solutions containing MPEG oligomer and a viscous PA-6 supporting solution. MPEG/PA-6 composite NFN membranes showed highly interconnected spider-web-like structures with ultrathin nanowire diameter of 15 ± 5 nm (Fig. 17A). The mechanical strength of the PA-6 nanofibrous membranes with low MPEG content (1 wt%) was greater than that of pure PA-6 and again decreased with increasing MPEG content (Fig. 17B). The enhanced mechanical strength up to 1 wt% MPEG is due to the highly interconnected spider-web structure of MPEG with the larger PA-6 backbone nanofibers. Upon increasing the MPEG content, the coverage rate of nano-nets was decreased, as can be observed in

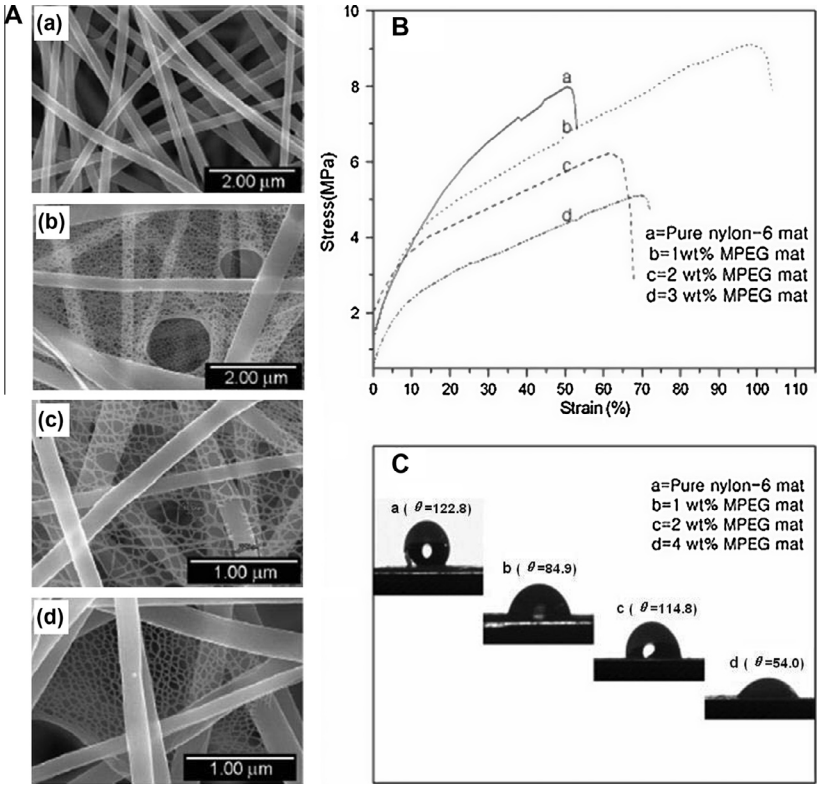

Fig. 17. FE-SEM images (A), mechanical strength (B) and contact angles (C) of MPEG/PA-6 fibrous membranes containing different amounts of MPEG oligomer: (a) 0, (b) 1 wt%, (c) 2 wt% and (d) 4 wt%. Reprinted with permission from [107]. © 2010 Elsevier B.V.

the FE-SEM images (Fig. 17A). Therefore, there was a decrease in mechanical strength. The results of contact angle measurement showed that MPEG/PA-6 NFN membrane with 1 wt% MPEG was not only much more hydrophilic than pure PA-6 membrane but also more hydrophilic than a 2 wt% MPEG membranes (Fig. 17C). It is probably due to the formation of more surface to volume ratio of well distributed nano-nets of hydrophilic MPEG throughout the 1 wt% MPEGN membrane than the others. Therefore, strongly interconnected thin MPEG spider-web-like nano-nets with thick PA-6 nanofibers are responsible to increase mechanical strength and hydrophilic nature of PA-6 fibrous membranes, which make composite MPEG/PA-6 NFN membranes great potential in air filtration and different biomedical application.

4.1.3. Lecithin/PA-6

Lecithin is a natural mixture of phospholipids and neutral lipids, which is a significant constituent of nervous tissue and brain substance [139,144–146]. It is a typical amphiphilic phospholipid with good biocompatibility and capable of mixing with different polymers, such as poly(lactic-co-glycolic acid) (PLGA), poly(lactic acid), poly(ε-caprolactone) (PCL) and poly-L-lactic acid (PLLA) [147,148]. Recently, lecithin blended in PA-6 nanofibers with spider-web-like nano-net structure (Fig. 18a–d) was successfully produced by ESN technique for human osteoblastic (HOB) cell culture applications [139]. From the water wettability test, it was observed that the water droplets sink into the lecithin/PA-6 NFN scaffold (Fig. 18b–d), indicating improved water wettability than that of the pristine PA-6 scaffolds (Fig. 18a). Fig. 18e shows the Fourier-transform infrared (FT-IR) spectrum of the lecithin/PA-6 NFN membranes, which indicated that the characteristic peaks of lecithin/PA-6 appeared at

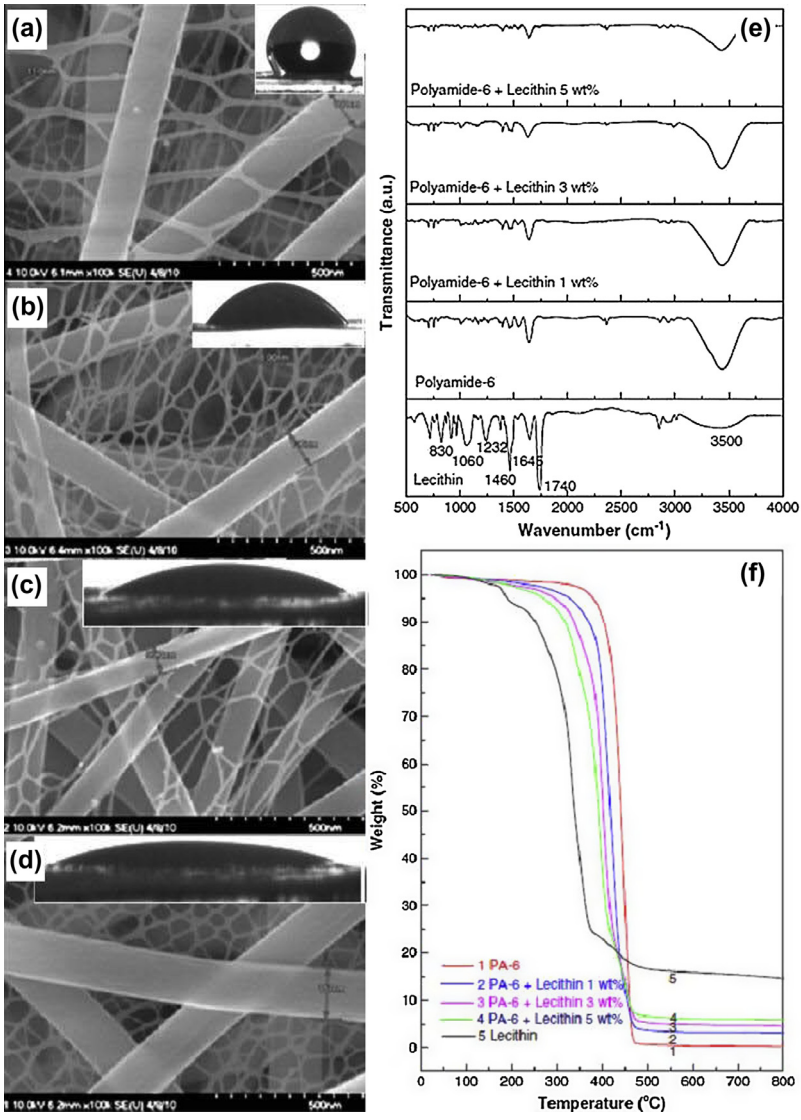

Fig. 18. FE-SEM images of lecithin/PA-6 NFN membranes with different contents of lecithin (a) 0, (b) 1, (c) 3 and (d) 5 wt%. Insets show the appearance of water droplet on the NFN membranes. (e) FT-IR spectra and (f) TGA graphs of lecithin/PA-6 NFN membranes with different lecithin concentrations of 0, 1, 3 and 5 wt%. Reprinted with permission from [139]. © 2011 Elsevier B.V.

500–1750 cm^{-1} in the composite fibers. One prominent peak was observed for the lecithin/PA-6 at 1645 cm^{-1} (amide I), which is attributed to the amino groups of blended nanofibers. On the other hand, one intense extra peak at 1740 cm^{-1} was observed for the pristine lecithin, which is attributed to the C═O groups in lecithin. The CH_2 group transmittance band in the 2800–3000 cm^{-1} region is slightly stronger than that of PA-6, indicating that lecithin contains more CH_2 groups. The broad peak between 3400 and 3500 cm^{-1} corresponds to a stretching of –OH and the intensity of this band was found to be decreased with increasing lecithin concentration in lecithin/PA-6 NFN membranes. The TGA results show that pristine PA-6 nanofibers had higher onset temperature (~400 °C) among all samples, while for pristine lecithin was around 160 °C (Fig. 18f). The onset decomposition temperature monotonically

decreased with increasing lecithin concentration in the in the composite NFN membranes, which demonstrated a significant difference in the thermal stabilities between the starting physical forms (i.e. lecithin and PA-6) of the composite NFN membranes.

4.1.4. Chitosan (CS)/PA-6

Very recently, Kim and co-workers reported on a one step preparation of CS/PA-6 composite NFN membranes with a single solvent system and investigated the electrical properties of the resultant membranes (Fig. 19) [138]. The resultant nanofibers are well-oriented and have good incorporation of CS. High density CS/PA-6 composite nano-nets with diameters of about 20–40 nm are bound in between main fibers (Fig. 19a–d). Current–voltage (*I–V*) measurements revealed interesting linear curve, including enhanced conductivities with respect to CS content (Fig. 19e), which could be due to the enhanced electrical pathways in the composite NFN membranes caused by the increased CS content. Moreover, the sheet resistance of composite nanofibers was decreased with increasing content of CS (Fig. 19f), which could be attributed to the formation of highly denser ultrafine nano-net structures. Furthermore, they also demonstrated that these novel NFN membranes could be used as nontoxic scaffold material for the osteoblast cell culture [149].

4.1.5. Polyaniline (PANI)/PA-6

Conducting polymers constitute an attractive class of materials for electronic, magnetic, and optical applications [150,151]. Among them, PANI has received much attention due to its environmental

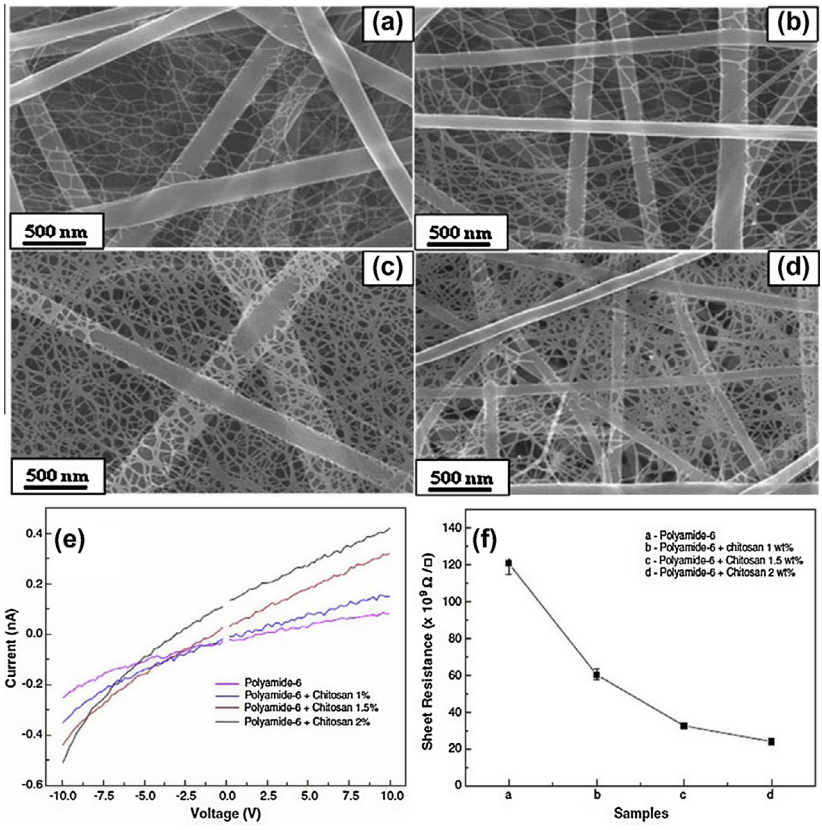

Fig. 19. FE-SEM images of CS/PA-6 composite NFN membranes with different contents of CS (a) 0, (b) 1, (c) 1.5 and (d) 2 wt.%. (e) Electrical conductivity and (f) *I–V* characteristic of the composite NFN membranes with different contents of CS. Reprinted with permission from [138]. © 2011 Elsevier B.V.

stability, controllable electrical conductivity, and interesting redox properties [152]. Considering the well-known fact that the yield of electrochemical reactions occurring at an electrode is proportional to its surface area, it is expected that nanostructures of this polymer offer great opportunities for potential applications in electronic nanodevices like sensors [153–155]. More recently, our group has presented continuous efforts toward the aim of generating PANI-based nanostructured materials and for the first time fabricated composite PANI/PA-6 NFN membranes (Fig. 20a), which were used as a platform for efficient sensing reaction by providing high specific surface area and porosity. Evidence for the formation of PANI/PA-6 composite NFN membranes comes from FT-IR spectral analysis (Fig. 20b). The bands at 1645, 3302, and 2861 cm^{-1} belong to C═O group, hydrogen bonded N–H stretch and $–CH_2–$ group of PA-6, respectively. The band corresponding to *p*-substituted chains of PANI appears around 820 cm^{-1}, and the bands corresponding to stretching vibration of N–B–N and N═Q═N structure of PANI appear around 1369 and 1504 cm^{-1}, respectively. Furthermore, we showed that PANI/PA-6 NFN membranes could be used as sensor strips for naked-eye colorimetric detection of Cu^{2+} in water, achieving a detection limit as low as 1 ppb by naked eye [28].

4.1.6. Polyacrylic acid (PAA)/PA-6

Acrylic acid monomer in a viscous supporting PA-6 solution was polymerized and fabricated simultaneously via an ESN process by Parajuli et al. [156]. Polymerization of acrylic acid was achieved via formic acid reduction during the ESN process. In this process, formic acid acted as a reducing agent, which was activated by the applied voltage (Fig. 21a). This voltage removed the hydride ion to electrically excite acrylic acid and induced a nucleophilic chain reaction polymerization. This polymerization method defines the fiber morphology as a network of interconnected membranes (i.e. nano-nets). This network consists of smaller PAA fibers (approximately 19 nm in diameter) and larger PA-6 fibers (approximately 75 nm in diameter) (Fig. 21b), which was demonstrated by the FE-SEM image of PAA/PA-6 NFN membranes after washing with water (Fig. 21c). Final observations of promoting experiments were taken several times and different feed ratios of acrylic acid monomer with a fixed viscous nylon solution remarkably enhanced mechanical properties along with the thermal behavior of PAA/PA-6 hybrid membranes. Research and observation are underway. Furthermore, they demonstrated smaller changes exhibited with an increase the volume ratio of acrylic acid (Fig. 21d).

4.2. Polyacrylic acid (PAA)

The close association of the charged polyelectrolytes in aqueous solutions and their counter ions is expected to play an important role in the conformation of polyelectrolyte molecules, thus molecular entanglement and solution viscosity, both of which are critical to fiber formation [157–159]. Furthermore, the investigation of the formation of polyelectrolyte fibers provides excellent models to understand how to generate fibers from proteins [160]. Therefore, it is of fundamental interest to understand the formation and properties of polyelectrolyte fibers from electrospinning and ESN

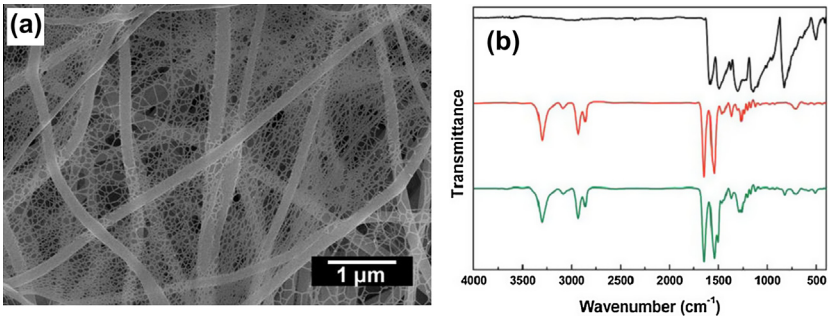

Fig. 20. (a) FE-SEM image of the PANI/PA-6 NFN membranes. (b) FT-IR spectra of PANI-EB powder (black), PA-6 (red) and PANI/PA-6 NFN membranes (green). Reprinted with permission from [28]. © 2011 Royal Society of Chemistry.

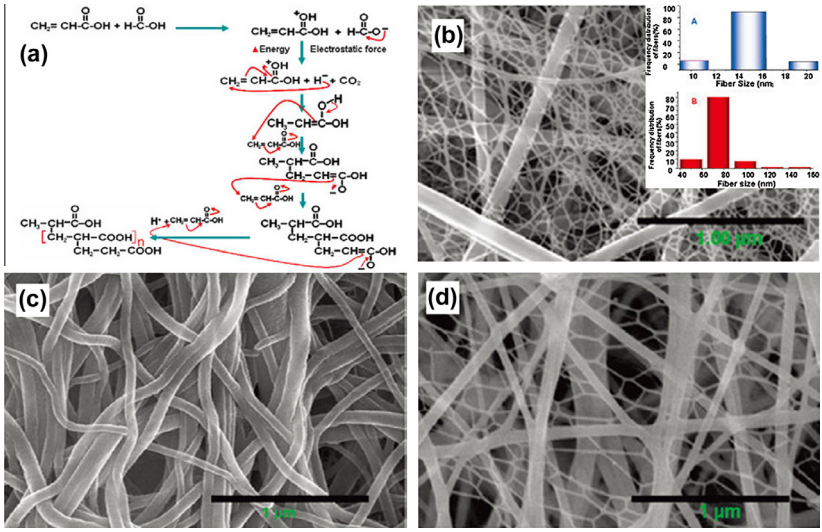

Fig. 21. (a) Formic acid initiated PAA polymerization mechanism. FE-SEM images of the PAA/PA-6 NFN membranes showing interconnected nano-nets appearing before (b) and (c) after washing with water. FE-SEM image of PAA/PA-6 NFN membranes obtained from more volume ratio of acrylic acid. Reprinted with permission from [156]. © 2009 American Chemical Society.

processes. PAA is a high water absorbing and protein resistive hydrogel polyelectrolyte widely used in medical field [161]. Growing attempts were reported to regulate the morphology of PAA fibers to achieve the designed functions [33,106,156]. Ding et al. [33] firstly reported the formation of PAA nano-nets, and concluded that nano-nets could be obtained by adjusting the solution properties and several parameters in the process of electrospinning (Fig. 22a). Wang et al. [31,106] demonstrated that highly sensitive sensors could be prepared by ESN deposition of PAA NFN membranes on the electrodes of quartz crystal microbalance (QCM). Additionally, in order to obtain PAA nano-nets in large quantities and with uniform size, various additives, such as formic acid (Fig. 22b), $AgNO_3$ (Fig. 22c), dodecylbenzene sulfonic acid (DBSA) (Fig. 22d), silica (Fig. 22e), and NaCl (Fig. 22f), were incorporated into the PAA solutions and their effects on the internal morphology of the electrospun nanofibrous membranes were also investigated [32]. Furthermore, the versatile nano-nets with small pore-widths create additional surface area, which would be particularly useful for applications such as ultrafiltration, ultrasensitive sensors, and catalyst supports.

4.3. Poly(vinyl alcohol) (PVA)

PVA, a water-soluble polyhydroxy polymer, is the largest volume synthetic resin produced in the world. The excellent chemical resistance, physical properties, and complete biodegradability of PVA resins have led to their broad practical applications [162,163]. Nanomaterials can be rationally designed to exhibit novel and significantly improved physical, chemical, and biological properties because of their size [163]. Thus, engineering PVA into nanomaterials has attracted extensive attentions. Fig. 23a showed the morphology of the electrospun pure PVA fibrous films. As a typical electrospun fibrous film, the PVA fibers were randomly oriented as a porous film with a wide fiber diameter distribution. Further investigations have demonstrated that PVA NFN membranes could be prepared by changing the solution properties, such as adding ZnO [164], SiO_2 [99], and NaCl [34] into the polymer solutions. The SEM image of composite PVA/ZnO NFN membranes is shown in Fig. 23b. It can be observed that the composite fibers have many junctions among the fibers, showing poor fiber uniformity compared with the pure PVA fibers. The average diameter of PVA/ZnO fibers (258 nm) was larger than that (239 nm) of pure PVA fibers due to its increased viscosity (from 420 to 600 cps). Additionally, the formation of nano-nets was observed among the fibers. The electrospun PVA/ZnO fibers acted as a support for the spider-web-like nano-nets comprising interlinked 1D nanowires. The

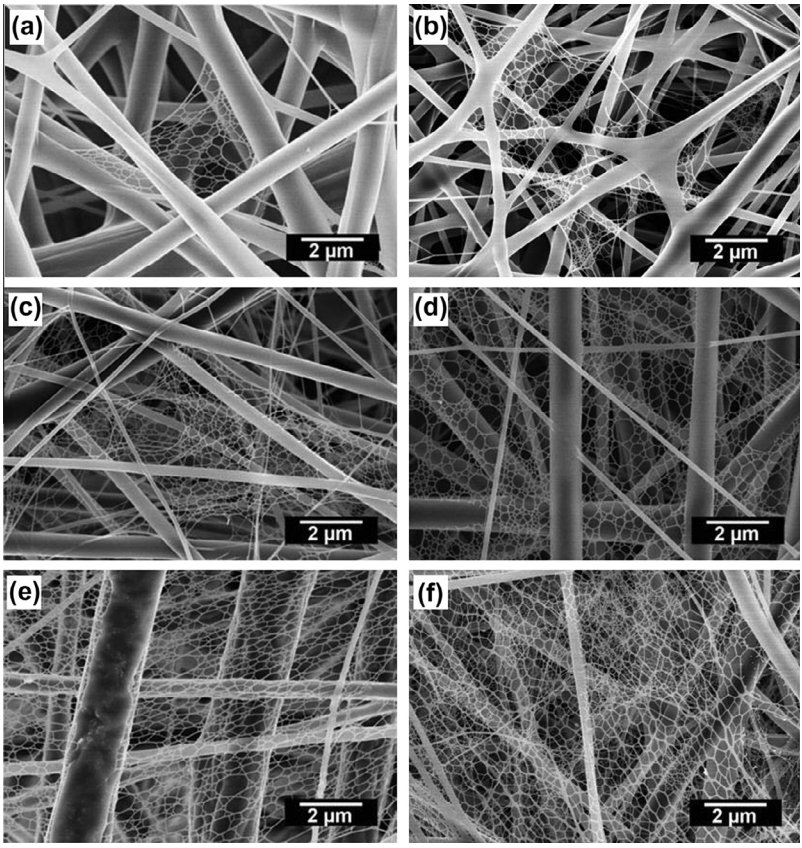

Fig. 22. FE-SEM images of (a) PAA, (b) PAA (prepared from the cosolvent of ethanol and formic acid), (c) PAA/$AgNO_3$, (d) PAA/DBSA (reprinted with permission from [32]. © 2011 Royal Society of Chemistry), (e) PAA/silica, and (f) PAA/NaCl NFN membranes.

average diameter of the PVA/ZnO nanowires (10 nm) contained in this nano-net was about one order magnitude less than that of conventional electrospun fibers.

Another example for nano-net formation is the PVA/SiO_2 nano-nets by ESN the suspension of PVA and SiO_2 nanoparticles (Fig. 23c). The formation of nano-nets probably was due to the increased instability by blending the high content nanoparticles in polymer solution. Recently, Barakat et al. [34] revealed that the addition of the utilized salts to the PVA solution resulted in formation of nano-nets (Fig. 14c). Despite the success in fabrication of PVA nano-nets, the small coverage rate of current PVA NFN membranes restricts the use of PVA in more extensive fields. Extensive research should be performed on developing more proficient strategies to regulate the structure of PVA NFN membranes, and thus further improving the quality of nano-nets.

4.4. Polyurethane (PU)

PU presents a class of thermoplastic polymer that possesses a lot of excellent properties, such as good mechanical properties, excellent elastomeric properties and high durability [165,166]. Meanwhile, 1D nanostructure has achieved a tremendous amount of attention in recent years due to their fascinating chemistry and size-, shape-, and material-dependent properties.[35,167,168]. Electrospinning has been paid a considerable attention due to production of micro- or nano-sized fibers by

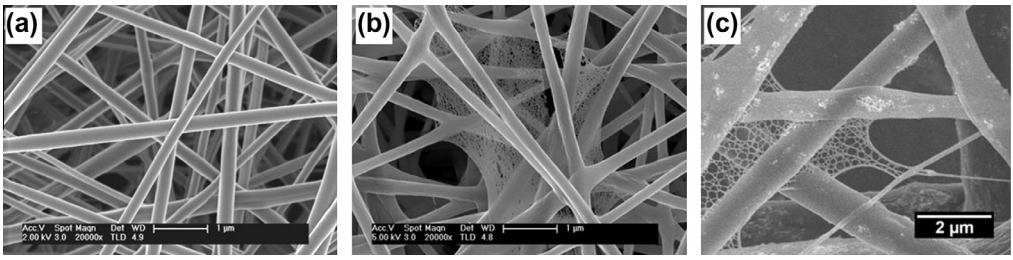

Fig. 23. SEM images of (a) pure PVA electrospun nanofibers, (b) PVA/ZnO NFN membranes and (c) PVA/SiO_2 NFN membranes [99].

applying high electric fields [45,105,169]. Many investigators have attempted to apply various degrees of control to this process in order to produce PU fibrous membranes with the designed functions [166,170–172]. However, the main hurdle for further applications in ultrafiltration, special protective clothing, ultrasensitive sensors, etc. is the larger fiber diameter (100–500 nm) of current electrospun PU fibers. Therefore, the procedures for manufacturing large-scale and ultrafine nanofibers with diameter less than 50 nm still require more investigation [31].

Recent investigations have revealed that different additives (e.g. multiwalled carbon nanotube (MWCNTs), salts, and surfactants) incorporated into the PU solutions could generate spider-web-like nano-nets with ultrathin nanowires [113]. For example, Kimmer et al. [113] reported the fabrication of the composite PU/MWCNTs NFN membranes containing a handful of nano-nets (Fig. 24a). The presence of the MWCNTs promoted the creation of net-like structures in comparison with the PU nanofibers without MWCNTs. They suggested that these nano-nets were created because of strong secondary

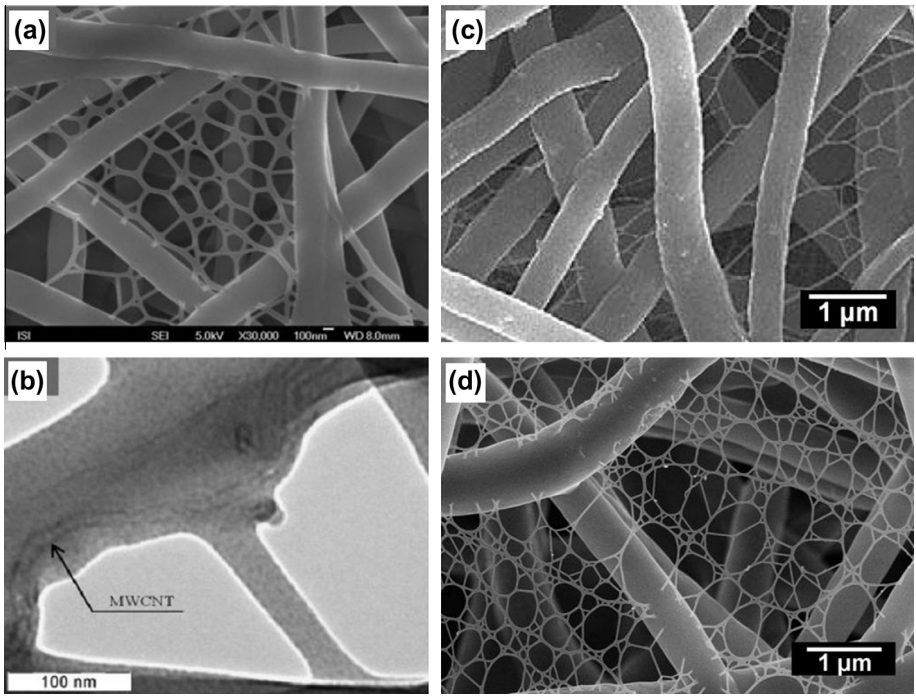

Fig. 24. (a) FE-SEM and (b) TEM images of the PU/MWCNTs NFN membranes. Reprinted with permission from [113]. © 2009 WILEY-VCH Verlag GmbH & Co. FE-SEM images of (c) PU/NaCl (reprinted with permission from [34]. © 2009 Elsevier B.V.) and (d) PU/SLS NFN membranes.

electric fields occurring between MWCNTs during the electrospinning process. TEM analysis of the PU/MWCNT NFN membranes showed that individual and very well aligned MWCNTs (except for a small curvature at the junction point) occurred in the outer surface of the main nanofiber from which nano-nets was created (Fig. 24b). In addition of MWCNTs, Kim et al. [34] added NaCl into the PU solution in which tetrahydrofolate (THF)/N,N-dimethylformamide (DMF) were utilized as solvents and found that nano-nets with small coverage rate were produced (Fig. 24c). To obtain nano-nets in large scale, Hu et al. [30] demonstrated that the addition of SLS surfactant at the critical micelle concentration (CMC) to the PU solution resulted in a significant improvement in the NFN morphology (Fig. 24d).

4.5. Poly(trimethylene terephthalate) (PTT)

PTT, as a new member in the linear aromatic polyester family, combines the desirable mechanical properties of poly(ethylene terephthalate) with the outstanding processing characteristics of poly(butylene terephthalate), which makes it a promising candidate in both fiber and engineering applications [173,174]. Of particular interest is recently developed nanocomposite technology consisting of PTT and nanofiller (e.g. CNT) because the obtained nanocomposites usually show fascinating properties and hence, both the structure and the performance of PTT/CNT nanocomposites have been studied extensively with the aim of exploring their potential applications [174,175]. More recently, PTT/CNT composite NFN membranes were fabricated by ESN the melt compounding solution (Fig. 25a) [174]. Carboxylic surface functionalized CNTs are well embedded by the PTT and oriented along the fiber axis during ESN process, leading to bead-free and uniform fiber morphology as well as spider-web-like nano-nets. They ascribed the formation of nano-nets to the self-governed network of CNTs. However, it is noteworthy mentioning that the determination of the actual composition of nano-nets should be carried out, whether the CNT composition existing in the nano-nets. Just as the authors said that "This is interesting and worthy of further study" [174]. Nevertheless, the formation feasibility of nano-nets based on PTT polymer system has been well revealed. Further studies are needed to focus on the controllable fabrication of PTT NFN membranes.

4.6. Polyethylene oxide (PEO)/cellulose nanocrystals (CNCs)

PEO, as a nontoxic, fully biodegradable, and biocompatible polymer, has attracted tremendous attention in the biomedical field for controlled drug release and tissue engineering [176,177]. Over

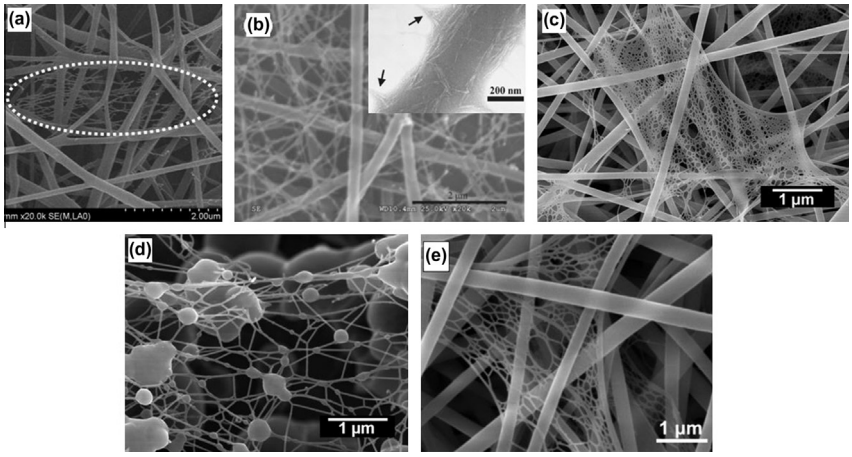

Fig. 25. SEM images of (a) PTT/CNT (reprinted with permission from [174]. © 2011 Elsevier B.V.), (b) PEO/CNCs (reprinted with permission from [177]. © 2011 American Chemical Society), (c) gelatin (reprinted with permission from [108]. © 2011 Elsevier B.V.), (d) CS (reprinted with permission from [198]. © 2010 Walter de Gruyter GmbH & Co. KG), and (e) *Bombyx mori* silk/SWCNT (reprinted with permission from [112]. © 2006 American Chemical Society) NFN membranes.

the past few years, extensive studies have been done on electrospun PEO fibers produced from PEO/water solutions to study the effects of process conditions and solution compositions [56,178–180]. On the other hand, CNC, as one of the strongest and stiffest natural biopolymer, is a suitable candidate for tailoring mechanical properties of polymer materials [181]. They have been successfully used as highly effective reinforcing nanofillers for various electrospun polymer nanofibers [182,183]. Additionally, because CNCs are nontoxic, biocompatible, and biodegradable, they have a significant potential in developing fully biodegradable polymer nanocomposites for biomedical applications [177]. Considering excellent dispersion of CNCs in water, the exploitation of an all-aqueous system for ESN based on a combination of CNCs with water-soluble polymers offers advantages in avoiding the use of organic solvents. Recently, PEO/CNCs NFN membranes have been fabricated when increasing wood-based CNC content to 7 wt% in the polymer solutions (Fig. 25b). The resultant heterogeneous composite NFN membranes were composed of rigid-flexible bimodal nanofibers, consisting of the primary nanofibers and secondary ultrafine nanofibers. The authors attributed this behavior to the unstable jet flow arising from the unbalanced forces among the surface tension, viscoelastic, and electrostatic forces. Furthermore, they have demonstrated that the CNCs and nano-nets effectively improved the mechanical properties of the NFN membranes [177].

4.7. Gelatin

Gelatin is a natural polymer that is derived from collagen, and is commonly used for pharmaceutical and medical applications because of its biodegradability and biocompatibility in physiological environments [184,185]. Generally, gelatin is of two types (i.e. Type A and Type B) depending on the hydrolysis condition of isolation from collagen [109,186]. Gelatin is a kind of temperature sensitive polymer. Temperature has a profound effect on gelatin aqueous solution properties. Zhang et al. [187] demonstrated the electrospinning of gelatin aqueous solution by elevating the spinning temperature from 35 to 50 °C. Previous studies have also revealed that gelatin nanofibers could be prepared from various organic solvents, such as 2,2,2-trifluoroethanol [188], formic acid [189], cosolvent (acetic acid/ethyl acetate/water) [190] and so on. Through some posttreatment or blending with other biodegradable polymer, gelatin can be used to prepare nanofibrous membranes for tissue scaffolds, wound healing and health caring devices, and other biomedical applications [184]. For this reason, gelatin has been electrospun into various forms for wide applications [189,190]. Recent studies have demonstrated that 2D gelatin nano-nets could be fabricated by regulating the solution properties and several process parameters during ESN process [108]. The spider-web-like nano-nets that comprise interlinked 1D ultrathin nanowires (10–35 nm) are stacked layer-by-layer and widely distributed in the 3D porous membranes (Fig. 25c). Moreover, they revealed that the occurrence of rapid phase separation on the splitting-film and the formation of hydrogen bond among gelatin molecules during ESN process were responsible for the formation of these spider-web-like nano-nets.

4.8. Chitosan (CS)

CS is a natural biopolymer derived by the deacetylation of chitin, possessing unique polycationic, chelating, and film-forming properties due to the presence of active amino and hydroxyl functional groups [138,191,192]. As a natural polymer, CS intrinsically exhibits a unique set of characteristics such as biocompatibility, biodegradability, antimicrobial activity, physiological inertness, non-toxicity remarkable affinity to proteins, and its adequate absorption capabilities [109,193]. These significant biological and chemical characteristics make CS as a desirable biomaterial used in many different fields, including medicine, food and chemical engineering, pharmaceuticals, cosmetics, nutrition, and agriculture [109,138]. Particularly, nanofibrous CS membranes have a great potential to be widely used in various applications derived from its biocompatibility and biodegradability [194,195]. Earlier work had revealed that electrospun fibers from pure CS were difficult, until 2004 when direct electrospinning of pure CS was performed by some researchers using THF and acetic acid as a solvent [196,197]. CS nano-nets have been fabricated by ESN CS solutions with 90 wt% acetic acid aqueous solution as solvent [198]. It is worthy to mention that the nano-nets bonded with polymer beads other than electrospun fibers in CS NFN membranes (Fig. 25d), which could be attributed to the lower

concentration (2 wt%) of the CS solution. In this case (i.e. polymer concentration was lower than critical entanglement concentration), insufficient chain entanglements are present to fully stabilize the jet, and thus bead-on-string structure was formed. Taking advantage of the large surface areas, CS NFN membranes as the template on which modified with polyethyleneimine (PEI) have been used as sensing materials on QCM for humidity detection [198].

4.9. Silk

Silk is a well-described natural fiber obtained from silkworms (*Bombyx mori* and *Antheraea mylitta*) and spiders and has been used in textile industries from thousands of years. Recently, net-like structures (containing very fine fibers 5–30 nm in diameter) occurring together with fibers with much higher diameters (100–150 nm) have also been identified in natural biopolymers [113], such as collagen spider silk [199] and *B. mori* silk [112]. Because of these structures mimic natural tissue structure; they can be used as scaffolds for biomedical tissue engineering. Such nano-net structure can also lead to enhanced mechanical properties in fibers prepared via electrospinning [112,199]. Lam [199] explained that the formation of net-like structure might be a result of the inclusion of single wall carbon nanotubes (SWCNTs) into the fibers. During electrospinning, the silk/SWCNT bundles were expelled from the polymer jet under extremely high force and velocity, which caused opening of the bundles to form the nano-net structure. Similarly, Ayutsede and coworkers [112] demonstrated the feasibility of fabricating nanocomposite *B. mori* silk/SWCNT NFN membranes through the ESN process (Fig. 25e). Additionally, they reported the reinforcement effects of SWCNT on the mechanical properties of electrospun silk nanofibers, which showed significant enhancement in Young's modulus (up to 460%) compared to the pristine electrospun silk fibers. Consequently, by adding SWCNT into the silk fibroin solution, strong and tough multifunctional nanocomposite fibrous membranes may be fabricated, which may open the gateway to producing multifunctional fibers that may be suitable for weaving into textiles. These results indicate that the SWCNT incorporated into the polymer solutions plays an important role in the formation of the nano-nets.

Despite the rapid increase of research on polymer-based NFN nanomaterials as documented in this section, several challenges need to be overcome to realize overall development of ESN NFN materials.

1. ESN is a newly emerging interdisciplinary field in materials science, nanotechnology, EHD and engineering. The design and fabrication of NFN membranes is one of the most promising scientific and technological challenges in the coming years. According to preparation process and formation of current polymer NFN materials, we found that polymers with hydrogen bonds favored creating interconnect nano-nets [107,108], adding ZnO [164], SiO_2 [99], NaCl [34], CNT [174], CNC [177] and SWCNT [112] into the polymer solutions could lead to nano-nets, and changing processing parameters could influence the morphology of NFN membranes. However, pursuing the universal law for explaining the formation of nano-nets is a complicated problem. Revealing the process's secret can help people to look for additional spinnable polymers.
2. It is worthy to mention that current NFN membranes are all organic-based materials. On the other hand, inorganic materials are potentially important for those applications in many areas that include electronics, photonics, mechanics, and sensing [200]. Fabrication of inorganic NFN membranes is of significant importance, which of course is a complicated process.

5. Effects of various parameters on ESN

NFN membranes have attracted considerable attention due to their unique fundamental properties and diverse polymer compositions, making them model systems for the observation of novel EHD phenomenon and ideal building blocks for future applications. However, in practical point of view it is necessary, (1) to create NFN structure in large quantities among the 3D fibrous membranes and (2) to provide a universal principle to readily control the structure of NFN membranes. Similar to electrospinning, the ESN process is also influenced by many parameters, classified broadly into solution parameters, process parameters, and ambient parameters. Solution parameters include concentration, conductivity, viscosity, surface tension, and solvent and process parameters include applied voltage

and tip to collector distance [33,109,111,137]. Each of these parameters significantly affects the NFN morphology (e.g. fiber and nanowire diameter, pore-width and coverage rate of nano-nets) obtained as a result of ESN, and through proper manipulation of these parameters we can obtain NFN membranes with desired morphology and diameters. In addition to these variables, ambient parameters encompass the temperature and humidity of the surroundings, which also play a significant role in determining the morphology of NFN membranes [30,33,108]. Table 2 overviews the "global effects" on the NFN morphology one can expect by changing the various parameters.

5.1. Solution parameters

5.1.1. Concentration

The typical NFN membrane is composed of traditional electrospun fibers and 2D spider-web-like nano-nets. The effects of solution concentration on the morphology of common electrospun fibers have been extensively studied [40,53,201]. Solution concentration determines the limiting boundaries for the formation of electrospun fibers due to variations in the viscosity and surface tension [40,52]. Low concentration solution forms bead-on-string fibers due to the influence of surface tension and as the solution concentration increases, the shape of the beads changes from spherical to spindle-like and finally uniform fibers with increased diameters are formed due to the higher viscosity [56,109,202,203]. Therefore, there should be an optimal concentration range for the electrospinning process, and higher polymer concentrations lead to increased fiber diameters within this optimal range [37,93]. Here, a question may come to mind, how morphology changes for nano-nets when we regulate the solution concentrations? Does the universal law of electrospinning process can be applied to the ESN process? Fortunately, several researchers have paid their attention to solve these problems. Previous studies have documented the ESN fabrication of polymers like PAA [33], PA-6 [111], and gelatin [108] in certain concentration levels. Ding and co-workers investigated the morphologies of PAA NFN membranes formed with various concentrations of PAA solution [33]. It can be observed that all the samples exhibit incomplete splitting of defect films and the PAA (6 wt%) NFN membranes show the largest average pore-width and diameter deviation of nano-nets among the three samples (Fig. 26a). As the PAA concentration is increased to 8 wt% (Fig. 26b), the pore-width and shape of the nano-nets become uniform and the average pore-width is decreased compared to the sample in Fig. 26a. Moreover, as shown in Fig. 26b, the shapes of the pores in the nano-nets are circular, triangular, quadrangular, pentagonal and hexagonal, while PAA (10 wt%) NFN membranes exhibited circular pores with the smallest average pore-width among the three samples (Fig. 26c).

Table 2
Effects of ESN parameters (solution, processing and ambient) on fiber morphology.

Parameters	Effect on NFN morphology	Reference
Polymer concentration ↑	Fiber and nanowire diameter ↑ (within optimal range), pore-width of nano-nets ↓	[33,108,111]
Solution conductivity ↑	Fiber and nanowire diameter ↓, coverage rate and density of nano-net ↑	[30,32,34,106]
Surface tension ↓	Fiber and nanowire diameter ↓, optimal morphology at CMC of surfactant in polymer solutions	[30,32]
Solvent	Lower boiling point and higher dielectric constant of solvent are beneficial to form nano-net; formic acid was identified as good solvent for producing nano-nets	[32,33,108,137]
Applied voltage ↑	Fiber and nanowire diameter ↓, coverage rate and pore-width of nano-net ↑ (within optimal range)	[31,136]
Tip to collector distance ↑	Fiber and nanowire diameter ↓, pore-width of nano-net ↑	[30]
Ambient temperature ↑	Coverage rate and density of nano-net ↑ initially (15–25 °C), then ↓ (>25 °C)	[30,108]
Ambient humidity ↑	Fiber and nanowire diameter ↓, coverage rate ↓, fiber-sticking and beads ↑	[30,31,108]

↑: Increasing the parameter; ↓: decreasing the parameter.

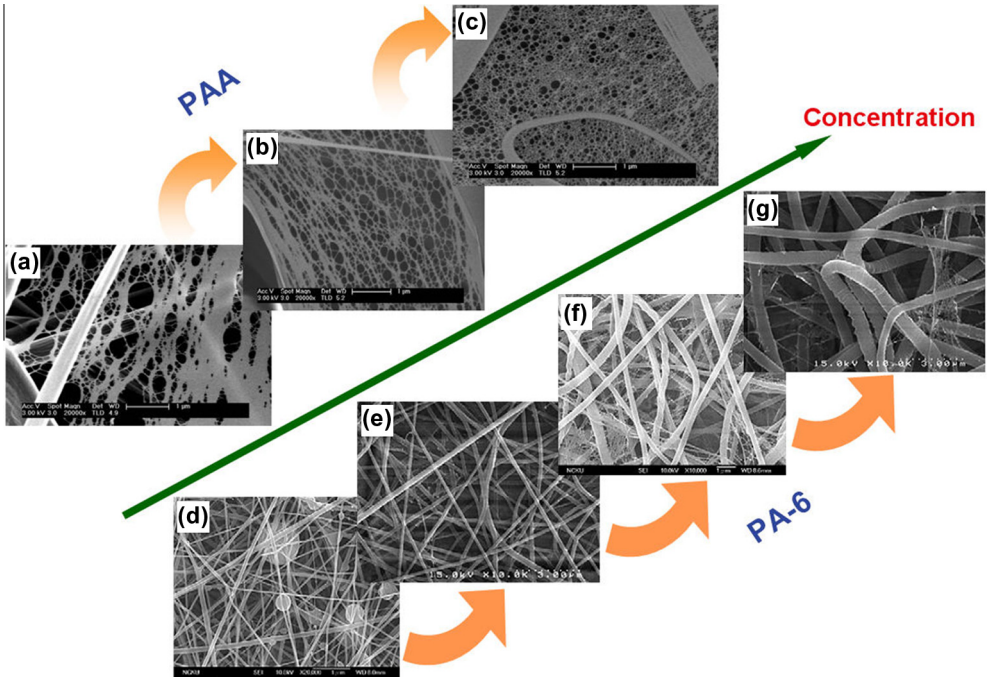

Fig. 26. SEM images of NFN membranes from different polymer concentration solutions. (a–c) SEM images of PAA NFN membranes formed with PAA concentrations of (a) 6, (b) 8 and (c) 10 wt%. Reprinted with permission from [33]. © 2006 IOP Publishing Ltd. (d–g) SEM images of PA-6 NFN membranes formed with PA-6 concentrations of (d) 7, (e) 12, (f) 15 and (g) 20 wt%. Reprinted with permission from [111]. © 2011 Elsevier B.V.

By increasing the concentration of PA-6 solution, a morphological transformation of electrospun products is seen from the beaded fibers with diameters lower than 100 nm at a concentration of 7 wt% to the ribbon-like fibers with widths of 2–3 mm at high concentrations (Fig. 26d-g) [111]. The ribbon-like fibers are initially discernible by electrospinning of the 15 wt% nylon 6 solution, and finally become the dominant feature in the products obtained from the 22 wt% solution. For nano-nets, they are barely seen from PA-6 solutions with low and high concentrations (Fig. 26d and e), but prevail as an intermediate concentration is used (i.e. the concentration of 15 wt%) (Fig. 26f). In the presence of nano-nets, the NFN membranes consisting of bimodal fiber diameter distribution have the advantage of capturing a wider range of particle sizes in the ultra-filtration application. As is evident from the discussions, the concentration of the polymer solution influences the spinning of fibers and splitting of nano-nets as well as NFN structure and morphology. Despite numerous discussions offered in the previous literatures on this subject, there remain several unresolved issues with the formation of nano-nets as a function of solution concentration. For example, the relationship between solution concentration and electrospun fiber diameter has been well established, however the theoretical model of this relationship for nano-nets need much concern.

5.1.2. Conductivity

Most of the polymers are conductive, and the charged ions in the polymer solution have a high effect on jet formation [52,89,204]. The ions increase the charge carrying capacity of the jet, and thus subjecting it to higher tension with the applied voltage [205]. Solution conductivity is mainly determined by the polymer type, solvent used, and the availability of ionisable salts [109]. The conductivity of the solution can influence the fiber morphology [206]. Highly conductive solutions will be extremely unstable in the presence of strong electric fields, leading to significant decrease in the fiber

diameter and dramatic bending instabilities and thus a broad diameter distribution [207]. Additionally, the formation and the resultant morphology of nano-nets are also highly depending on the solution conductivity [30–32,34]. Increasing the conductivity of the solution could enhance the instability of the Taylor cone, which would greatly improve formation probability of microsized droplets and thus dense nano-nets [31]. Kim et al. [34] demonstrated the effect of ions by adding ionic salt on the morphology of PA-6, PVA and PU NFN membranes. The electrical conductivity is proportional to the salt amount in the solution, which can be explained as increasing in the amount of the free ions in the solution (Fig. 27e). They found that PA-6 fibers with the addition of ionic salts like NaCl, KBr, and $CaCl_2$ produced multi-layers spider-web-like nano-nets within the electrospun nanofibers (Fig. 27a–c), while the nano-nets became trivial when a weak metallic acid (H_2PtCl_6) was used (Fig. 27d). Additionally, Yang et al. [32] reported that the atomic radii of ions also exhibited effects on the structure of NFN membranes and they investigated the morphology of PAA NFN membranes containing the same content of NaCl, $AgNO_3$ and $Cu(NO_3)_2$. Ions with smaller atomic radius have a higher charge density and thus a higher mobility under an external electric field [208]. Thus the elongational forces imposed on the jet with NaCl should be higher than that with $AgNO_3$ and $Cu(NO_3)_2$, since Na^+ and Cl^- have smaller radius than Ag^+, Cu^{2+} and NO_3^-. Therefore, the PAA/NaCl composite membranes possessed the smallest average fiber and nanowire diameter.

Concerning the nano-net formation within the electrospun nanofiber, increase the salt concentration had distinct impact on the internal morphology of the NFN membranes (Fig. 28). Fig. 28a–c compares SEM images of PAA/NaCl NFN membranes formed with different NaCl concentrations. The as-prepared PAA fibers have a diameter ranging from 160 to 1600 nm, in which a few nano-nets with ultrathin nanowire (~30 nm) was observed. In order to manufacture extremely small nanofibers in large quantities and a uniform size, salt was added into the ESN PAA solutions. Fig. 28b provides the morphology of PAA/NaCl NFN membranes containing 0.1 wt% NaCl. The fibers show a dramatically decreased average diameter (526 nm) which corresponds to the sharply increased conductivity (Table 3). A high-magnification FE-SEM image in Fig. 28b clearly shows that dense nano-nets, stacked

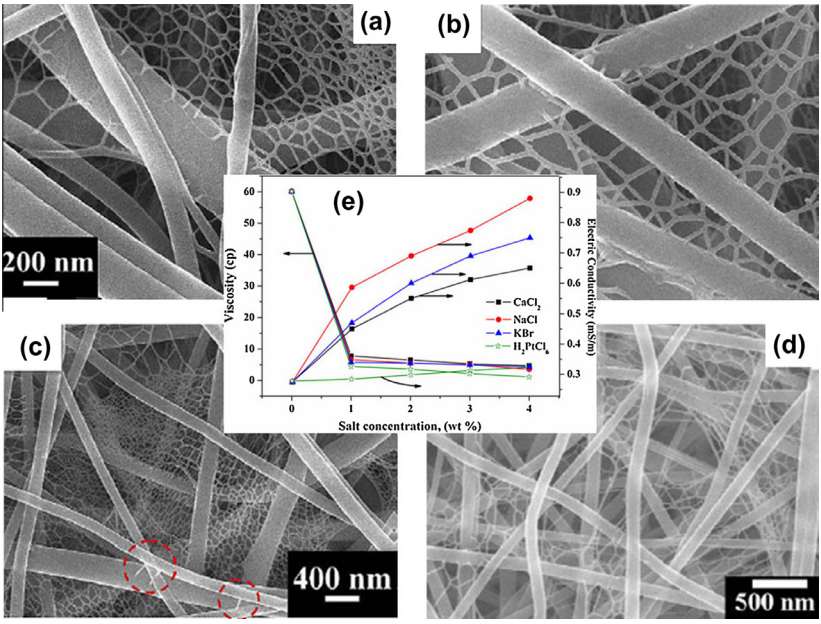

Fig. 27. FE SEM images showing the PA-6 NFN membranes containing 1.5 wt% salts: (a) NaCl, (b) KBr, (c) $CaCl_2$, and (d) H_2PtCl_6. (e) Effect of the salt addition on the viscosity and electrical conductivity of PA-6 solutions. Reprinted with permission from [34]. © 2009 Elsevier B.V.

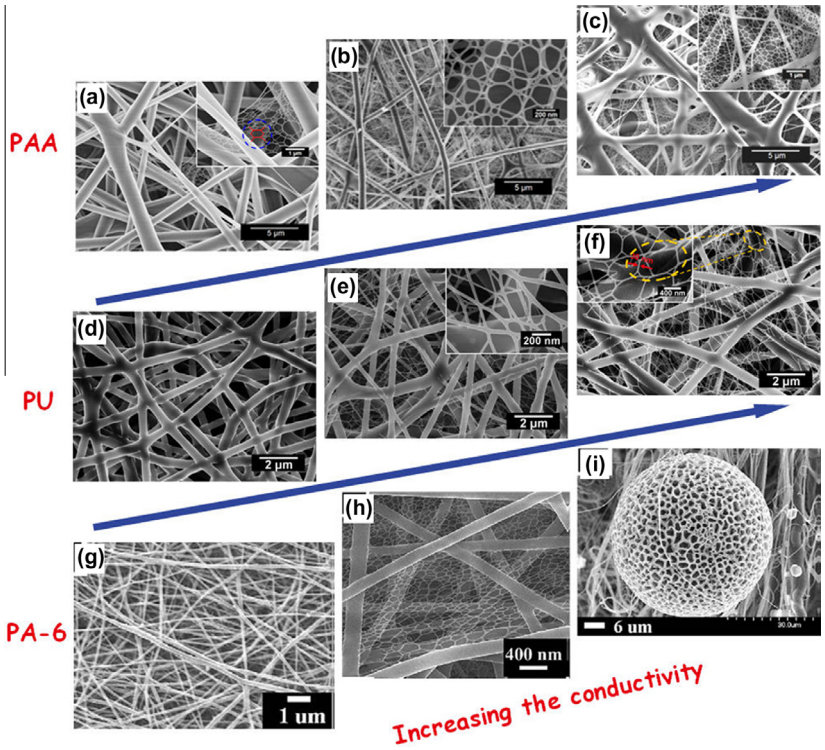

Fig. 28. Effect of salt concentration on the morphology of fibrous membranes. (a–c) FE-SEM images of PAA/NaCl NFN membranes formed with different NaCl concentrations: (a) 0 (pristine PAA), (b) 0.1, and (c) 0.2 wt%. Reprinted with permission from [31]. © 2011 Royal Society of Chemistry. (d–f) FE-SEM images of PU/NaCl NFN membranes formed with different NaCl concentrations: (d) 0 (pristine PU), (e) 0.05, and (f) 0.1 wt%. Reprinted with permission from [30]. © 2011 WILEY-VCH Verlag GmbH & Co. (g–i) FE-SEM images of PA-6/NaCl NFN membranes formed with different NaCl concentrations: (g) 0 (pristine PA-6), (h) 1.5, and (i) 2.5 wt%. Reprinted with permission from [34]. © 2009 Elsevier B.V.

Table 3
Solution properties and characteristics of the PAA, PU, and PA-6 nanofibers.

Polymer	Contents of NaCl (wt%)	Voltage (kV)	Viscosity (cps)	Conductivity ($\mu S\ m^{-1}$)	Average fiber diameter (nm)	Average nanowire diameter (nm)	BET surface area ($m^2\ g^{-1}$)
PAA	–	30	336	6.4	835	30	3.30
	0.1	30	337	240	526	20	6.57
	0.2	30	330	412	850	28	5.91
PU	–	30	2900	5.44	464	–	–
	0.05	30	2200	259.7	450	35	–
	0.1	30	2000	272.5	418	31	–
PA-6	–	20	60	~280	~350	–	–
	1.5	20	6	~640	~250	15	–
	2.5	20	5	~725	~200	–	–

layer-by-layer, almost completely covering the electrospun fibers and a strong bonding among them was also formed. Further increase in the NaCl concentration (from 0.1 to 0.2 wt%) resulted in a fiber-sticking morphology as well as an increase in the diameter of the spun fibers (Fig. 28c, Table 3), in contrast to the conventional view that a more conductive solution causes a reduction in diameter [209]. This surface morphology change could be attributed to the localized charge effects on the surface of

the fibers [210], as well as changed chain conformation of PAA (from the extended linear conformation to the coil one) with increasing the ionic strength of the solution [211], causing the fibers to stick together during the formation process. Additionally, Hu et al. [30] revealed that the NaCl concentration plays an important role in determining the morphology of the PU NFN membranes. With increasing the NaCl concentration, the morphology of PU NFN membranes was changed from no nano-nets to dense nano-nets (Fig. 28d–f). For PA-6 system, the pristine PA-6 electrospun fibrous membranes did not contain nano-nets (Fig. 28g), and very clear spider-nets fastening the main nanofibers are observed when the salt concentration was 1.5 wt% (Fig. 28h), while microballs was obtained instead of the nano-nets when the salt concentration was increased to 2.5 wt% (Fig. 28i) [34]. Increasing content of NaCl brings increase in electric conductivity, changes rheological behavior and considerably influences spinnability of the solution. As shown in Fig. 28i, fiber morphology was getting worse with the further increased NaCl salt concentration (2.5 wt%) and more non-fibrous bodies appear in the fibrous membranes. The increased electric conductivity meanwhile enhanced the instability of Taylor cone, which may lead to the formation of micro-sized droplets. The droplets may form porous microballs due to the fast phase separation with the evaporation of the solvents. In addition to salts, the solvents used in polymer solution for ESN process is strongly related to the final morphology of NFN membranes. Addition of formic acid to the PAA solution increased the number of free ions in the solution as well as the electrical conductivity of the polymer solution, and hence improved the formation of nano-nets [106]. In another report, Wang et al. [108] compared the gelatin NFN membranes obtained from formic acid and acetic acid, respectively, and found that gelatin solution from formic acid possesses the larger conductivity due to the high dielectric constant of formic acid, which favors forming thinner fibers and dense nano-nets.

5.1.3. Surface tension

Surface tension, more likely to be a function of surfactants added into the solution plays an important role in the common electrospinning process and by reducing the surface tension of a polymer solution, defect-free nanofiber can be obtained [212,213]. Recent studies have shown that surface tension was likely to be the primary factor that contributed to regulate the morphology of the nano-nets [30,32]. Inspired by the soap bubbles, which exhibits a highly stable Steiner networks, Yang et al. [32] considered the addition of DBSA into the ESN PAA solutions to decrease the surface tension and mimic the fascinating structure of soap bubbles. The surfactant was so effective that a concentration as low as 0.1 wt% was enough to produce nano-nets with large area and uniform size (Fig. 29a). High

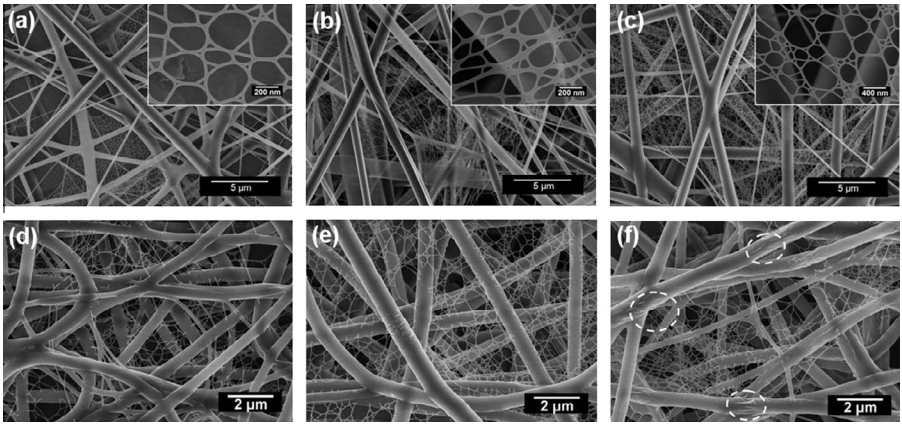

Fig. 29. Effect of surfactant concentration on the morphology of (a–c) PAA and (d–f) PU NFN membranes. FE-SEM images of PAA/DBSA NFN membranes formed with different DBSA concentrations: (a) 0.1, (b) 0.3, and (c) 0.5 wt%. Reprinted with permission from [32]. © 2011 Royal Society of Chemistry. FE-SEM images of PU/SLS NFN membranes formed with different SLS concentrations: (d) 0.1, (e) 0.25, and (f) 0.5 wt%. Reprinted with permission from [30]. © 2011 WILEY-VCH Verlag GmbH & Co.

magnification images (insets of Fig. 29a–c) reveal that nano-nets are more regular due to a more stable jet that encounters fewer perturbations from the surface tension effect of reducing surface area. Additionally, the average fiber and nanowire diameter were both slightly decreased with increasing the contents of DBSA in the solutions, which could be attributed to the lower surface tension and increased solution conductivity [96]. Recently, Hu et al. [30] also demonstrated the effect of surfactant in improving the structure of NFN membranes at CMC of surfactant in polymer solutions (Fig. 29d–f). Addition of sodium laurylsulfonate (SLS) at CMC to the PU solution results in significant improvement in nanofiber morphology as evinced from reduced fiber-sticking phenomenon and uniform fiber diameter (Fig. 29e). By close observation of Fig. 29e, it can be seen that nano-nets are more regular due to more stable jet that encounters fewer perturbations from the surface tension effect of reducing surface area. Addition of small amounts of nonionic surfactant was found to no obviously change the nanofiber morphology (Fig. 29d). For SLS concentration at higher level (>CMC), PU/SLS NFN membranes displayed defected nanofiber morphology (Fig. 29f), which could be attributed to that surfactants may self-assemble to form colloidal aggregates above CMC. Therefore, polymer–surfactant interactions may modulate the molecular structure and interactions of polymer molecules thereby altering rheological and interfacial properties of polymer dispersions, which are critical factors in the successful preparation of NFN membranes by ESN.

5.1.4. Solvent

For the electrospinnability of a polymer solution, the solvent plays a major role, and thus its selection is a crucial step in the electrospinning and even ESN process. According to the investigation by Ding et al. [33], the formation of nano-nets from defect films was considered to be due to the fast phase separation of polymer and solvent in the charged droplet, which is thought to be caused by solvent evaporation during the flight inside the high electric field. Therefore, the volatility of the solvent is very critical as it determines the process of the phase separation. PAA fibrous membranes formed from various kinds of solvents (H_2O, H_2O/ethanol, and ethanol) have been investigated. Several discontinuous irregular defect films with maximum lengths of up to 20 μm are found among the electrospun PAA fibers that are spun from the solvent of H_2O (Fig. 30a), while the defect films partly split into nano-nets due to the fast phase separation of polymer and highly volatile solvent in the charged droplet when the cosolvent of ethanol and H_2O is used (Fig. 30b). It is worth noting that the fibers formed from the cosolvent show a slightly increased diameter (745 nm) which corresponds to the increased viscosity (585 cps) and decreased conductivity (129 $\mu S\ m^{-1}$) (Table 4). In comparison with the fibers formed from the solvents of H_2O or cosolvent, the fibers formed from the sole solvent of ethanol show an increased average diameter (841 nm) due to the sharply decreased conductivity [214]. More interestingly, the formation of a few nano-nets with soap-bubble-like structure (Fig. 30c) is observed among the main fibers. Besides PAA system, our group also studied the structure of gelatin NFN membranes as a function of different solvents (i.e. formic acid and acetic acid), and the result showed that gelatin NFN membranes obtained from formic acid exhibited better morphology (Fig. 30d and e) [108].

Fig. 30 and Table 4 also summarize morphological observations of the PA-6 fibrous membranes for the various solvent systems. From these results, it is interesting to note that well-aligned uniform electrospun nanofibers and nano-nets (diameters in the range from 8 to 35 nm) of PA-6 can be produced from formic acid and its mixture solutions (Fig. 30f–i). However, the other single solvent system (i.e. chlorophenol and hexafluoroisopropanol) can also be used as solvents for PA-6, in which the expected nano-nets are not produced (Fig. 30j and k). Consequently, the formation of nano-nets in PA-6 NFN membranes can strongly depend on the polyelectrolytic behavior in the solvent. As a result, the electrical conductivity of the polymer solution was increased due to the formation of enormous free ions. By changing the polymer concentration and solvent ratio one can obtain nano-nets with uniform diameters [137].

5.2. Processing parameters

5.2.1. Applied voltage

The applied electric field strength plays important roles in the morphology of the ESN NFN membranes. The influence was so significant that earlier investigators held the point that only higher

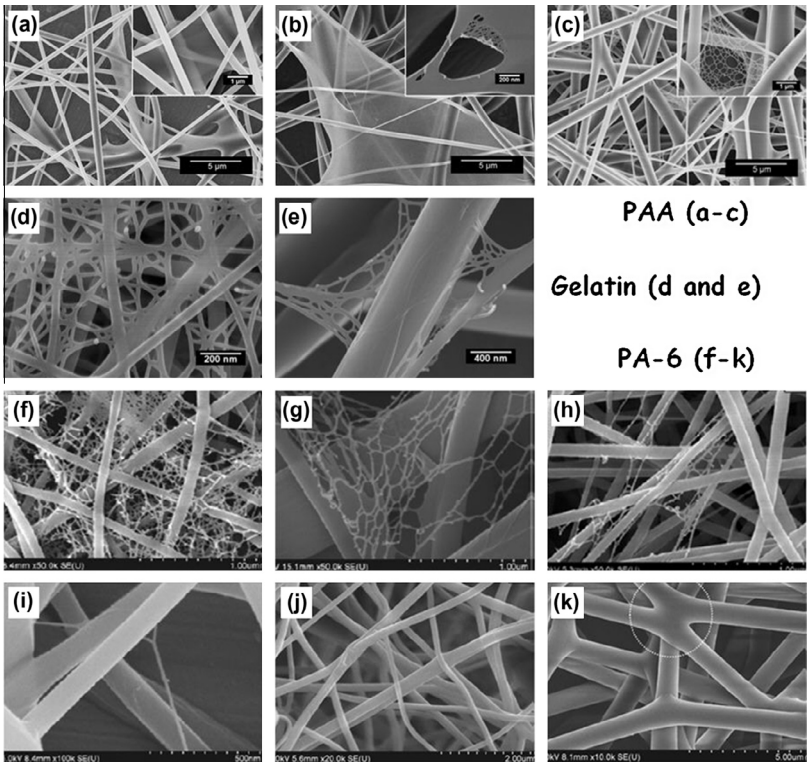

Fig. 30. (a–c) FE-SEM images of PAA fibrous membranes obtained from different solvents: (a) H_2O, (b) H_2O/ethanol, and (c) ethanol. Reprinted with permission from [32]. © 2011 Royal Society of Chemistry. (d and e) FE-SEM images of gelatin NFN membranes obtained from different solvents: (d) formic acid and (e) acetic acid. Reprinted with permission from [108]. © 2011 Elsevier B.V. (f–k) FE-SEM images of PA-6 fibrous membranes obtained from different solvents: (f) formic acid, (g) Formic acid/dichloromethane, (h) formic acid/acetic acid, (i) formic acid/chlorophenol, (j) chlorophenol and (k) hexafluoroiso propanol. Reprinted with permission from [137]. © 2010 Springer-Verlag.

Table 4
Effect of solvents on the solution properties and morphologies of fibrous membranes.

Polymers	Solvents	Viscosity (cps)	Conductivity ($\mu S\ m^{-1}$)	Av. fiber dia. (nm)	Av.nanowire dia. (nm)	Reference
PAA	H_2O	170	1401	510	–	[32]
	H_2O/ethanol (50/50 wt%)	585	129	745	–	
	Ethanol	336	6.4	841	20	
Gelatin	Formic acid	–	–	90	24	[108]
	Acetic acid	–	–	730	30	
PA-6	Formic acid	1375	412000	80–110	10–24	[137]
	Formic acid/dichloromethane (60/40 wt%)	2338	157000	150–300, 600–800	13–34	
	Formic acid/acetic acid (60/40 wt%)	2326	112700	100–220	8–32	
	Formic acid/chlorophenol (50/50 wt%)	13,354	60,800	175–220	18–28	
	Chlorophenol	5255	42	100–220	–	
	Hexafluoroiso propanol	11,787	308	900–1200	–	

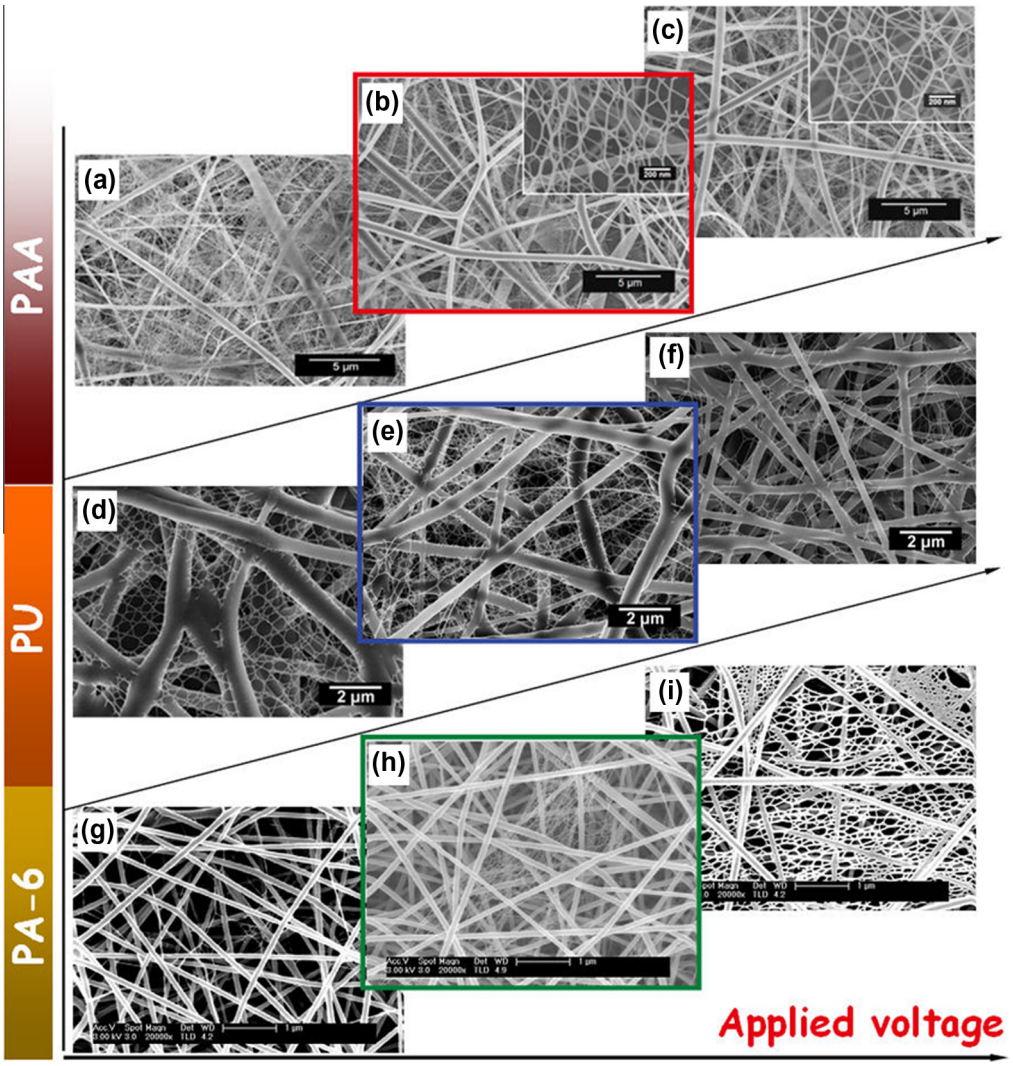

Fig. 31. Effect of applied voltage on the morphology of (a-c) PAA/NaCl, (d–f) PU/NaCl and (g–i) PA-6 NFN membranes. FE-SEM images of PAA/NaCl NFN membranes obtained at different voltages: (a) 30, (b) 40, and (c) 50 kV. Reprinted with permission from [31]. © 2011 Royal Society of Chemistry. FE-SEM images of PU/NaCl NFN membranes obtained at different voltages: (d) 20, (e) 30, and (f) 40 kV. Reprinted with permission from [30]. © 2011 WILEY-VCH Verlag GmbH & Co. FE-SEM images of PA-6 NFN membranes obtained at different voltages: (g) 10, (h) 20, and (i) 30 kV. Reprinted with permission from [33]. © 2006 IOP Publishing Ltd.

applied voltage can lead to formation of nano-nets [33]. High voltage is able to generate more charges to the solution or droplet surface located at the tip of the needle as well as larger electrostatic forces, both of which stretch the jets fully for the favorable formation of the thinner fibers and completely split nano-nets [215,216]. Fig. 31a–c shows the variation in morphology as the PAA/NaCl NFN membranes formed at applied voltages of 30, 40 and 50 kV, respectively. It was seen that increasing voltage decreased the average diameters of nanofibers and nanowires, while enhanced the pore-width and end breakages of the nano-nets [31]. Hu and co-workers have reported that the pores of the PU nano-nets were less erratic at the lower voltage of 20 kV, possibly due to lower instability of phase separation process for the thin liquid film. Additionally, they also found that increasing the voltage

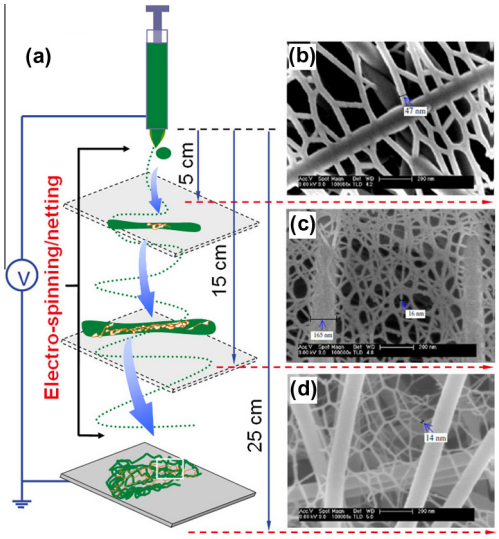

Fig. 32. (a) Schematic diagrams illustrating the ESN process. SEM images of nylon-6 fibers formed with tip to collector distance of (b) 5, (c) 15, and (d) 20 cm. Reprinted with permission from [33]. © 2006 IOP Publishing Ltd.

decreased the average diameter of the nanofibers and nanowires, and increased the pore width of the nano-nets from 413 nm (20 kV) to 643 nm (40 kV) (Fig. 31d–f) [30]. Similar behavior of applied voltage on NFN morphology is also observed by Ding et al. [33]. They have showed the area density of nano-nets in PA-6 NFN membranes sharply increased along with the applied voltage and ascribed this result to the increase of bead defect density along with increasing applied voltage (Fig. 31g–i).

5.2.2. Tip to collector distance

The structure of ESN NFN membranes is easily affected by the tip to collector distance because of their dependence on the deposition time, evaporation rate, and whipping or instability interval. Recent investigations have demonstrated that a minimum distance was required to give the electrospun fibers sufficient time to dry before reaching the collector, otherwise with distances that are either too close or too far, beads would form [217]. Although the effect of tip and the collector distance on fiber morphology is not as significant as other parameters, the studies on this aspect have been done with ESN of PA-6, gelatin and PU. For example, Ding et al. [33] examined the morphological changes in ESN PA-6 NFN membranes with variations in the distance between the tip and the collector (Fig. 32). They showed that lesser tip-collector distance was responsible for the relatively large wire diameter of about 30–50 nm and strong bonding between fibers and nano-nets (Fig. 32b). As the distance increased to 25 cm, the relatively sufficient expansion of nano-nets enabled them to form thinner wire diameter (10–20 nm) as well as larger pore-width at this long spinning distance (Fig. 32d).

5.3. Ambient parameters

Apart from solution and processing parameters, ambient parameters that include temperature relative humidity (RH), etc., also influence the structure and morphology of ESN NFN membranes. Investigations have been conducted to examine the effects of ambient parameters (i.e., temperature and humidity) on the ESN process. Wang et al. [108] investigated the effect of low ambient temperature (15 °C) on the morphology of gelatin nano-nets and found that the area density of nano-nets in membranes sharply decreased along with the decreased temperature from 25 to 15 °C (Fig. 33a and b). However, they did not investigate the morphology of nano-nets when the ambient temperature was at higher state. Therefore, for a supplement, Wang et al. [218] investigated the formation of

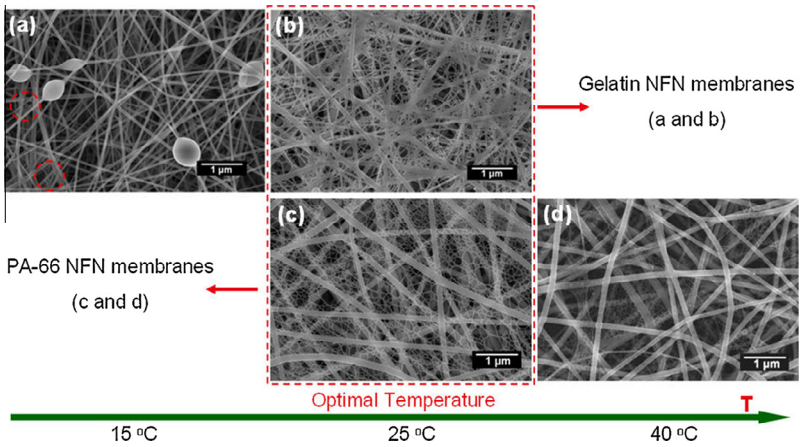

Fig. 33. Effect of ambient temperature on the morphology of (a and b) gelatin/NaCl and (c and d) PA-66/$BaCl_2$ NFN membranes. FE-SEM images of gelatin/NaCl NFN membranes obtained at ambient temperature: (a) 15 and (b) 25 °C. Reprinted with permission from [108]. © 2011 Elsevier B.V. FE-SEM images of PA-66/$BaCl_2$ NFN membranes obtained at ambient temperature: (c) 25 and (d) 40 °C [218].

PA-66/$BaCl_2$ nano-nets at much higher ambient temperature of 40 °C (Fig. 33d). It is obvious that the coverage rate of nano-nets was decreased with increased temperature (from 25 to 40 °C), which indicated that 25 °C was the optimal temperature (Fig. 33c and d). Additionally, the average diameter (171 nm) of the nanofibers increased at higher temperature. Increasing the temperature will accelerate the evaporation rate of the solvent and thus taking a shorter time for the jet to solidify, which favors the less elongation of the jet and the formation of thicker fibers. At a lower temperature, the evaporation rate of the solvent decreases exponentially with temperature. The polymer chains have more freedom to move at higher temperatures, resulting in lower solution viscosity. Thus, these two effects may play negative role in nano-net formation and result in the decreased coverage rate of nano-nets.

According to recent progress in controllable fabrication of polymer based NFN membranes, one can find that the RH plays an important role in formation of nano-nets. Ding et al. [33] observed that PAA fibrous membranes electrospun in an atmosphere of RH more than 45% showed the fiber-sticking phenomenon without the appearance of nano-nets, and they attributed this structure to the solubility of PAA in water and the retarded evaporation of solvents caused by the high RH. In another report, the effect of RH on the morphology of PAA/NaCl composite NFN membranes was also studied, and the results suggested that the microsized defect films were partly split into nano-nets at a RH of 45% (Fig. 34a) and sticking ribbon-like fibers with small parts of nano-nets were observed when the RH was increased to 60% (Fig. 34b) [31]. Besides of PAA system, the variation in humidity while ESN gelatin solutions has also been studied and shows that by increasing humidity there is an appearance of bead-on-string structured fibers in the membranes (Fig. 34c) [108]. The situation is much better for ESN PU solution; it was possible to produce NFN morphology for the PU system even in a high humidity environment (55% RH) (Fig. 34d). In comparison with the samples obtained at lower humidity, the fibers and nanowires in the 3D network became thinner and a slight fiber-sticking structure could be observed [30].

6. Applications of NFN membranes: solving global issues

The past few years have witnessed significant progresses in applications of the electrospun nanomaterials, demonstrated by numbers of recent scientific publications on this area [24,44,82,219–221]. NFN membranes possess almost all the applications that traditional electrospun fibrous membranes have, and due to its much smaller fiber diameter and unique net-like structure, which bring ESN

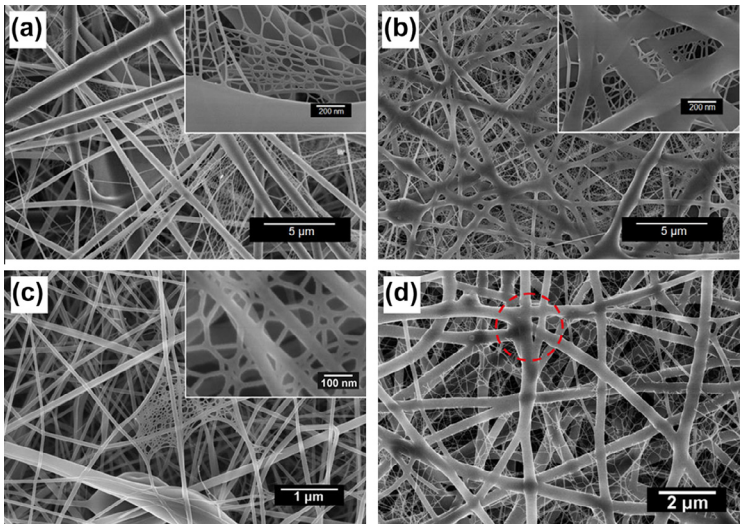

Fig. 34. FE-SEM images of PAA/NaCl NFN membranes obtained at different RH: (a) 45% and (b) 60%. Reprinted with permission from [31]. © 2011 Royal Society of Chemistry. (c) FE-SEM image of gelatin/NaCl NFN membranes obtained at RH of 45%. Reprinted with permission from [108]. © 2011 Elsevier B.V. (d) FE-SEM image of PU/NaCl NFN membranes obtained at RH of 55%. Reprinted with permission from [30]. © 2011 WILEY-VCH Verlag GmbH & Co.

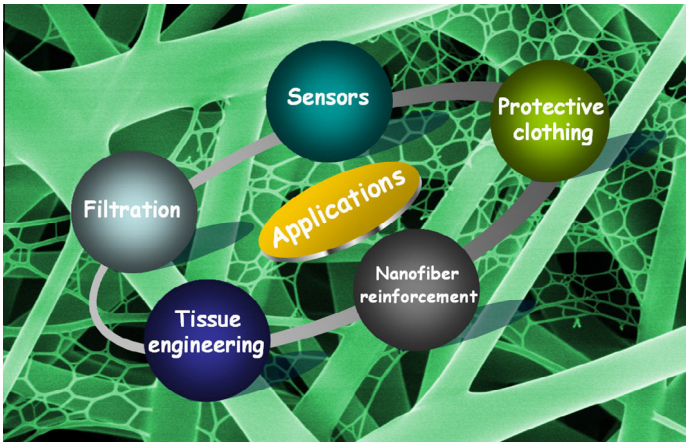

Fig. 35. Current applications of ESN NFN membranes.

NFN membranes highly attractive to some special area, such as ultra-fine filters to intercept viruses, ultrasensitive sensors, as well as biomedicine. A schematic diagram illustrating the perspective application areas are summarized in Fig. 35. It should be realized that most of these applications have not reached their industry level, but just at a laboratory research and development stage. However, their promising potential is believed to be attracting attentions and investments from academia, governments, and industry all over the world.

6.1. Filtration applications

Atmospheric and liquid environment pollutions caused by the uncontrolled development of industrial technologies, has now reached the dangerous point, which leads to the optimal selection

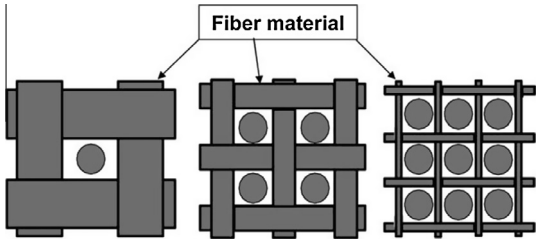

Fig. 36. The efficiency of a filter increases with decrease in fiber diameter. Reprinted with permission from [53]. © 2003 Elsevier B.V.

of environmental filtration and separation technologies [36,222,223]. It was estimated that future filtration market would be up to US $700b by the year 2020 [53,224]. Nonwoven fibrous membrane as a kind of porous media has been widely used in different filtration applications, from indoor air filter to personal protective equipment (e.g. N95 respirator) [225]. For filtration, the channels and structural elements of a filter must be matched to the size of the particles or droplets that are to be captured in the filter (Fig. 36). To filter increasingly finer particles, a transition from micro-sized to nano-sized fibers is required. In addition, it is generally understood that the smaller the fiber diameter, the better are their filtration performance [36,225–227]. Nanofibers provide dramatic increases in filtration efficiency at relatively small decreases in permeability [223,228–230]. Additionally, nanofiber filter media also demonstrate improved filter lifetime and more contaminant holding capacity in many laboratory tests and actual operating environments [231]. NFN possess the general properties and functions of conventional electrospun nanofibers, as well as the fascinating feature characters (i.e. extremely small diameter, unique geometric characteristic, controllable coverage rate) donated by the novel 2D nano-nets structure. It has been realized that ESN technique is rising to the challenge of providing solutions for the removal of unfriendly particles in such submicron ranges.

Recently, our group has developed a new concept of two-tier filter by ESN depositing PA-66 NFN membranes (as core filter medium) on the nonwoven polypropylene (PP) scaffold (Fig. 37) [218]. It

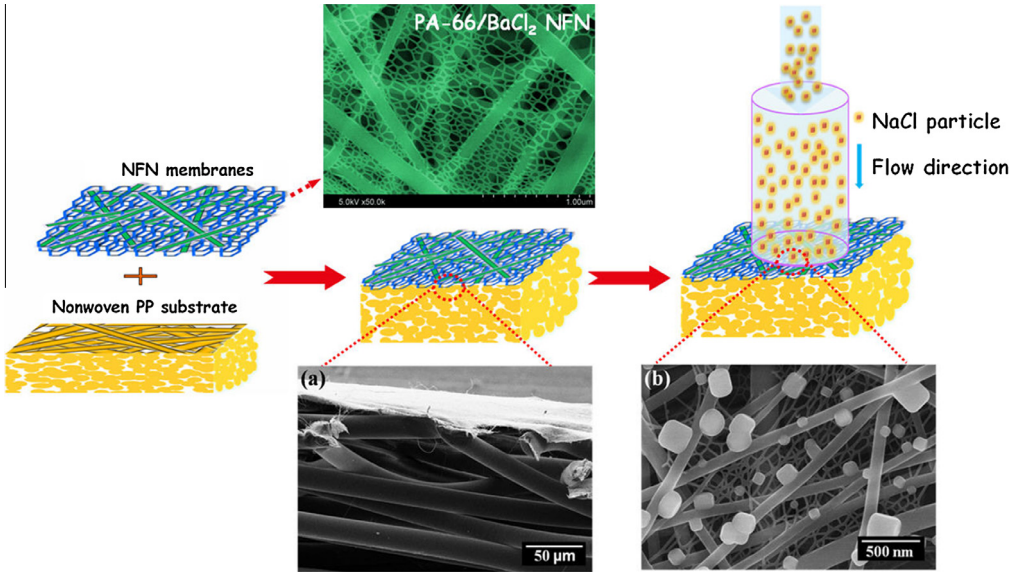

Fig. 37. Schematic diagrams illustrating the fabrication of the nonwoven PP scaffold with a NFN layer and the filtration process of the composite membrane. FE-SEM images of the composite membrane: (a) cross section before filtration and (b) top view after filtration [218]. Reprinted with permission from [218]. © 2012 Royal Society of Chemistry.

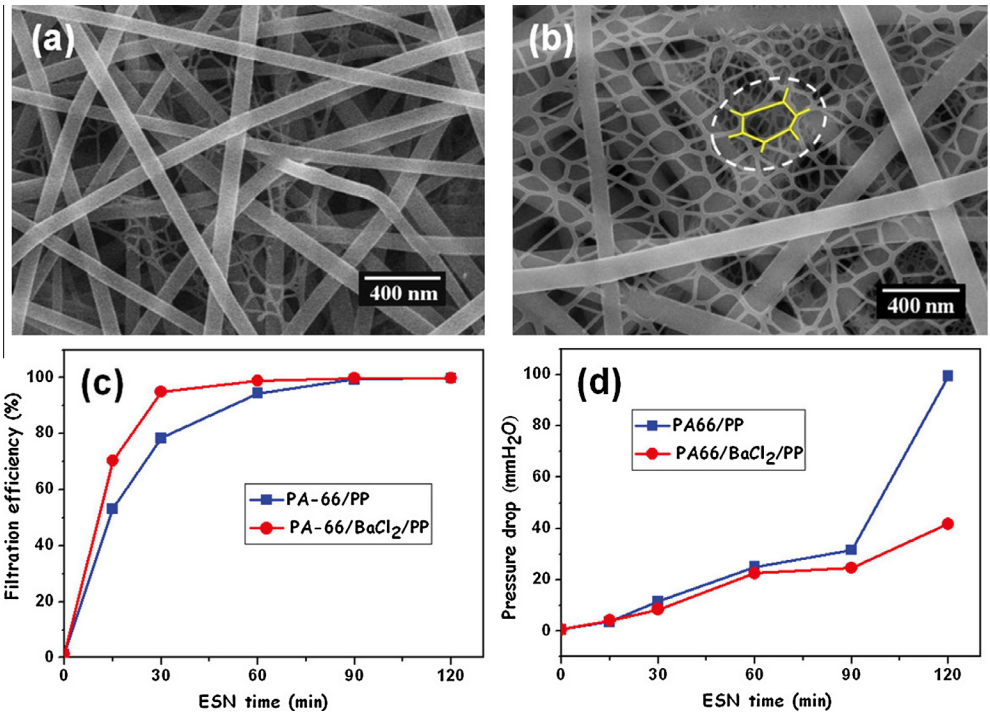

Fig. 38. FE-SEM images of (a) PA-66 and (b) PA-66/$BaCl_2$ NFN membranes. Filtration efficiency (c) and (d) pressure drop of composite membranes variation versus ESN time [218]. Reprinted with permission from [218]. © 2012 Royal Society of Chemistry.

was found that the morphology of the NFN membranes and the filtration performance towards NaCl aerosols (diameter ~300 nm) were both strongly dependent on the ESN time and addition of chloride (Fig. 38). Fig. 38c compares the ESN time dependence-filtration efficiency of PA-66/PP and PA-66/$BaCl_2$/PP composite membranes. The filtration performance undergoes a dramatical rise and reaches a steady value after 90 min. The filtration efficiency is increased with the prolonging of ESN time, which is induced by the increased fiber mass and thickness. Additionally, the PA-66 membranes doping with $BaCl_2$ show a better filtration performance (up to 99.9%) than pristine PA-66 fibers, which further demonstrating the key role of nano-nets played in enhancing the filtration efficiency (Fig. 38a and b). Furthermore, the stacked nano-nets among the conventional electrospun fibers can greatly improve the porosity of PA-66/$BaCl_2$/PP composite membranes, which can account for the lower pressure drop compared with PA-66/PP composite membranes (Fig. 38d).

Based on the fascinating features of nano-nets and the filtration mechanism, the NFN membranes-containing filters possess the following three outstanding advantages: (1) a much higher efficiency and lower pressure drop for particulate filtration. Considering the simple fiber filtration theory involving only a single fiber, smaller fiber diameter may lead to higher filtration efficiency. The nano-nets in NFN membranes played the role of "second doorkeeper" that could intercept particles smaller than its aperture size, which may further increase the filtration efficiency. Meanwhile, the high porosity of nano-nets facilitated the flow of airflow through the membranes and thus resulted in decreased pressure drop; (2) the two-tier filter allowed the particles captured at the surface other than deep inside, which facilitated the cleaning of NFN/PP composite filters through air back blowing and/or mechanical shaking and thus improved the filter lifetime [35]; (3) in the event of the same filtration performance, the deposition amount of NFN membranes was much smaller than that of electrospun membranes, which significantly reduced the thickness of filtering membranes and made them more lightweight [218].

Even though NFN membranes have exhibited great advantages over conventional media in environmental applications, such as air and water filtration, there remain a large number of challenges. The challenges include the mass production strategies of high quality NFN membranes and NFN-based composites, the selection of suitable materials and of appropriate chemistry to introduce the desired functionality to meet specific needs [36]. Additionally, NFN membranes show the promising application as filters to intercept viruses and bacteria such as influenza A (H1N1) virus, severe acute respiratory syndrome (SARS) virus, and *Escherichia coli* [105], however, further verify its feasibility by experiments is imperative. None of these challenges are trivial but they are also not insurmountable.

6.2. Sensor applications

Developments of nanomaterials have provided researchers with an opportunity to construct electronic interfaces with components whose sizes are comparable to the size of molecules, potentially leading to a much more efficient interface [232–234]. Nanometer cross-section of nanomaterials gives them enhanced surface sensitivity, and allows them to utilize the benefits of size effects, such as quantization and single-molecule sensitivity [105,235]. Taking advantages of comparatively large surface area and high porosity, nano-nets create enhanced interconnectivity and additional surface area and facilitate the diffusion of analytes into the NFN membranes, which make them attractive candidates for use in ultrasensitive sensors [31]. This is one of the most desirable properties for improving the sensitivity of sensors because a larger surface area will absorb more analytes and change the sensor's signal more significantly [44]. In this section, we will review recent progress in the development of ESN NFN materials having applications in two predominant sensing approaches (i.e. QCM and colorimetric sensors), illustrate them with current examples showing how they have been applied, and discuss their intrinsic fundamentals and optimal designs. It will emphasize trends, but will also highlight gaps requiring further research. A comprehensive summary of sensors based on the ESN NFN materials is illustrated in Table 5.

6.2.1. QCM sensors

QCM as a mass sensitive device is widely used for detecting very small mass changes of even less than a nanogram deposited on electrode surface [236]. Through surface modification of the electrodes with sensitive materials, QCM devices have been used as highly sensitive sensors for environmental monitoring, chemical and biochemical analysis due to their sensitive interface measurement capability [237,238]. Sauerbrey [239] first derived the mass-frequency shift relation for quartz crystal resonators as follows:

$$\Delta f = -2f_o^2 \Delta m / A(\mu\rho)^{1/2} \tag{2}$$

where Δf the measured frequency shift, f_o the fundamental frequency of a bare QCM chip, Δm the mass change per unit area, A the electrode area, ρ the density of quartz, and μ the shear modulus of quartz crystal.

Table 5
ESN NFN materials based sensors.

Materials	Sensor types	Synthesis method of sensing structures	Targets tested	Detection limit	Reference
PAA	QCM	ESN	RH	6%	[106]
PEI-CS	QCM	ESN and surface modification	RH	8%	[198]
PEI/PA-6	QCM	ESN and surface modification	RH	2%	[29]
PAA/NaCl	QCM	ESN	TMA	1 ppm	[31]
PEI/PA-6	QCM	ESN and surface modification	HCHO	50 ppb	[27]
PANI/PA-6	Colorimetric	ESN and hydrazine deoxidation	Cu^{2+}	1 ppb	[28]
Methyl Yellow/PA-6	Colorimetric	ESN and Methyl Yellow-impregnated	HCHO	50 ppb	[281]

Up to now, enormous materials such as metals, ceramics, polymers, self-assembled monolayers, dendrimers, lipids, and waxes [236,240], have been used as sensitive coatings on QCM to improve the sensor sensitivity and selectivity for chemical analytes. QCM sensors have been demonstrated to be versatile in various applications, whereas one major challenge lies in that the flat electrode surface limits the immobilization degree of the absorbing sites per unit area [241]. To solve this problem, increasing attention has been paid to the development of nanostructured coatings on QCM to improve the sensor sensitivity, including nanotube [242,243], nanofibers [244], nano-assembled thin films [245], and nanogold hollow balls [246]. Taking advantage of large specific surface area of the nanostructured sensing materials, the performance of the QCM sensors is greatly enhanced. In this part, we review recent progress in the development of ESN NFN materials having applications in QCM sensing approaches.

6.2.1.1. Relative humidity (RH) sensing. Humidity monitoring is significant to a wide variety of fields, such as meteorology, process controlling, agriculture, textiles, and manufacturing [247–249]. It is well known that the sensitivity of chemical sensors towards a specific analyte is enhanced by increasing the specific surface area of the sensing materials [250]. Growing efforts have been put in the development of nanostructured materials based humidity sensors to further improve the sensing characteristics [251,252]. Among various sensing strategies used to detect humidity such as impedance [253], capacity [254], and optics [255], QCM have been emerging as very stable sensors for humidity detection [106]. On the other hand, many approaches for fabricating humidity-sensitive membranes such as spin coating [256], dip coating [257], layer-by-layer self-assembly [258], and ink-jet printing [259], have been reported. As a nanofabrication technique, ESN has been identified as a remarkably robust and versatile method for fabricating fibrous membranes with net-like structure. The remarkable specific surface area and high porosity provide ESN nanomaterials potential application in ultrasensitive and highly miniaturized sensors [105].

Wang et al. [106] fabricated a humidity sensor by electrospinning and ESN deposition of nanofibrous polyelectrolyte membranes as sensitive coatings on QCM. In their RH testing system, the controlled humidity environments were achieved using water injections into the chamber, which yielded the required humidity ranging from 6% to 95%. The sensing properties of the sensors to humidity were examined by measuring the resonance frequency shifts of QCM due to the additional mass loading. The results of sensing experiments shown in Fig. 39c indicated that the response of the sensors increased by more than two orders of magnitude with increasing RH from 6% to 95% at room temperature, exhibiting high sensitivity and that, in the range of 20–95% RH, the $Log(\Delta f)$ showed a good linearity (Fig. 39c, inset). The sensitivity of fibrous composite PAA/PVA membranes (Fig. 39a) was two times higher than that of corresponded flat films at 95% RH. Compared with fibrous PAA/PVA membranes, the PAA NFN membranes (Fig. 39b) exhibited remarkably enhanced humidity sensitivity due to their high PAA content and large specific surface caused by the formation of ultrathin nano-nets among electrospun fibers, which can facilitate fast mass transfer of water molecules to and from the interaction region [253]. Additionally, the developed sensors exhibited good long term stability (Fig. 39d). The measurements were repeated at 26 °C every 5 days for 1 month. The variation of frequency shift is less than 6% at each humidity region.

Directly ESN sensing materials onto QCM electrode provides one-step strategy to fabricate highly sensitive QCM sensors. However, this strategy is only appropriate for those materials that can be ESN, which will inevitably limit the application of more sensing materials on QCM. Therefore, it is urgent to explore other general platforms to meet these challenges. Recently, a simple two-step strategy for fabricating RH sensing coatings on QCM has been developed, which include the ESN deposition of NFN membranes on the surface of a QCM resonator followed by the surface modification process [29,198]. For instance, PEI modified CS (PEI/CS) NFN membranes were used as sensing materials coated on QCM for humidity detection (Fig. 40) [198]. Increasing the coating load of the membranes introduced more absorption sites in the sensing membranes, and hence greatly enhanced the sensor sensitivity (Fig. 40a). Fig. 40b shows the response curve of sensor coated with PEI/CS membranes with the RH changing from 8% to 95%. When the RH was increased from 8% to 95%, the response time were 10, 20, 47, 64, 81, 120, and 300 s, respectively. Additionally, the resultant sensors possessed good

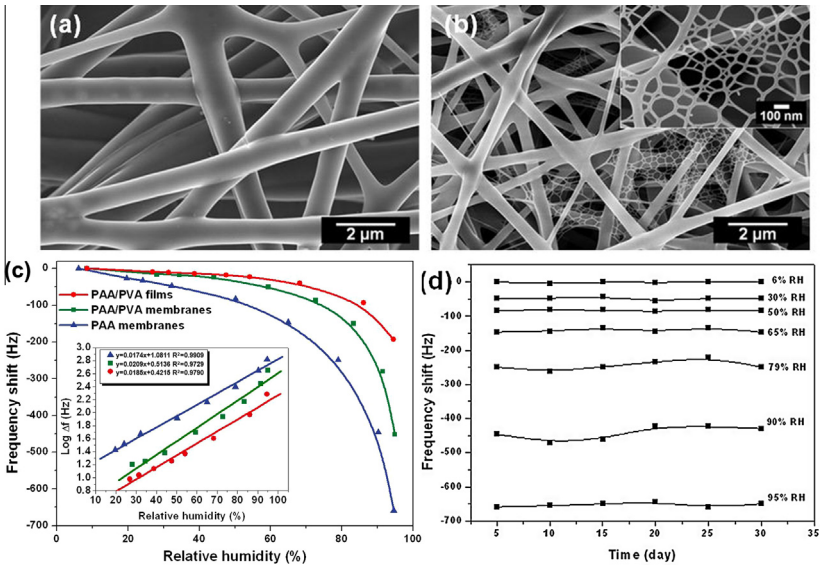

Fig. 39. FE-SEM images of (a) PAA/PVA and (b) PAA fibrous membranes. (a) Frequency shifts of polyelectrolyte coated QCM humidity sensors with a coating load of 600 Hz as a function of the RH. (b) Dependence of the frequency shifts of sensors on RH (20–95%) and the calibration curves obtained from (a). Stability of the PAA NFN membranes coated QCM sensors with a coating load of 600 Hz after exposing in air for 30 days. Reprinted with permission from [106]. © 2010 IOP Publishing Ltd.

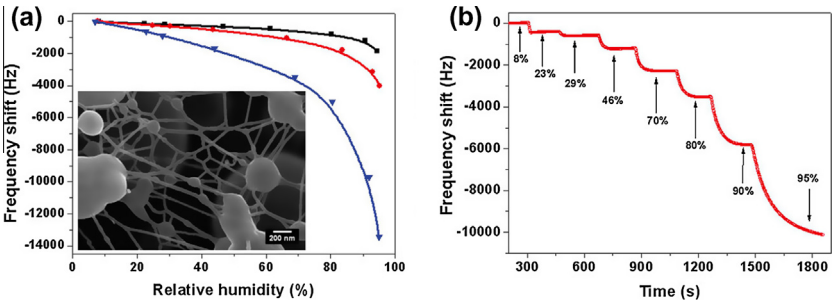

Fig. 40. (a) Frequency shifts of PEI/CS NFN membranes-based QCM sensors as a function of the RH with different PEI coating loads 0 (black), 1200 (red), and (blue) 6000 Hz. (Coating load of CS: 4000 Hz). Inset shows the FE-SEM images of CS NFN membranes. (b) Response curves of PEI/CS membranes coated QCM humidity sensors with the RH changing from 8% to 95%. (Coating load of CS: 5000 Hz; Coating load of PEI: 3600 Hz.) Reprinted with permission from [198]. © 2010 Walter de Gruyter GmbH & Co. KG.

Log(Δf) linearity (20–95% RH), wide RH range of response, and small hysteresis, which exhibited great potential for humidity sensing applications at room temperature operations [198].

Although the PEI/CS NFN membranes-based QCM sensors have presented good performance to RH sensing, a main drawback of using CS NFN membranes as substrate is the lower productivity of CS NFN membranes due to the low concentration (2 wt%). Therefore, a few researchers have made effort to ESN deposition other polymer-based NFN membranes (e.g. PA-6) as substrates on QCM (Fig. 41) [27,29]. Recent study of Wang and coworkers revealed the PEI functionalized PA-6 (PEI/PA-6) NFN-based QCM sensor that exhibited high sensitivity and fast response/recovery time (120 s/50 s) to humidity, which outperform flat film-based sensors and even current porous structure-based sensors (Fig. 42a). The frequency changed approximately three orders of magnitude with RH varied from 2% to

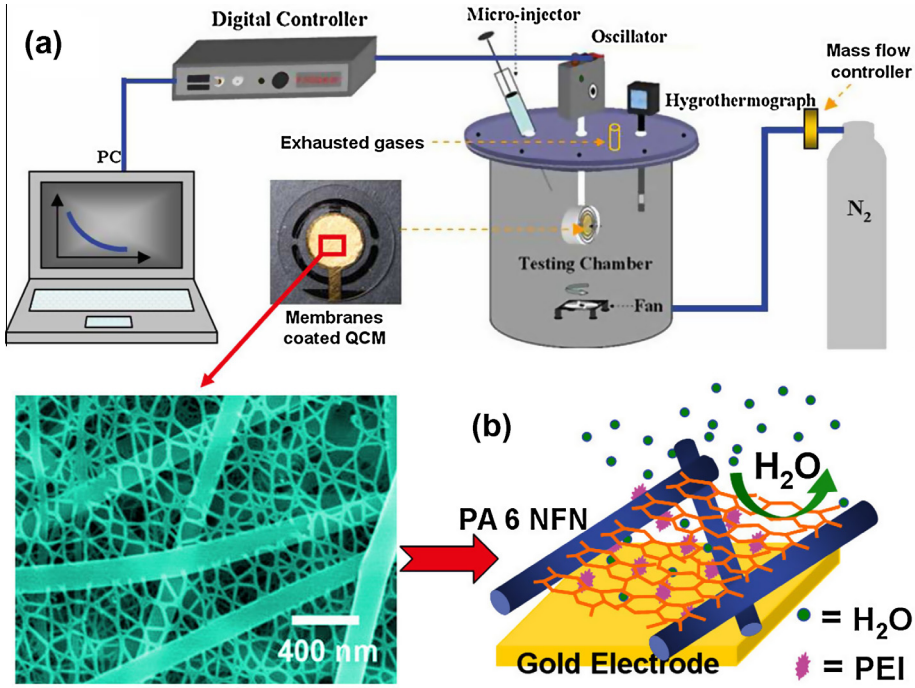

Fig. 41. Schematic diagrams illustration of (a) a gas testing system for RH detection and (b) sensing coating of PEI/PA-6 NFN on QCM gold electrode. Reprinted with permission from [29]. © 2011 Royal Society of Chemistry.

95%. Repeated humidity cycling tests demonstrated stable device operation and high repeatability of sensor response (Fig. 42b). Additionally, the resultant sensors also presented relatively small hysteresis with a maximum humidity hysteresis rate of 3.5% at 60% RH (Fig. 42c), indicating a good reliability of the humidity sensor. Fig. 42d shows the possible humidity sensing mechanism of QCM-based PEI/PA-6 NFN sensor. For low RH levels, the response of the QCM sensor is dependent on water molecules adsorbed/desorbed masses on NFN membranes, whereas for increasing RH levels variations in interlayer expansion stress of NFN membranes derived from swelling effect becomes prevalent. Several possible reasons may be responsible for the improved sensor properties: (1) the spider-web-like nano-nets can provide an effective channel for the fast mass transfer of the water molecules toward and away from the interaction region, as well as greatly reduced interfacial areas between nanofibers and substrate; (2) the piezoelectric QCM is an ultrasensitive mass-measuring device and has been used as a mass sensor in the air phase. Therefore, the tiny mass of water molecules adsorbed in the fibrous membranes could be detected and calculated. This study demonstrates that NFN structured materials are of the potential applications for fabricating high performance humidity sensors [29].

6.2.1.2. Trimethylamine (TMA) sensing. TMA can cause headache and nausea, severe skin burns, as well as irritation to the eyes and the respiratory tract. Safe exposure of 10 ppm TMA as a time weighted average concentration for up to a 10 h workday has been standardized by the World Health Organization [260]. On the other hand, TMA has attracted considerable research attention in recent years as an indicator for food freshness, in particular for fish, seafood, meat, wine, and milk. Therefore, the detection of TMA is a very important problem in food industry and fish-processing industry.

Recently, it was demonstrated that PAA/NaCl composite NFN membranes could be used as sensing materials in a TMA-selective QCM sensor [31]. Fig. 43a and b depicts the response of membranes coated QCM sensors with three kinds of structures, exposed to increasing TMA concentrations ranging from 1 to 100 ppm. The response caused by the additional mass loading was primarily attributed to

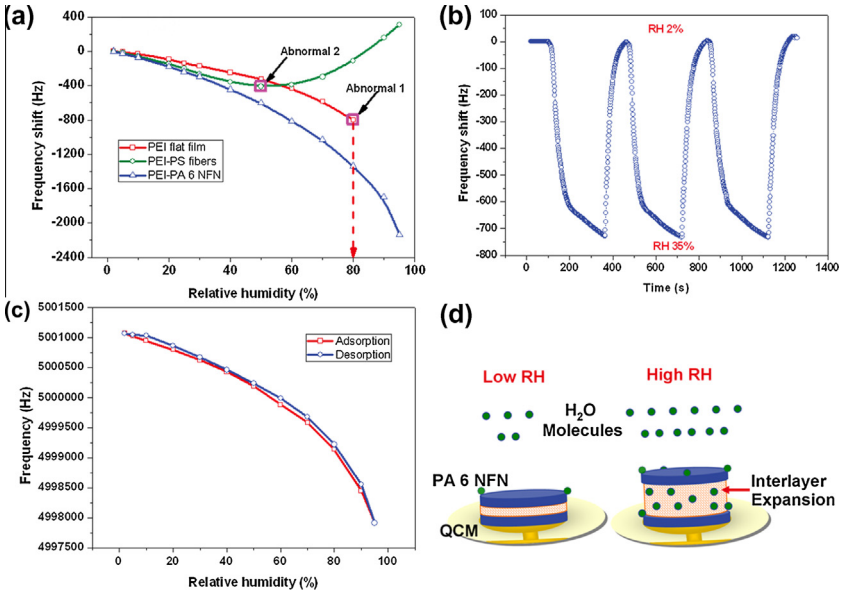

Fig. 42. (a) Frequency shifts as a function of RH for QCM sensors coated with three different sensing structures. (b) Response and recovery characteristic curves (three cycles) of QCM-based PEI/PA-6 NFN sensors with RH cycling between 2% RH and 35% RH. (c) Humidity hysteresis characteristic of QCM-based PEI/PA-6 NFN sensor. The coating loads of PEI and PA-6 were 4000 and 1400 Hz, respectively. (d) Schematic illustration of the humidity sensing mechanism of QCM-based PEI/PA-6 NFN sensor. Reprinted with permission from [29]. © 2011 Royal Society of Chemistry.

the interaction between the TMA molecules and the carboxyl groups of PAA (Fig. 43c, inset). The rapid response time, approximately 180 s to reach the 90% of the maximum value for each gas exposure, is comparable to similar TMA exposure levels on polyaniline (PANI)–TiO_2 nano-composite coated QCM sensor (~280 s) [261]. It is obvious from the figures that the gas sensor based on PAA/NaCl (0.1 wt%) composite nanofibrous membranes exhibits the best performance, which may be attributable to the abundant of active sites available for faster gas diffusion into the membranes because of the high surface and volume ratio of the nano-nets. Additionally, the resultant sensors coated with PAA/NaCl NFN membranes exhibited an excellent selectivity to TMA (Fig. 43c).

According to the Sauerbrey equation, Δf is directly proportional to the attached mass of gas molecules. The absorption behavior of TMA molecule in nano-nets is a Fickian process and Fickian equation can thus be expressed as [262]:

$$\frac{\Delta f_t}{\Delta f_\infty} = 4\sqrt{\frac{D}{\pi}}\frac{t^{1/2}}{h} \tag{3}$$

where Δf_t and Δf_∞ are the frequency changes at any time, t, and at equilibrium, respectively. Therefore, the diffusion coefficient (D) can be determined from the initial slope of the absorption curve plotted in the form of $\Delta f_t/\Delta f_\infty$ versus $t^{1/2}/h$ (Fig. 43d). As a result, PAA/NaCl (0.1 wt%) composite nanofibrous membranes showed the largest D value (1.4723×10^{-14} cm^2/s), which may be due to enhanced interconnectivity and additional surface area induced by the large density of nano-nets. Nano-nets facilitate the diffusion of analytes into the membranes and significantly boosted the gas sensing properties [31].

6.2.1.3. Formaldehyde sensing. Formaldehyde, one of the most serious indoor air pollutants among volatile organic compounds (VOCs), can cause central nervous system damage, immune system disorders, as well as asthma and nasopharyngeal cancer [263]. The detection of formaldehyde in air is of

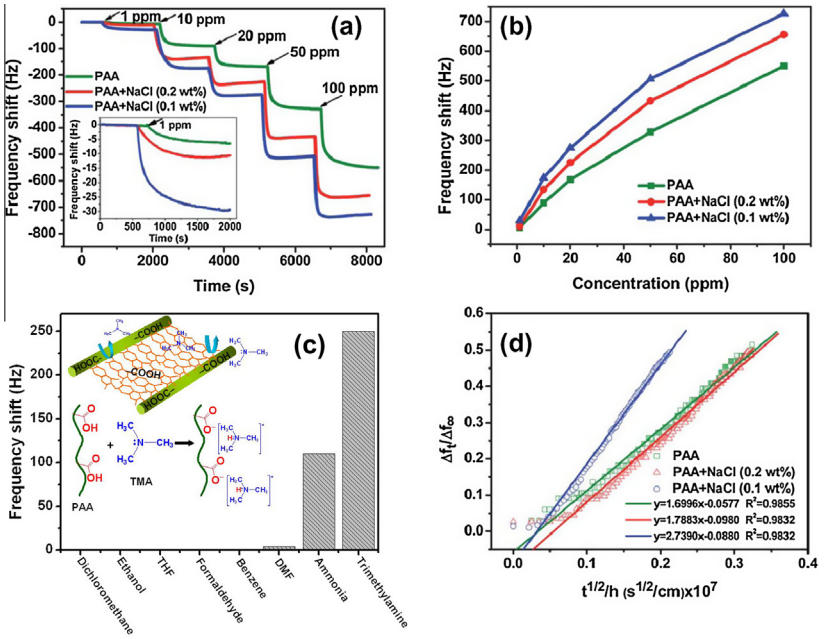

Fig. 43. (a) Response of sensors coated with PAA/NaCl NFN membranes containing different concentrations of NaCl: 0 (green), 0.1 (blue), and 0.2 wt% (red), exposed to increasing TMA concentrations ranging from 1 to 100 ppm. The coating load was 3500 Hz for each sensor. The inset is the amplified image in the range of 0–2000 s. (b) Frequency shift versus TMA concentration (1–100 ppm) for three nanofibrous membranes coated QCM sensors. (c) Frequency shift of the PAA/NaCl (0.1 wt%) NFN membranes $\Delta f_t/\Delta f_\infty$ coated sensor with a coating load of 3500 Hz versus 20 ppm of various VOCs. The inset shows the schematic of gas-sensing mechanism between PAA nano-nets and TMA. (d) The ($\Delta f_t/\Delta f_\infty < 0.5$) as a function of $t^{1/2}/h$ when exposed to 1 ppm of TMA vapors for three nanofibrous membranes coated QCM sensors. The lines are linear fits to Fickian diffusion. Reprinted with permission from [31]. © 2011 Royal Society of Chemistry.

significance for environmental monitoring and process control because of its high toxicity. The World Health Organization (WHO) has set a safe exposure limit of 80 ppb (30 min average) and the established limit by Chinese Environmental Protection Agency (EPA) is 60 ppb averaged over 30 min [264,265]. Considerable efforts have been made to develop formaldehyde-selective QCM sensors in the past few years [244,250,266–268]. Various sensing structures such as molecularly imprinted polymers films [268], electrospun fibrous PEI/PVA membranes [250], PEI modified electrospun polystyrene (PS) (PEI/PS) nanoporous fibers [244], PEI modified bacterial cellulose [269] have been deposited on QCM for formaldehyde detection. However, all of these QCM sensors have a limited ability to detect formaldehyde at low concentrations. Therefore, it is very important to develop a rapid, simple and ultrasensitive device for detection of gaseous formaldehyde.

Taking advantage of several attractive features such as extremely large specific surface area, high porosity, large stacking density and strongly tight adhesive force to the devices, the NFN structured membrane (Fig. 44e) can lead to enhancement in the facilitation of the analytes diffusion and oscillation transmission into the membranes and thus can detect formaldehyde at lower concentration level [27,102]. More recently, an effective formaldehyde detection system was developed by ESN depositing PA-6 NFN membranes on QCM and then modifying sensing PEI onto the NFN membranes (Fig. 44a–d). After PEI modification, the 3D porous fibrous membranes with NFN structure were still maintained in the samples (Fig. 44f). When exposed to 100 ppm of formaldehyde, QCM-based PEI/PA-6 NFN (30 kV) sensor has achieved the largest response value, approximately three times as much as PEI flat film coated sensor. To detect formaldehyde at very low concentration, they developed a moisture-compensating-based detecting method, i.e., firstly injected the dilute formaldehyde aqueous solution (1 wt%)

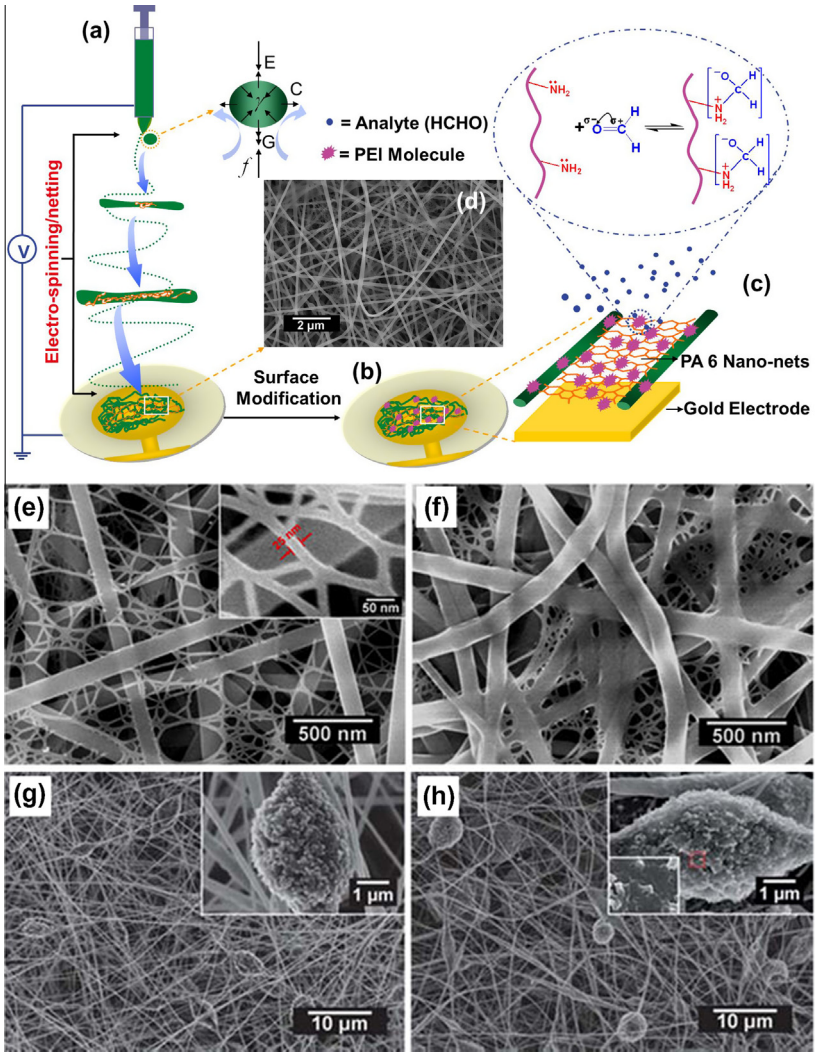

Fig. 44. Schematic diagram illustrating the fabrication of sensing layers on QCM. (a) ESN deposition of fibrous membranes onto the electrode of QCM. (b) Surface modification of NFN with diluted PEI solutions. (c) Illustration of PEI/PA-6 NFN on gold electrode and the reaction mechanism between formaldehyde and PEI. (d) Typical FE-SEM image of PA-6 NFN membranes. FE-SEM images of PA-6 NFN (e) and (g) PS fibrous membranes and their corresponding samples modified with PEI: (f) PEI/PA-6 and (h) PEI/PS. Reprinted with permission from [27]. © 2011 Royal Society of Chemistry.

into the chamber and then eliminated the influence of moisture. Fig. 45a shows the responses of QCM-based PEI/PA-6 NFN sensors upon injection of water and the dilute formaldehyde solution. The response of moisture-compensating QCM sensor exposing to formaldehyde was shown in Fig. 45b, indicating that the PEI/PA-6 NFN sensors exhibits a reduced detection limit for formaldehyde down to 50 ppb and a rapid response time (<100 s). In comparison with previous works using QCM platform for formaldehyde sensing, the present QCM-based PEI/PA-6 NFN sensor had not only the lowest detection limit but also the fastest time response (Table 6). Additionally, the sensor showed the highest response to formaldehyde with a value of up to 22 Hz, while for other gases the response is less than 5 Hz, implying a high selectivity to formaldehyde and can be considered as an excellent candidate

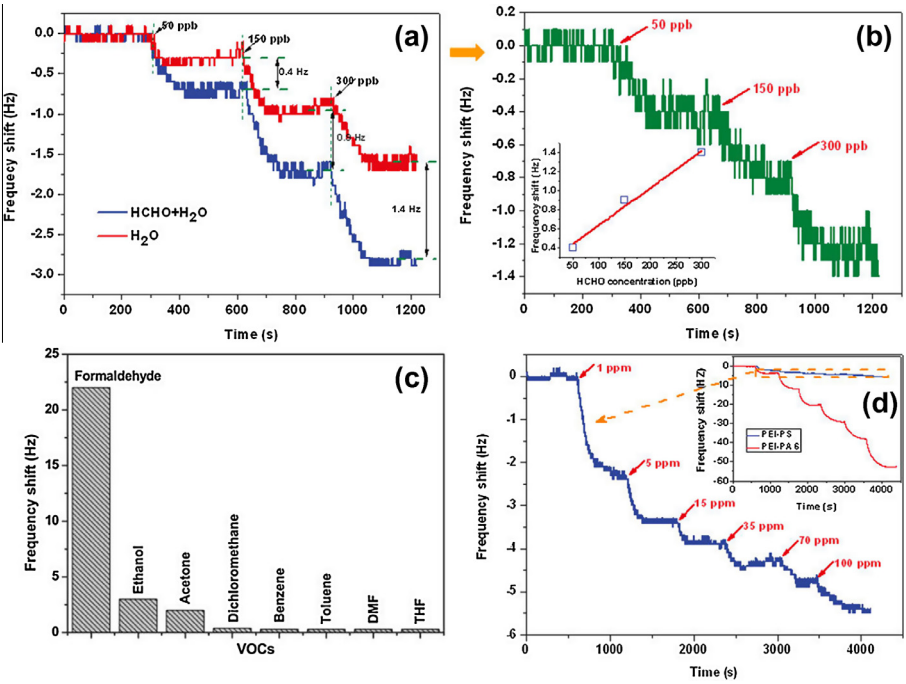

Fig. 45. (a) Responses of QCM-based PEI/PA-6 NFN (30 kV) sensors upon injection of water and the dilute formaldehyde solution, respectively. (b) Response of the QCM sensor to formaldehyde (50, 150, and 300 ppb), which derivate from (a) and removes effects of water. The inset in (b) shows the frequency shift versus the formaldehyde concentration. (c) Frequency shift of the QCM-based PEI/PA-6 NFN (30 kV) sensor versus 20 ppm of various VOCs. (d) Dynamic response of QCM-based PEI/PS sensors upon exposure to increasing formaldehyde concentrations. The inset shows the comparison of sensing property between PEI/PS porous fibers and PEI/PA-6 NFN (30 kV) membranes. The coating loads of PEI and PS (PA-6) were 2000 and 850 Hz, respectively. Reprinted with permission from [27]. © 2011 Royal Society of Chemistry.

for gas sensing applications (Fig. 45c). Furthermore, the PEI/PA-6 NFN nanostructure reported here possesses a higher sensitivity compared with the PEI-PS structure, which further demonstrated the advantages of the NFN structure (Fig. 45d). The lower sensitivity of the PEI-PS sensor could be due to the energy dissipation during vibration transfer in soft PS membranes on QCM as well as the blocking phenomenon on the surface of porous fibers after PEI modification.

6.2.2. Colorimetric sensors

Increasing public health and environmental protection demands have motivated researchers to look for more convenient detecting methods for low concentration of pollutants. Among various alternatives, a considerable attention has been given to the colorimetric sensor array system due to its effectiveness, simplicity, low cost and allows assays to be detected with the naked eye [270,271]. The investigation of NFN nonmaterial-based colorimetric detection strategy is really a novel topic and only few reports have been developed so far [28].

The determination of heavy metals in the environment has been an important worldwide concern since their dangerous effects on the ecosystem and human health depend on dose and toxicity. Copper, one of the heavy metals, is also an essential trace element in the human body and plays pivotal roles in a variety of fundamental physiological processes in organisms. The EPA gives an enforceable drinking water standard for Cu^{2+} of 1.3 ppm to prevent potential health problems and a secondary Cu^{2+} standard of 1 ppm for aesthetic considerations. Hence, sensitive, facile, and accurate detection of the levels of Cu^{2+} in water is especially important from the practical point of view. Ding et al. [28] reported a novel, ultrasensitive, selective and flexible sensor strip based on PANI/PA-6 NFN membranes for naked-eye colorimetric detection of Cu^{2+} ions in water. The sensing mechanism involves the

Table 6
Comparison of the QCM-based formaldehyde sensor parameters. Reprinted with permission from [27]. © 2011 Royal Society of Chemistry.

QCM platform	Sensing structures	Synthesis method of sensing structures	Detection limit (ppm)	Response time (s)	Reference
AT-cut, 6 MHz	Polyaniline-TiO_2 nano-composite	Chemical polymerization and sol–gel method	150	–	[261]
AT-cut, 9 MHz	Molecularly imprinted polymers film	Self-assembly and UV light radiation	49	~270	[268]
AT-cut, 5 MHz	PEI/PVA fibrous membranes	Electrospinning	10	~800	[250]
AT-cut, 5 MHz	PEI/PS nanoporous fibers	Electrospinning and surface modification	3	~1000	[244]
AT-cut, 5 MHz	PEI/PA-6 NFN	ESN and surface modification	0.05	<150	[27]

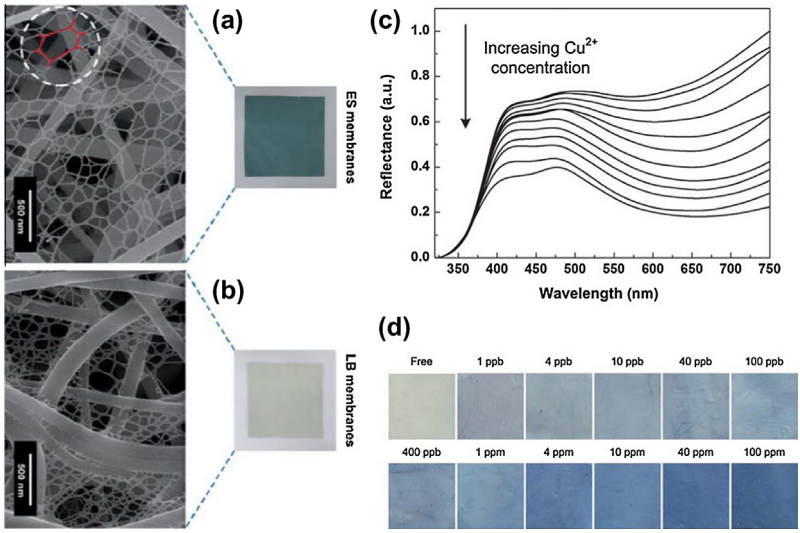

Fig. 46. (a and b) FE-SEM and optical images of the PANI/PA-6 NFN membranes (a) before (over) and (b) after (down) treated with hydrazine aqueous solution (40 wt%) for 2 h. (c) Reflectance spectra and (d) optical colorimetric response of the sensor strips after incubation for 30 min in Cu^{2+} aqueous solutions with concentrations of (0, 1 ppb, 4 ppb, 10 ppb, 40 ppb, 100 ppb, 400 ppb, 1 ppm, 4 ppm, 10 ppm, 40 ppm, and 100 ppm). Reprinted with permission from [28]. © 2011 Royal Society of Chemistry.

transformations between different oxidation and doping forms of PANI. Fig. 46a and b presents the changes of FE-SEM and optical images that accompany the treatment of PANI/PA-6 NFN membranes with hydrazine aqueous solution. During the process, PANI emeraldine salt in NFN membranes reacted with the hydrazine, and the semiquinone segments in polymer backbone were reduced into benzenoid segments yielding the PANI leucoemeraldine base, and thus the color changed from green to white vividly. Upon exposure to Cu^{2+} aqueous solution, the sensors exhibit two significant reflectance intensity decreasing bands at 435 and 650 nm which induce the color changes from white to blue dramatically (Fig. 46c and d). This new sensor shows colorimetric response specifically to Cu^{2+} ions (white-to-blue color change) over other possible interfering metal cations and allows for detection of Cu^{2+} in aqueous solution with a low detection limit of 1 ppb observing by naked eye. Additionally, the colorimetric responses could be quantitatively visualized by using a color-differentiation map prepared form converted RGB (red, green and blue) values (Fig. 47). With increasing Cu^{2+} concentration,

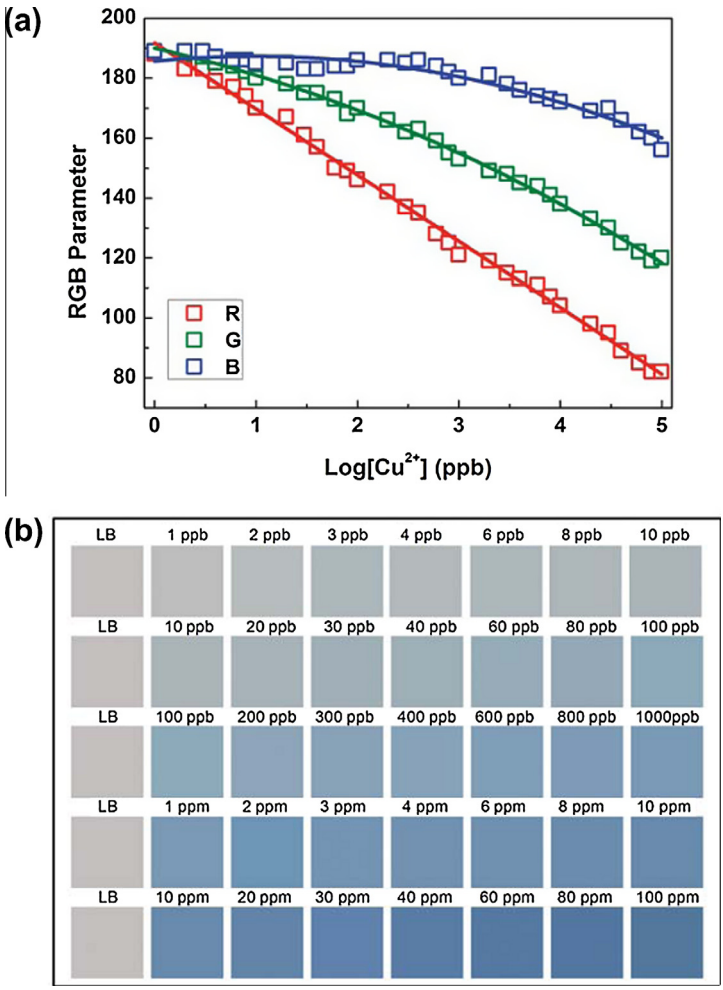

Fig. 47. (a) The RGB values converted from the reflectance spectrum of sensor strips variation versus the logarithmic concentration of Cu^{2+}. (b) Color-differentiation map comprising the converted RGB colors versus a series of Cu^{2+} concentrations. Reprinted with permission from [28]. © 2011 Royal Society of Chemistry.

the three parameters were decreased within different rates; the R (red) parameter has the highest decreasing rate while the B (blue) parameter has the lowest one, resulting in the dark blue of the sensor strips (Fig. 47a). Furthermore, the as-prepared PANI/PA-6 NFN sensor strips could successfully combine with the color map (Fig. 47b), which suggested a promising analytical method as an economical alternative to traditional Cu^{2+} sensors and also provided a new insight into the design and development of novel colorimetric sensing system based on the NFN platform.

Another colorimetric sensor based on NFN membranes has been developed for formaldehyde detection. The exploitation of highly efficient sensors for the detection of formaldehyde continues to be a significant scientific endeavor due to its possible threat to public health. Up to now, numerous formaldehyde-induced color changes of sensors that are composed of arrays of metalloporphyrins [272,273], pH indicators [274–276], chromotropic acid [277], and nanoporous pigments [278,279] have been successfully designed to detect formaldehyde with high selectivity. However, current colorimetric sensors for formaldehyde often use polymer film [274], cellulose tape [275,276] or even

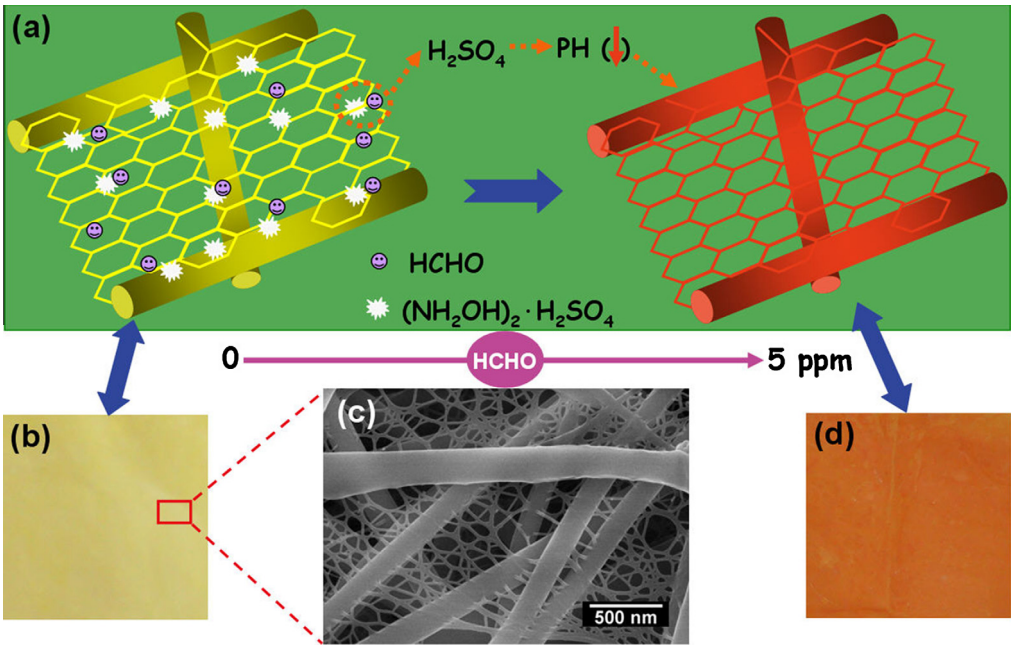

Fig. 48. (a) Schematic illustration of the colorimetric detection of formaldehyde based on the Methyl Yellow-impregnated PA-6 NFN membranes. Optical images of Methyl Yellow-impregnated PA-6 NFN membranes (b) before and (d) after exposure to 5 ppm formaldehyde. (c) FE-SEM image of the Methyl Yellow-impregnated PA-6 NFN membranes [281]. Reprinted with permission from [281]. © 2012 Elsevier B.V.

glass [280] as platform for immobilization of colorimetric sensing elements, which will inevitably cause relatively slow response and low sensitivity. Therefore, it is urgent to explore other general platforms to meet these challenges.

Wang et al. [281] demonstrated a label-free colorimetric sensor strip for real-time formaldehyde detection based on Methyl Yellow-impregnated PA-6 NFN membranes (Fig. 48). When the sensor strip was exposed to formaldehyde, the Methyl Yellow on the tape reacted with sulfuric acid produced by the reaction of hydroxylamine sulfate with formaldehyde to produce a yellow-to-red color change (Figs. 48 and 49) [275]. The degree of color change could be recorded by measuring the intensity of reflecting light (550 nm). This novel sensor strip not only maintains the high surface area and porosity of NFN structure, but also effectively improves the reflectance signal. Taking advantage of extremely large specific surface area and high porosity of the NFN structured membrane, the as-prepared sensors offers easy handling, as well as ultrasensitive and selective color change for gaseous formaldehyde, achieving detection limit as low as 50 ppb by naked eye (Fig. 49a). The kinetic sensing response was studied by continuously monitoring the reflectance spectra of sensor strips upon exposure to 5 ppm formaldehyde as a function of time, which showed that the reflectance intensity kept decreasing with increasing reaction time and the reflectance intensity at 550 nm varied nonlinearly with the exposure time between 0 and 30 min (Fig. 49b). Moving forward, it is envisioned that this strategy will facilitate the design and development of other label-free colorimetric sensors toward various analytes in the future.

6.3. Protective clothing application

Knowing that the essential properties of protective clothing are high moisture vapor transport, increased fabric breathability, and enhanced toxic chemical resistance [52,282], ESN NFN membranes have been recognized as potential candidates for these applications [30]. Actually, as the supporter of nano-nets, conventional electrospun nanofibers have played an important role in defense and

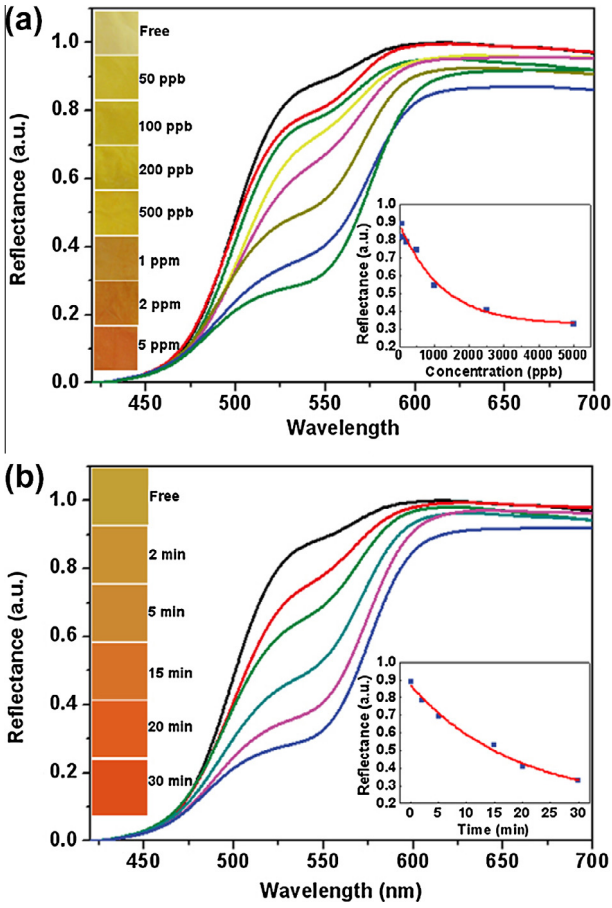

Fig. 49. (a) Reflectance spectra and (left inset) optical colorimetric response of the PA-6 NFN sensor strips upon exposure to increasing formaldehyde concentrations (0, 50 ppb, 100 ppb, 200 ppb, 500 ppb, 1 ppm, 2 ppm, 5 ppm).Exposure time for each concentration is 30 min. Right inset: the reflectance intensity of PA-6 NFN membranes at 550 nm versus formaldehyde concentration. (b) The kinetic reflectance response and (left inset) time dependent converted RGB color changes of PA-6 NFN membrane as a function of time upon exposure to formaldehyde concentrations of 5 ppm. Right inset: the reflectance intensity of PA-6 NFN membranes at 550 nm versus exposure time [281]. Reprinted with permission from [281]. © 2012 Elsevier B.V.

security applications as protective materials. Kang et al. [283] developed waterproof-breathable fabric by applying electrospun web of PU directly onto the substrate fabric (Fig. 50a and b). The electrospun PU fibers/fabric showed higher air permeability and vapor transmission properties than resin-coated fabrics, which could be attributed to the open porous structure of electrospun fibrous membranes. Electrospun PP webs and laminates were developed using melt-electrospinning to explore an alternative way of manufacturing protective clothing materials for agricultural workers [284]. The electrospun PP layer significantly enhanced barrier performance for challenge liquids. The potential of electrospun webs for future protective clothing systems has also been investigated. The U.S. Army Natick Soldier Center studied enhancement of barrier materials via a fine layer of electrospun fibers, focusing on preventing penetration of chemical warfare agents in aerosol form [285]. They found that the electrospun fibrous membranes of PA-66, polybenzimidazole, polyacrylonitrile and PU provided good aerosol particle protection, without a significant change in moisture vapor transport of the system.

As mentioned above, PU have been used successfully in clothing and textile coatings for garments, such as rain coats and industrial safety clothing, and they are distinguished as being comfortable to

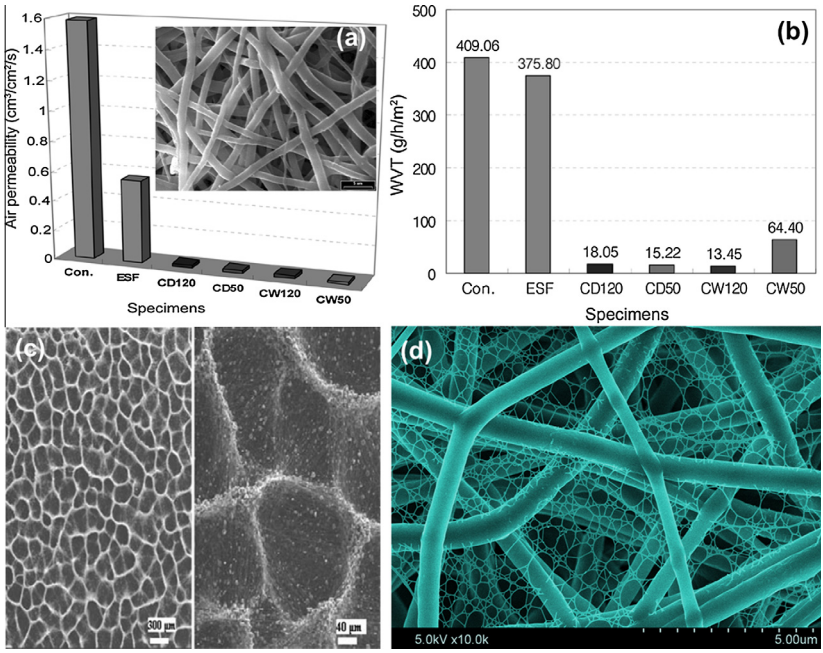

Fig. 50. Air permeability (a) and (b) water vapor transmission rate of specimens (Con.: plain face fabric, ESF: electrospun PU web/fabric, CD and CW: PU resin coated fabrics). Reprinted with permission from [283]. © 2007 Springer-Verlag. SEM images of (c) self-assembled PU nanofibrous membranes with honeycomb-like structure (reprinted with permission from [287]. © 2006 WILEY-VCH Verlag GmbH & Co.) and (d) PU NFN membranes. Reprinted with permission from [30]. © 2011 WILEY-VCH Verlag GmbH & Co.

wear and easy to care for [286]. Lee and Obendorf [286] prepared protective clothing materials by electrospinning PU fibrous membranes onto nonwoven fabric substrates. Barrier performance of layered fabric systems with an electrospun PU fiber web layer was evaluated against challenge liquids of different physicochemical properties. The air permeability of layered fabric systems is higher than most protective clothing materials currently in use. The water vapor transmission rates of layered fabric systems were in a range comparable to typical woven work clothing fabrics [286]. Thandavamoorthy et al. [287] demonstrated that self-assembled PU nanofibrous membranes with honeycomb-like structure are very useful in protective liners and filters for chemical warfare, because the honeycomb filters can trap and retain particles more efficiently, providing enhanced adsorption and filtration capabilities (Fig. 50c). Similarly, here we can expect that PU NFN membranes interspersing with 2D soap bubble-like or honeycomb-like structured nano-nets can also be a potential candidate for protective clothing application (Fig. 50d) [30].

Besides PU NFN membranes, Pant and coworkers demonstrated the fabrication of spider-web-like PA-6 NFN membranes containing TiO_2 nanoparticles, with superior mechanical strength, high hydrophilicity, and good antimicrobial as well as UV blocking ability [124]. These spider-web-like organic–inorganic nanocomposite NFN membranes with good UV blocking capacity and antimicrobial properties would have great potentiality for different kinds of protective clothing. As shown in Fig. 51a, the reflectance decreased as the amounts of TiO_2 in the composite mats increased because of the absorbance of UV light by TiO_2 nanoparticles for transferring the electron from the valance band to the conduction band, indicating that the novel PA-6/TiO_2 nanocomposite NFN membranes can be used for UV blocking. Additionally, the survival numbers of bacterial cells decreased with increasing amounts of TiO_2 in the composite NFN membranes, suggesting good bactericidal ability (Fig. 51b).

Via the ESN technique, which produces very thin membrane-like webs with very small pore size, the obtained protective materials provide resistance to liquid penetration while allowing moisture

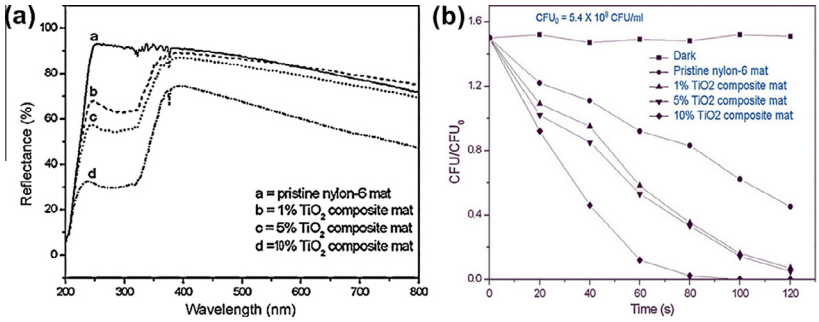

Fig. 51. UV–visible spectra and antimicrobial efficiency of pristine PA-6 and different PA-6/TiO_2 nanocomposite NFN membranes. Reprinted with permission from [124]. © 2011 Elsevier B.V.

vapor and thermal transport. In addition, controlling pore size by varying the area density of electrospun fiber and the pore-width of nano-nets would be useful for developing materials with different levels of protection and thermal comfort depending on the need and use [286]. Furthermore, combined with other functional materials through composite spinning or surface modification, multifunctional nanocomposite NFN membranes can be facilely prepared.

6.4. Nanofiber reinforcement

The mechanical properties of fibrous membranes are highly depending on the fiber structure, geometrical arrangement of the fibers, individual fiber properties and interaction between fibers [38,288,289]. Recent investigations have demonstrated that the size of the fiber influenced their tensile response. For example, Wong et al. [290] determined the tensile deformation of individual PCL fibers and found that the mechanical properties (i.e. tensile strength and tensile modulus) were enhanced when the diameter of the fibers was reduced below the critical diameter (Fig. 52). They ascribed the enhanced properties of finer diameter fibers to the gradual ordering of the molecular

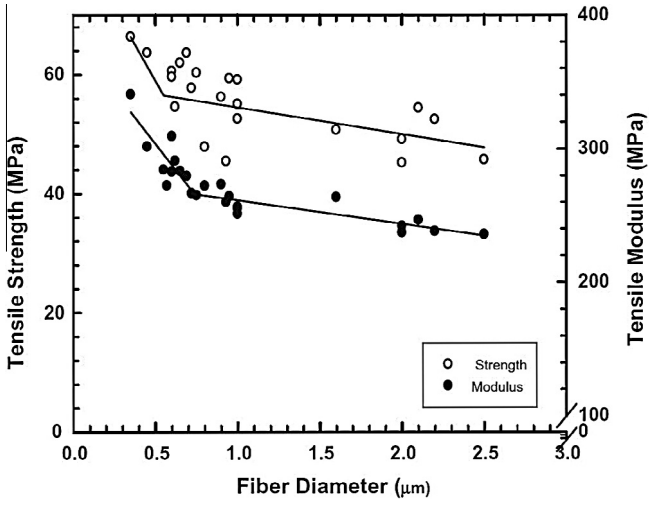

Fig. 52. Plot of tensile modulus and tensile strength versus fiber diameter. Tensile modulus increases with decreasing fiber diameter. These results can be attributed to the better molecular orientation and crystallinity in smaller fiber diameters. Larger than 2 lm, both tensile modulus and tensile strength appear invariant with fiber diameter. Reprinted with permission from [290]. © 2008 Elsevier B.V.

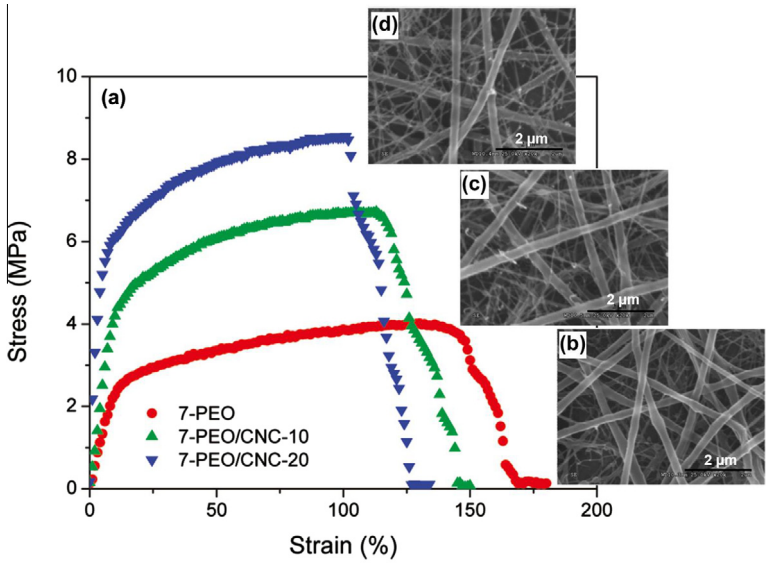

Fig. 53. (a) Stress–strain curves of ESN 7-PEO and 7-PEO/CNC NFN membranes. (b–d) SEM images of (b) 7-PEO, (c) 7-PEO/CNC-10, and (d) 7-PEO/CNC-20 NFN membranes. Reprinted with permission from [177]. © 2011 American Chemical Society.

chains, modest increase in the crystallinity of the fibers, and the densely packed lamellae and fibrillar structures. Based on these observations, NFN membranes containing ultrathin nanowires possess great potential as reinforcements for development of high strength/high toughness materials and materials with good thermal and electrical conductivity.

From the point of view of NFN nature, the existence of spider-web-like nano-nets further enhanced the mechanical properties of NFN membranes, which could be attributed to the extremely small fiber diameter and the net-like structure. Zhou et al. [177] demonstrated that mechanical performances of heterogeneous 7-PEO/CNC fibrous membranes with nano-nets were stronger than their homogeneous counterparts (5-PEO/CNC fibrous membranes) for all compositions (0–20 wt% CNC contents). For the 7-PEO/CNC nanofibrous membranes (Fig. 53), the values of maximum tensile stress (σ_{max}) and Young's modulus (E) increased with increased CNC contents (from 0 to 20 wt%) from 4.00 ± 0.10 to 8.52 ± 0.25 MPa and 23.8 ± 0.9 to 59.6 ± 3.8 MPa, respectively, which correspond to the increased density of nano-nets in the NFN membranes. These results indicated that the especially heterogeneous network microstructure was beneficial to the mechanical properties of electrospun composite nanofibrous membranes. Because the crystallinity of the PEO/CNC composite nanofibrous membranes is lower than that of the PEO nanofibrous membranes, their enhanced mechanical properties should be attributed to the efficient stress transfer from PEO to CNCs originating from the uniform dispersion and high alignment of CNCs in the PEO matrix. Such reinforcements also benefited from the formation of strong hydrogen bonding between the PEO matrix and the CNCs [177]. Moreover, the SEM-based morphologies of heterogeneous 7-PEO/CNC-20 NFN membranes in different stages of the tensile process were also studied (Fig. 54). Before the yield point (i.e., the initial stage of tensile testing), NFN morphology (Fig. 54a) did not show obvious changes, which was ascribed to the strong interaction among the nanofibers originating from the strong polar of PEO and CNCs. The improved Young's modulus of heterogeneous NFN membranes (compared with homogeneous mats) could be attributed to the strong bonding and entanglement between nano-nets and primary nanofibers. Increasing the tensile stress, most of the nanofibers in the NFN membranes gradually reached their tightened state and aligned along the tensile direction (Fig. 54b) due to the destroyed bonding points between nanofibers. Additionally, many nano-nets were also broken off from the primary fibers, which could defer the rupture of primary nanofibers and thus increase the elongation at break for NFN membranes. Further

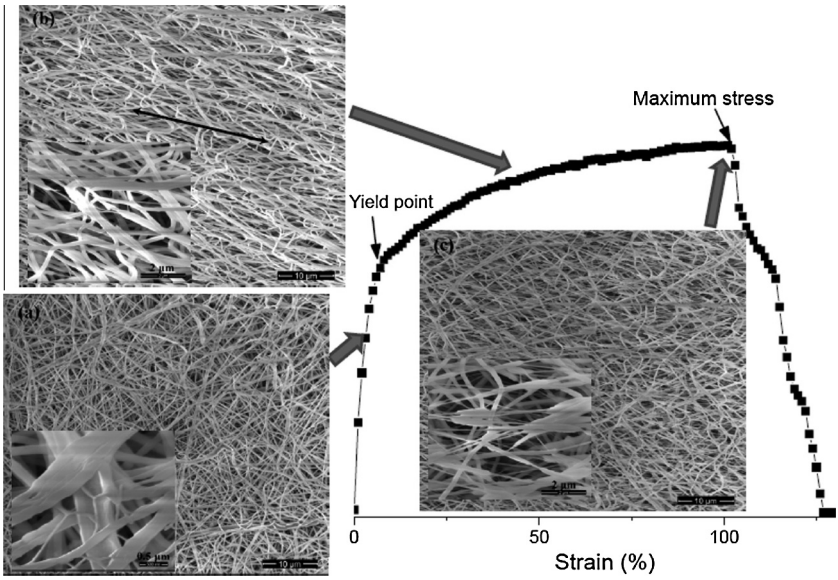

Fig. 54. Morphology observation of the tensile process of the 7-PEO/CNC-20 nanofibrous mats. Reprinted with permission from [177]. © 2011 American Chemical Society.

increasing the tensile stress, most nanofibers were necked and fractured; leading to the final NFN membranes rupture (Fig. 54c).

From the point of view of NFN reinforced polymer composites, nano-nets reinforced NFN membranes can significantly enhance the mechanical integrity of the polymer matrix compared to common electrospun fibers. Additionally, nano-nets bring NFN structured membrane several advantages as reinforcement materials: (1) the materials saving and the reduced brittleness of the matrix. To achieve the same reinforcement effect as electrospun fibers, smaller loadings of NFN in the matrix are required. (2) The enhanced mechanical strength caused by the interlocking mechanism, the high percentage of porosity and irregular pores between the fibers can lead to an interpenetrated structure when dispersed in the matrix. (3) The improved impact strength of the reinforced matrix induced by the large specific surface area between the nanofibers and the matrix promotes relaxation processes. Despite these attractive advantages of NFN membranes used as reinforcement materials, the number of investigations on this topic is rather small. The research on NFN reinforcement is still at its beginnings.

6.5. Tissue engineering

Tissue engineering is a multidisciplinary field that contains both the principles of engineering and life sciences for the development of biological substitutes and also for restoration, maintenance, or improvement of tissue function [41,88,291–293]. Target tissue and organs include skin, bones, cartilage, lymph knots, arteries, muscles, as well as heart, lung, and liver tissue [41,294,295]. Nanofiber is an emerging material which plays a pivotal role in tissue engineering by serving as matrices for cellular in growth, proliferation, differentiation, and new tissue formation in three-dimensions due to their high surface area to volume ratios and high porosity of the fibers [35,39,296]. An inherent feature of nanofibers is that they mimic the extracellular matrices (ECM) (i.e. a complex composite of fibrous proteins such as collagen and fibronectin, and glycoproteins) of tissues and organs [44]. ESN technique allows preparation of nanofibers and nano-nets in dimensions which resemble closely those of the cellular cytoskeleton or the diameter of collagen fibers within the ECM [28,168,297]. NFN membrane is highly porous which is favorable for cell proliferation and the mechanical properties of the scaffold

can be matched to those of the tissue to be replaced. In comparison with other fiber fabrication methods such as self-assembly and phase separation techniques, ESN provides a simpler and more cost-effective strategy to produce fibrous scaffolds with an inter-connected pore structure and fiber diameters in the sub-micron range. During the past few years, the field of application for ESN NFN membranes has evoked much attentions [27,31,102]; a series of natural polymers, such as gelatin [108], *B. mori* silk [112], CS [198] and synthetic polymers such as PA-6 [27,33,34], PA-66 [218], PAA [32,106], PU [30,113], PVA [34,164], PEO [177], and PTT [174] have been ESN into NFN structures. Such ESN NFN materials have great potential application in tissue engineering, immobilized enzymes, wound healing, artificial blood vessels, drug delivery, and so on.

Natural polymers (e.g. collagen, alginate, silk protein, hyaluronic acid, fibrinogen, CS) are often used for preparing nanofibrous scaffolds because of their enhanced biocompatibility and bio-functional motifs, as well as their blending into synthetic polymers can improve the overall cytocompatibility of the scaffold [8,291]. Collagen, for instance, is usually used as a scaffold for cells since it makes up a major component of the ECM [291].Gelatin is a natural polymer that is derived from collagen by controlled hydrolysis, and is commonly used for pharmaceutical and medical applications because of its biodegradability and biocompatibility in physiological environments [185,298]. Li et al. [299] demonstrated that electrospun gelatin nanofibrous scaffolds with diameter ranging from 200 to 500 nm could support attachment and growth of human embryonic palatal mesenchymal (HEPM) cells (Fig. 55a). More recently, our group have demonstrated the large-scale fabrication of gelatin NFN membranes by regulating the solution properties and several process parameters during ESN process [108]. Gelatin nano-nets that comprise interlinked 1D ultrathin nanowires (10–35 nm) are stacked layer-by-layer and widely distributed in the 3D porous membranes exhibited great potential application in tissue engineering (Fig. 55b), although this application was not investigated in this study. *B. mori* silk is another proteins found that have been ESN into NFN structures. Ayutsede and coworkers have demonstrated the feasibility of fabricating nanocomposite NFN membranes comprising *B. mori* silk and SWCNT through the ESN process [112]. Further study is needed for exploiting their applications in tissue engineering and other biomedical applications.

A variety of synthetic polymer nanofibers have been considered for use as scaffolds for engineering tissues such as PLGA [42], PLLA [300], PCL [43], PA-6 [149], and PU [301]. However, the limited properties of synthetic polymer NFN membranes with only one component restrict their application in biomedical engineering. Therefore, the feasibility of incorporating natural polymers into polymer to form composite NFN membranes has revealed ESN as an attractive technique to meet several specific functional applications. Kim's group pioneered the application of NFN membranes in tissue engineering [139,149,301]. They have demonstrated the one-step preparation of CS/PA-6 composite NFN scaffolds via ESN technique for the osteoblastic cell culture applications [149]. Fig. 56a–d shows the FE-SEM images of CS/PA-6 composite NFN membranes for the different concentration of CS. The diameter of the composite nanofibers were observed to be in the range of 300–600 nm, whereas the nano-nets consisted of regularly distributed very fine nanofibers with diameters of about 20–60 nm. The density of high aspect ratio fibers increases with increasing the concentration of CS. The adhesion, viability

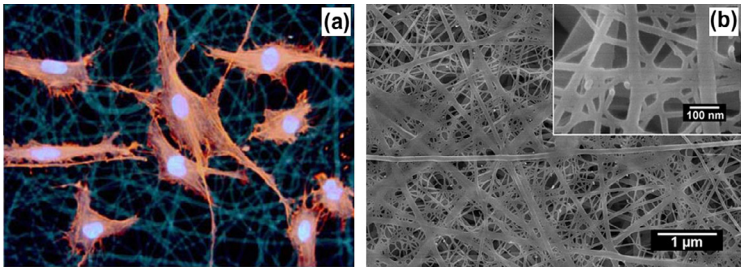

Fig. 55. (a) Morphology of HEPM cells on gelatin fiber matrices after 48 h in culture (original magnification 400×). Reprinted with permission from [299]. © 2005 Elsevier B.V. (b) FE-SEM image of gelatin NFN membranes. Reprinted with permission from [108]. © 2011 Elsevier B.V.

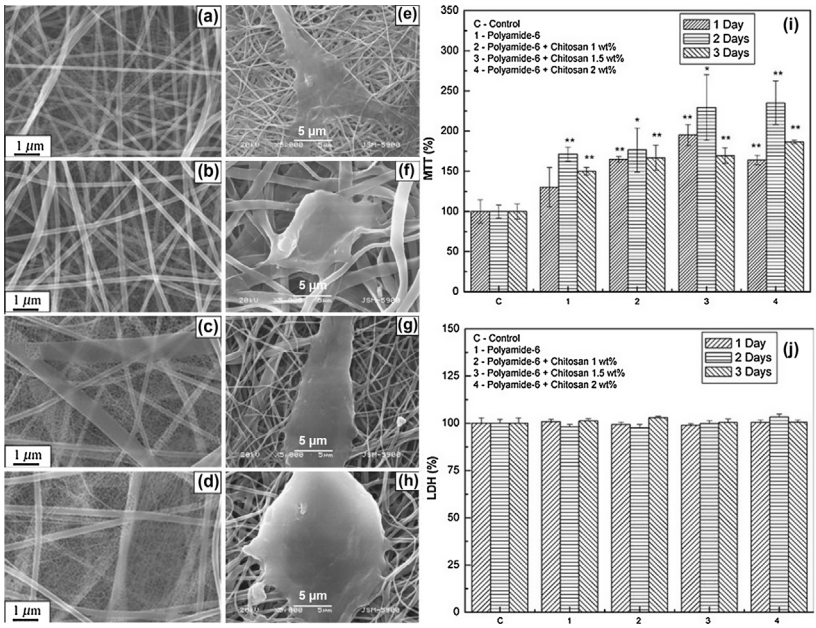

Fig. 56. FE-SEM images of (a–d) CS/PA-6 composite NFN membranes and (e–h) their corresponding samples cultured with osteoblast cells. The concentration of CS in CS/PA-6 NFN membranes were (a and e) 0, (b and f) 1, (c and g) 1.5 and (d, h) 2 wt%, respectively. Cell growth measurement of (i) MTT and (j) LDH on CS/PA-6 composite NFN membranes with different CS concentration of 0, 1, 1.5 and 2 wt%. Cell viability was determined in accordance with LDH and MTT test. The viability of control cells was set at 100%, and viability relative to the control was expressed. The experiments were conducted at least in triplicate. $^{*}P < 0.01$ vs. control. $^{**}P < 0.005$ vs. control. Reprinted with permission from [149]. © 2011 Elsevier B.V.

and proliferation properties of osteoblast cells on the CS/PA-6 blended nanofibers were analyzed by in vitro cell compatibility test. The results showed that the cells spread over the scaffold fibers, linked with fibers by cytoplasmic extensions (Fig. 56e–h). The MTT (3-[4,5-dimethylthiazol-2-yl]2,5-diphenyl tetrazolium bromide) and lactate dehydrogensae (LDH) level appeared to be increased with increasing CS concentration, and this was attributable to the density of nanofibers (Fig. 56i and j). However, the MTT level of all the samples was observed to be higher than that of the negative control. The in vitro cytotoxicity evaluation of the CS/PA-6 blended nanofibers indicated that this scaffold material was nontoxic for the osteoblast cell culture. In another work, they used lecithin to replace the CS and successfully prepared lecithin/PA-6 homogenously composite NFN membranes. Lecithin/PA-6 NFN membranes showed non-cytotoxic behavior for the osteoblast cell culture [139]. Besides PA-6 based NFN membranes, they also investigated the preparation of PU NFN membranes blended with $CaCl_2$ for osteoblastic cell culture applications. The $CaCl_2$ was adapted in the composite scaffolds owing to its cell permeability and cellular metabolic activity. The MTT and LDH measurements of the composite NFN membranes demonstrated the cytocompatibility of this novel scaffold. Because of good attachment and formation behaviors, there is a potential to utilize PU/$CaCl_2$ composite NFN scaffold for the bone regeneration applications [301].

7. Concluding remarks and perspectives

This article presents a comprehensive review of the progress in a novel nanomaterials fabrication technique (i.e. ESN technique), starting from an overview about conventional electrospinning technique (the rudiment of ESN technique), continuing with the illustration of ESN technique (historical background and basic setup), and finishing with the discussion on the proposed formation mechanisms of NFN structures. Additionally, we also present the fundamental properties

(e.g. extremely small diameter, high porosity, Steiner tree network geometry, controllable coverage rate, and controllable density) of NFN nanomaterials. The selection of polymers used for ESN is outlined by the introduction of various polymer based NFN materials such as PA-6, PAA, PVA, gelatin, CS, and PU. The following section fully highlights the state-of-the-art strategies for the controllable fabrication of NFN membranes based on the regulation of solution, processing, and ambient parameters. The remarkable level of a synthetic control for NFN nanostructures and their rich morphologies at the nanoscale has paved the way to the unique applications in the fields of environment, energy and healthcare.

It has become evident that the fundamental properties of ESN NFN membranes (e.g. extremely small diameter, high porosity, Steiner tree network geometry, controllable coverage rate, controllable density) made it compelling for various engineering applications. Intensive efforts have been devoted to exploring the fundamental structure control and outstanding applications. Novel structure with 2D soap-bubble-like structured or spider-web-like nano-nets supported by conventional electrospun nanofibers have not been observed earlier from most conventional 3D electrospun nanomaterials. Research publications in the past several years indicate that the importance of NFN nanomaterials might surpass traditional electrospun fibers in the development of filtration and ultrasensitive sensors. While electrospinning technique is at its mature stage to overcome the technological barrier, ESN NFN nanomaterials are being extensively investigated as it overcomes the bottleneck problem of electrospinning technique. Both ESN and 3D NFN membrane as novel technique and new structured material still face many challenges ranging from formation theory and fabrication to the final practical applications and there are a number of areas where future work should be directed.

- The formation mechanism of the NFN structures is complicated, which relate to physical, chemical, EHD processes, etc., and thus consensus on the formation mechanism has not been reached currently. The main confused problem is this: What happens to the charged polymer jets and droplets during such small distance from tip to collector? Theoretical modeling, calculation and prediction of this process, its collective behavior and inherent mutual interaction, have received little attention, which will potentially hinder the rapid process in this field. There have been so far only few publications dealing with the interpretation and theory background behind the observed phenomena of ESN process. Thorough understanding the formation mechanisms of nano-nets makes for preparing optimal nano-nets with ideal structure and extending the range of spinnable polymers. Thus, more rigorous experimental and theoretical work is also required to consummate this novel technique.
- The design and fabrication of NFN membranes is one of the most promising scientific and technological challenges in the coming years. According to preparation process and formation of current polymer NFN materials, we found that polymers with hydrogen bonds favored creating interconnect nano-nets, adding ZnO, SiO_2, NaCl, CNT, CNC, and SWCNT into the polymer solutions could lead to nano-nets, and changing processing parameters could influence the morphology of NFN membranes. However, pursuing the universal law for explaining the formation of nano-nets is a complicated problem. Revealing the process's secret can help people to look for additional spinnable polymers.
- As described in the section of polymers and polymer composites used in ESN process, as can be seen, current NFN membranes are all organic-based materials while the ESN of materials other than polymers has not yet received much attention. Particularly, inorganic materials are potentially important for those applications in electronics, photonics, mechanics, sensing, etc. As far as we know, fabrication of inorganic NFN membranes via ESN process needs incorporation of inorganic materials or their precursors into the ESN polymer solutions and followed by the calcinations process. In order to obtain the inorganic nano-nets after calcinations, the content of inorganic materials should be as much as possible, which will certainly influence the solution properties and final morphology of resultant membranes. Therefore, several core issues such as the homogeneity of the composite solutions, the optimization of calcinations technique, and the brittleness of the inorganic fibrous membranes still require more investigation.

- We have shown in this review that NFN nanostructures have become one of the popular research pursuits due to the unique properties and wide range of potential applications. Amongst various applications, the NFN based filters is very important as it can prevent harmful nanoparticles and even virus from getting into the environment and the human body, which fulfill the rising demand for healthier and safer living and working environments. However, there are still many unresolved issues, such as the mass production of NFN materials, the compounding technology between NFN membranes and nonwoven scaffold and the experimental validation of their filtration performance to viruses, which need to be investigated both experimentally and theoretically. Additionally, fabrication of nanostructured sensing materials may significantly improve their performances in the existing devices or open the doors to new types of applications. The ability to narrow the compatibility gap between sensing devices and nanomaterials, however, remains a major challenge in the field.

The past several years have witnessed a remarkable progress in research activities leading to exploitation of ESN NFN nanomaterials and figuring out of the crucial challenges as documented in this review. We anticipate that the continuous efforts on exploration of NFN nanostructures inspired by their significant properties will address the current challenges and push forward the rapid development of ESN technology.

Acknowledgments

This work is supported by the National Basic Research Program of China (2011CB606103, 2012CB525005 and 2013CB228301), the National Natural Science Foundation of China (No. 51173022, 51176089, U1232116 and 51273038), the "111 Project" (B07024), the Shanghai Nano Special Projects (11nm0502900), the Innovation Program of Shanghai Municipal Education Commission (11ZZ59), the "Dawn" Program of Shanghai Education Commission (10SG32), the Huo Yingdong Foundation (131070), the recruitment program of global young experts (1000plan), the Scientific Research Foundation for the Returned Overseas Chinese Scholars, Ministry of Education of China, the Program for New Century Talents of the University in China, and the Fundamental Research Funds for the Central Universities.

References

[1] Fang X, Bando Y, Gautam UK, Ye C, Golberg D. Inorganic semiconductor nanostructures and their field-emission applications. J Mater Chem 2008;18:509–22.
[2] Fang X, Zhai T, Gautam UK, Li L, Wu L, Bando Y, et al. ZnS nanostructures: From synthesis to applications. Prog Mater Sci 2011;56:175–287.
[3] Zhang L, Fang M. Nanomaterials in pollution trace detection and environmental improvement. Nano Today 2010;5:128–42.
[4] Xiao K, Li YP, Luo JT, Lee JS, Xiao WW, Gonik AM, et al. The effect of surface charge on in vivo biodistribution of PEG-oligocholic acid based micellar nanoparticles. Biomaterials 2011;32:3435–46.
[5] Lu X, Zhang W, Wang C, Wen T, Wei Y. One-dimensional conducting polymer nanocomposites: synthesis, properties and applications. Prog Polym Sci 2011;36:671–712.
[6] Yuan J, Xu Y, Müller AHE. One-dimensional magnetic inorganic–organic hybrid nanomaterials. Chem Soc Rev 2011;40:640–55.
[7] Xia Y, Yang P, Sun Y, Wu Y, Mayers B, Gates B, et al. One-dimensional nanostructures: synthesis, characterization, and applications. Adv Mater 2003;15:353–89.
[8] Lu X, Wang C, Wei Y. One-dimensional composite nanomaterials: synthesis by electrospinning and their applications. Small 2009;5:2349–70.
[9] Lauhon LJ, Gudiksen MS, Wang D, Lieber CM. Epitaxial core–shell and core–multishell nanowire heterostructures. Nature 2002;420:57–61.
[10] Zach MP, Ng KH, Penner RM. Molybdenum nanowires by electrodeposition. Science 2000;290:2120–3.
[11] Hu J, Odom TW, Lieber CM. Chemistry and physics in one dimension: synthesis and properties of nanowires and nanotubes. Acc Chem Res 1999;32:435–45.
[12] Hu MS, Chen HL, Shen CH, Hong LS, Huang BR, Chen KH, et al. Photosensitive gold-nanoparticle-embedded dielectric nanowires. Nat Mater 2006;5:102–6.
[13] Huang Y, Duan XF, Wei QQ, Lieber CM. Directed assembly of one-dimensional nanostructures into functional networks. Science 2001;291:630–3.
[14] Barth S, Hernandez-Ramirez F, Holmes JD, Romano-Rodriguez A. Synthesis and applications of one-dimensional semiconductors. Prog Mater Sci 2010;55:563–627.

[15] Xiao YJ, Cao HQ, Liu KY, Zhang SC, Chernow V. The synthesis of superhydrophobic Bi_2S_3 complex nanostructures. Nanotechnology 2010;21:145601.
[16] Ebadzadeh T, Shojaee N, Aghaei A. Effect of concentration and heating conditions on microwave-assisted hydrothermal synthesis of ZnO nanorods. Mater Charact 2010;61:1418–23.
[17] Jiang L, Zhao Y, Zhai J. A lotus-leaf-like superhydrophobic surface: a porous microsphere/nanofiber composite film prepared by electrohydrodynamics. Angew Chem Int Ed 2004;43:4338–41.
[18] Taylor G. Studies in electrohydrodynamics. I. The circulation produced in a drop by electrical field. Proc Roy Soc Lond A 1966;291:159.
[19] Wang JK, Wang M, Li ZX. Lattice Poisson–Boltzmann simulations of electro-osmotic flows in microchannels. J Colloid Interface Sci 2006;296:729–36.
[20] Wang M, Liu J, Chen S. Electric potential distribution in nanoscale electroosmosis: from molecules to continuum. Mol Simulat 2007;33:1273–7.
[21] Du J, Hsieh YL. Nanofibrous membranes from aqueous electrospinning of carboxymethyl chitosan. Nanotechnology 2008;19:125707.
[22] Wang XF, Ding B, Yu JY, Wang MR. Engineering biomimetic superhydrophobic surfaces of electrospun nanomaterials. Nano Today 2011;6:510–30.
[23] Dzenis Y. Spinning continuous fibers for nanotechnology. Science 2004;304:1917–9.
[24] Kim ID, Rothschild A, Lee BH, Kim DY, Jo SM, Tuller HL. Ultrasensitive chemiresistors based on electrospun TiO_2 nanofibers. Nano Lett 2006;6:2009–13.
[25] Ding B, Wang MR, Yu JY, Sun G. Gas sensors based on electrospun nanofibers. Sensors 2009;9:1609–24.
[26] Sarkar K, Gomez C, Zambrano S, Ramirez M, de Hoyos E, Vasquez H, et al. Electrospinning to forcespinning (TM). Mater Today 2010;13:12–4.
[27] Ding B, Wang X, Yu J, Wang M. Polyamide 6 composite nano-fiber/net functionalized by polyethyleneimine on quartz crystal microbalance for highly sensitive formaldehyde sensors. J Mater Chem 2011;21:12784–92.
[28] Ding B, Si Y, Wang X, Yu J, Feng L, Sun G. Label-free ultrasensitive colorimetric detection of copper(II) ions utilizing polyaniline/polyamide-6 nano-fiber/net sensor strips. J Mater Chem 2011;21:13345–53.
[29] Wang X, Ding B, Yu J, Wang M. Highly sensitive humidity sensors based on electro-spinning/netting a polyamide 6 nano-fiber/net modified by polyethyleneimine. J Mater Chem 2011;21:16231–8.
[30] Hu J, Wang X, Ding B, Lin J, Yu J, Sun G. One-step electro-spinning/netting technique for controllably preparing polyurethane nano-fiber/net. Macromol Rapid Commun 2011;32:1729–34.
[31] Wang XF, Ding B, Yu JY, Si Y, Yang SB, Sun G. Electro-netting: fabrication of two-dimensional nano-nets for highly sensitive trimethylamine sensing. Nanoscale 2011;3:911–5.
[32] Yang SB, Wang XF, Ding B, Yu JY, Qian JF, Sun G. Controllable fabrication of soap-bubble-like structured polyacrylic acid nano-nets via electro-netting. Nanoscale 2011;3:564–8.
[33] Ding B, Li CR, Miyauchi Y, Kuwaki O, Shiratori S. Formation of novel 2D polymer nanowebs via electrospinning. Nanotechnology 2006;17:3685–91.
[34] Barakat NAM, Kanjwal MA, Sheikh FA, Kim HY. Spider-net within the N6, PVA and PU electrospun nanofiber mats using salt addition: novel strategy in the electrospinning process. Polymer 2009;50:4389–96.
[35] Greiner A, Wendorff JH. Electrospinning: a fascinating method for the preparation of ultrathin fibres. Angew Chem Int Ed 2007;46:5670–703.
[36] Yoon K, Hsiao BS, Chu B. Functional nanofibers for environmental applications. J Mater Chem 2008;18:5326–34.
[37] Huang C, Soenen SJ, Rejman J, Lucas B, Braeckmans K, Demeester J, et al. Stimuli-responsive electrospun fibers and their applications. Chem Soc Rev 2011;40:2417–34.
[38] Baji A, Mai Y, Wong S, Abtahi M, Chen P. Electrospinning of polymer nanofibers: effects on oriented morphology, structures and tensile properties. Compos Sci Technol 2010;70:703–18.
[39] Frenot A, Chronakis IS. Polymer nanofibers assembled by electrospinning. Curr Opin Colloid Interface Sci 2003;8:64–75.
[40] Deitzel JM, Kleinmeyer J, Harris D, Tan NCB. The effect of processing variables on the morphology of electrospun nanofibers and textiles. Polymer 2001;42:261–72.
[41] Agarwal S, Greiner A, Wendorff JH. Electrospinning of manmade and biopolymer nanofibers-progress in techniques, materials, and applications. Adv Funct Mater 2009;19:2863–79.
[42] Li WJ, Laurencin CT, Caterson EJ, Tuan RS, Ko FK. Electrospun nanofibrous structure: a novel scaffold for tissue engineering. J Biomed Mater Res 2002;60:613–21.
[43] Yoshimoto H, Shin YM, Terai H, Vacanti JP. A biodegradable nanofiber scaffold by electrospinning and its potential for bone tissue engineering. Biomaterials 2003;24:2077–82.
[44] Ramakrishna S, Fujihara K, Teo W-E, Yong T, Ma Z, Ramaseshan R. Electrospun nanofibers: solving global issues. Mater Today 2006;9:40–50.
[45] Li D, Xia YN. Electrospinning of nanofibers: reinventing the wheel? Adv Mater 2004;16:1151–70.
[46] Bose GM. Recherches sur la cause et sur la veritable theorie de l'electricite. Wittenberg, 1745.
[47] Rayleigh L. On the equilibrium of liquid conducting masses charged with electricity. Philos Mag 1882;14:184–6.
[48] Morton WJ. Method of dispersing fluids. U.S. Patent No. 705691, 1902.
[49] Cooley JF. Apparatus for electrically dispersing fluids. U.S. Patent No. 692631, 1902.
[50] Formhals A. Process and apparatus for preparing artificial threads. U.S. Patent No. 1975504, 1934.
[51] Taylor G. Electrically driven jets. Proc Roy Soc Lond A 1969;313:453.
[52] Subbiah T, Bhat GS, Tock RW, Parameswaran S, Ramkumar SS. Electrospinning of nanofibers. J Appl Polym Sci 2005;96:557–69.
[53] Huang Z, Zhang Y, Kotaki M, Ramakrishna S. A review on polymer nanofibers by electrospinning and their applications in nanocomposites. Compos Sci Technol 2003;63:2223–53.
[54] Doshi J, Reneker DH. Electrospinning process and applications of electrospun fibers. J Electrostat 1995;35:151–60.
[55] Reneker DH, Chun I. Nanometre diameter fibres of polymer, produced by electrospinning. Nanotechnology 1996;7:216–23.

[56] Fong H, Chun I, Reneker DH. Beaded nanofibers formed during electrospinning. Polymer 1999;40:4585–92.
[57] Bognitzki M, Czado W, Frese T, Schaper A, Hellwig M, Steinhart M, et al. Nanostructured fibers via electrospinning. Adv Mater 2001;13:70–2.
[58] Sun ZC, Zussman E, Yarin AL, Wendorff JH, Greiner A. Compound core–shell polymer nanofibers by co-electrospinning. Adv Mater 2003;15:1929–32.
[59] Buchko CJ, Chen LC, Shen Y, Martin DC. Processing and microstructural characterization of porous biocompatible protein polymer thin films. Polymer 1999;40:7397–407.
[60] Teo W, Ramakrishna S. A review on electrospinning design and nanofibre assemblies. Nanotechnology 2006;17:R89–R106.
[61] Guerrini LM, Branciforti MC, Canova T, Bretas RES. Electrospinning and characterization of polyamide 66 nanofibers with different molecular weights. Mater Res-Ibero-Am J Mater 2009;12:181–90.
[62] Zhang DM, Chang J. Electrospinning of three-dimensional nanofibrous tubes with controllable architectures. Nano Lett 2008;8:3283–7.
[63] Liu YQ, Zhang XP, Xia YN, Yang H. Magnetic-field-assisted electrospinning of aligned straight and wavy polymeric nanofibers. Adv Mater 2010;22:1–4.
[64] Agbenyega J. Electrospinning has nanofibers in alignment. Mater Today 2008;11. 10-.
[65] Li D, Wang YL, Xia YN. Electrospinning of polymeric and ceramic nanofibers as uniaxially aligned arrays. Nano Lett 2003;3:1167–71.
[66] Matthews JA, Wnek GE, Simpson DG, Bowlin GL. Electrospinning of collagen nanofibers. Biomacromolecules 2002;3:232–8.
[67] Zussman E, Theron A, Yarin AL. Formation of nanofiber crossbars in electrospinning. Appl Phys Lett 2003;82:973–5.
[68] Mathew G, Hong JP, Rhee JM, Leo DJ, Nah C. Preparation and anisotropic mechanical behavior of highly-oriented electrospun poly(butylene terephthalate) fibers. J Appl Polym Sci 2006;101:2017–21.
[69] Zhang DM, Chang J. Patterning of electrospun fibers using electroconductive templates. Adv Mater 2007;19:3664–7.
[70] Li D, Ouyang G, McCann JT, Xia Y. Collecting eectrospun nanofibers with patterned electrodes. Nano Lett 2005;5:913–6.
[71] Ding B, Li C, Du J, Shiratori S. Biomimetic super-hydrophobic micro/nanoporous fibrous mat surfaces via electrospinning. Nanotechnology research: new nanostructures, nanotubes and nanofibers. New York: Nova Science Publishers; 2008. p. 131–66.
[72] Lin JY, Ding B, Yu JY, Hsieh Y. Direct fabrication of highly nanoporous polystyrene fibers via electrospinning. ACS Appl Mater Interfaces 2010;2:521–8.
[73] Ding B, Lin J, Wang X, Yu J, Yang J, Cai Y. Investigation of silica nanoparticle distribution in nanoporous polystyrene fibers. Soft Matter 2011;7:8376–83.
[74] Koombhongse S, Liu WX, Reneker DH. Flat polymer ribbons and other shapes by electrospinning. J Polym Sci Pt B-Polym Phys 2001;39:2598–606.
[75] Kessick R, Tepper G. Microscale polymeric helical structures produced by electrospinning. Appl Phys Lett 2004;84:4807–9.
[76] Shin MK, Kim SI, Kim SJ. Controlled assembly of polymer nanofibers: from helical springs to fully extended. Appl Phys Lett 2006;88:223109.
[77] Jin Y, Yang DY, Kang DY, Jiang XY. Fabrication of necklace-like structures via electrospinning. Langmuir 2010;26:1186–90.
[78] Lu X, Zhang D, Zhao Q, Wang C, Zhang W, Wei Y. Large-scale synthesis of necklace-like single-crystalline $PbTiO_3$ nanowires. Macromol Rapid Commun 2006;27:76–80.
[79] Chang ZJ. "Firecracker-shaped" ZnO/polyimide hybrid nanofibers via electrospinning and hydrothermal process. Chem Commun 2011;47:4427–9.
[80] Yang SY, Zhu PN, Nair AS, Ramakrishna S. Rice grain-shaped TiO_2 mesostructures-synthesis, characterization and applications in dye-sensitized solar cells and photocatalysis. J Mater Chem 2011;21:6541–8.
[81] Zhao Y, Cao XY, Jiang L. Bio-mimic multichannel microtubes by a facile method. J Am Chem Soc 2007;129:764–5.
[82] Kokubo H, Ding B, Naka T, Tsuchihira H, Shiratori S. Multi-core cable-like TiO_2 nanofibrous membranes for dye-sensitized solar cells. Nanotechnology 2007;18:165604.
[83] Mou FZ, Guan JG, Shi WD, Sun ZG, Wang SH. Oriented contraction: a facile nonequilibrium heat-treatment approach for fabrication of maghemite fiber-in-tube and tube-in-tube nanostructures. Langmuir 2010;26:15580–5.
[84] Chen HY, Wang N, Di JC, Zhao Y, Song YL, Jiang L. Nanowire-in-microtube structured core/shell fibers via multifluidic coaxial electrospinning. Langmuir 2010;26:11291–6.
[85] Zhang ZY, Li XH, Wang CH, Wei LM, Liu YC, Shao CL. ZnO hollow nanofibers: fabrication from facile single capillary electrospinning and applications in gas sensors. J Phys Chem C 2009;113:19397–403.
[86] Li D, Xia YN. Direct fabrication of composite and ceramic hollow nanofibers by electrospinning. Nano Lett 2004;4:933–8.
[87] Chen M, Dong M, Havelund R, Regina VR, Meyer RL, Besenbacher F, et al. Thermo-responsive core–sheath electrospun nanofibers from poly (N-isopropylacrylamide)/polycaprolactone blends. Chem Mater 2010;22:4214–21.
[88] Chigome S, Darko G, Torto N. Electrospun nanofibers as sorbent material for solid phase extraction. Analyst 2011;136:2879–89.
[89] Rutledge GC, Fridrikh SV. Formation of fibers by electrospinning. Adv Drug Deliv Rev 2007;59:1384–91.
[90] Ding B, Kimura E, Sato T, Fujita S, Shiratori S. Fabrication of blend biodegradable nanofibrous nonwoven mats via multi-jet electrospinning. Polymer 2004;45:1895–902.
[91] Theron S, Yarin A, Zussman E, Kroll E. Multiple jets in electrospinning: experiment and modeling. Polymer 2005;46:2889–99.
[92] Wu DZ, Huang XP, Lai XT, Sun DH, Lin LW. High throughput tip-Less electrospinning via a circular cylindrical electrode. J Nanosci Nanotechnol 2010;10:4221–6.
[93] Um IC, Fang D, Hsiao BS, Okamoto A, Chu B. Electro-spinning and electro-blowing of hyaluronic acid. Biomacromolecules 2004;5:1428–36.
[94] Thoppey NM, Bochinski JR, Clarke LI, Gorga RE. Edge electrospinning for high throughput production of quality nanofibers. Nanotechnology 2011;22:345301.

[95] Bellan LM, Craighead HG. Nanomanufacturing using electrospinning. J Manuf Sci Eng 2009;131:034001.
[96] Lin K, Chua KN, Christopherson GT, Lim S, Mao HQ. Reducing electrospun nanofiber diameter and variability using cationic amphiphiles. Polymer 2007;48:6384–94.
[97] Huang CB, Chen SL, Lai CL, Reneker DH, Qiu H, Ye Y, et al. Electrospun polymer nanofibres with small diameters. Nanotechnology 2006;17:1558–63.
[98] Wang C, Chien HS, Hsu CH, Wang YC, Wang CT, Lu HA. Electrospinning of polyacrylonitrile solutions at elevated temperatures. Macromolecules 2007;40:7973–83.
[99] Ding B, Li C, Wang D, Shiratori S. Fabrication and application of novel two-dimensional nanowebs via electrospinning. In: Dixon CJ, Curtines OW, editors. Nanotechnology: nanofabrication, patterning, and self assembly. New York: Nova Science Publishers, Inc.; 2010. p. 51–69.
[100] http://www.rsc.org/chemistryworld/News/2011/July/28071103.asp.
[101] http://nanotechweb.org/cws/article/lab/41675.
[102] Dooley E. The beat. Environ Health Perspect 2011;119:a384–5.
[103] Kong C, Lee T, Lee S, Kim H. Nano-web formation by the electrospinning at various electric fields. J Mater Sci 2007;42:8106–12.
[104] Lee YJ, Shin DS, Kwon OW, Park WH, Choi HG, Lee YR, et al. Preparation of atactic poly (vinyl alcohol)/sodium alginate blend nanowebs by electrospinning. J Appl Polym Sci 2007;106:1337–42.
[105] Ding B, Wang MR, Wang XF, Yu JY, Sun G. Electrospun nanomaterials for ultrasensitive sensors. Mater Today 2010;13:16–27.
[106] Wang X, Ding B, Yu J, Wang M, Pan F. A highly sensitive humidity sensor based on a nanofibrous membrane coated quartz crystal microbalance. Nanotechnology 2010;21:055502.
[107] Pant HR, Bajgai MP, Nam KT, Chu KH, Park SJ, Kim HY. Formation of electrospun nylon-6/methoxy poly(ethylene glycol) oligomer spider-wave nanofibers. Mater Lett 2010;64:2087–90.
[108] Wang XF, Ding B, Yu JY, Yang JM. Large-scale fabrication of two-dimensional spider-web-like gelatin nano-nets via electro-netting. Colloids Surf, B 2011;86:345–52.
[109] Bhardwaj N, Kundu SC. Electrospinning: a fascinating fiber fabrication technique. Biotechnol Adv 2010;28:325–47.
[110] Han T, Reneker DH, Yarin AL. Buckling of jets in electrospinning. Polymer 2007;48:6064–76.
[111] Tsou S, Lin HS, Wang C. Studies on the electrospun Nylon 6 nanofibers from polyelectrolyte solutions: 1. Effects of solution concentration and temperature. Polymer 2011;52:3127–36.
[112] Ayutsede J, Gandhi M, Sukigara S, Ye HH, Hsu CM, Gogotsi Y, et al. Carbon nanotube reinforced *Bombyx mori* silk nanofibers by the electrospinning process. Biomacromolecules 2006;7:208–14.
[113] Kimmer Da, Slobodian P, Petrás D, Zatloukal M, Olejník R, Sáha P. Polyurethane/multiwalled carbon nanotube nanowebs prepared by an electrospinning process. J Appl Polym Sci 2009;111:2711–4.
[114] Mit-uppatham C, Nithitanakul M, Supaphol P. Ultrafine electrospun polyamide-6 fibers: effect of solution conditions on morphology and average fiber diameter. Macromol Chem Phys 2004;205:2327–38.
[115] Grimm RL, Beauchamp J. Dynamics of field-induced droplet ionization: time-resolved studies of distortion, jetting, and progeny formation from charged and neutral methanol droplets exposed to strong electric fields. J Phys Chem B 2005;109:8244–50.
[116] Olumee Z, Callahan JH, Vertes A. Droplet dynamics changes in electrostatic sprays of methanol-water mixtures. J Phys Chem A 1998;102:9154–60.
[117] Hong SH, Moon JH, Lim JM, Kim SH, Yang SM. Fabrication of spherical colloidal crystals using electrospray. Langmuir 2005;21:10416–21.
[118] Hartman R, Brunner D, Camelot D, Marijnissen J, Scarlett B. Electrohydrodynamic atomization in the cone-jet mode physical modeling of the liquid cone and jet. J Aerosol Sci 1999;30:823–49.
[119] Hartman RPA, Marijnissen JCM, Brunner DJ, Camelot DMA, Scarlett B. Jet break-up in electrohydrodynamic atomization in the cone-jet mode. J Aerosol Sci 2000;31:65–95.
[120] Wang MR, Kang QJ. Electrokinetic transport in microchannels with random roughness. Anal Chem 2009;81:2953–61.
[121] Cloupeau M, Prunetfoch B. Electrostatic spraying of liquids in cone-jet mode. J Electrost 1989;22:135–59.
[122] Gomez A, Tang KQ. Charge and fission of droplets in electrostatic sprays. Phys Fluids 1994;6:404–14.
[123] Kim H, Kim JH, Ogata A. Time-resolved high-speed camera observation of electrospray. J Aerosol Sci 2011;42:249–63.
[124] Pant HR, Bajgai MP, Nam KT, Seo YA, Pandeya DR, Hong ST, et al. Electrospun nylon-6 spider-net like nanofiber mat containing TiO_2 nanoparticles: a multifunctional nanocomposite textile material. J Hazard Mater 2011;185:124–30.
[125] Pant HR, Bajgai MP, Yi C, Nirmala R, Nam KT, Baek W, et al. Effect of successive electrospinning and the strength of hydrogen bond on the morphology of electrospun nylon-6 nanofibers. Colloids Surf, A 2010;370:87–94.
[126] Bean C, Livingston J. Superparamagnetism. J Appl Phys 1959;30:S120–9.
[127] Choi SH, Hwang IS, Lee JH, Oh SG, Kim ID. Microstructural control and selective C_2H_5OH sensing properties of Zn_2SnO_4 nanofibers prepared by electrospinning. Chem Commun 2011;47:9315–7.
[128] Wang HY, Wu DY, Li DZ, Niu ZW, Chen YZ, Tang DH, et al. Fabrication of continuous highly ordered mesoporous silica nanofibre with core/sheath structure and its application as catalyst carrier. Nanoscale 2011;3:3601–4.
[129] Yang Y, Centrone A, Chen L, Simeon F, Hatton TA, Rutledge GC. Highly porous electrospun polyvinylidene fluoride (PVDF)-based carbon fiber. Carbon 2011;49:3395–403.
[130] Zha ZB, Cohn C, Dai ZF, Qiu WG, Zhang JH, Wu XY. Nanofibrous lipid membranes capable of functionally immobilizing antibodies and capturing specific cells. Adv Mater 2011;23:3435–40.
[131] Molla S, Compan V, Gimenez E, Blazquez A, Urdanpilleta I. Novel ultrathin composite membranes of Nafion/PVA for PEMFCs. Int J Hydrogen Energy 2011;36:9886–95.
[132] Wang M, Pan N. Predictions of effective physical properties of complex multiphase materials. Mater Sci Eng R 2008;63:1–30.
[133] Gilbert E, Pollak H. Steiner minimal trees. SIAM J Appl Math 1968:1–29.
[134] Yin Y, Chen Y, Yin J, Huang K. Geometric conservation laws for perfect Y-branched carbon nanotubes. Nanotechnology 2006;17:4941–5.

[135] Li G, Yin Y, Li Y, Zhong Z. "Steiner trees" between cell walls of sisal. Chin Sci Bull 2009;54:3220–4.
[136] Nirmala R, Nam KT, Park S-J, Shin Y-S, Navamathavan R, Kim HY. Formation of high aspect ratio polyamide-6 nanofibers via electrically induced double layer during electrospinning. Appl Surf Sci 2010;256:6318–23.
[137] Nirmala R, Panth HR, Yi C, Nam KT, Park SJ, Kim HY, et al. Effect of solvents on high aspect ratio polyamide-6 nanofibers via electrospinning. Macromol Res 2010;18:759–65.
[138] Nirmala R, Navamathavan R, El-Newehy MH, Kim HY. Preparation and electrical characterization of polyamide-6/chitosan composite nanofibers via electrospinning. Mater Lett 2011;65:493–6.
[139] Nirmala R, Park HM, Navamathavan R, Kang HS, El-Newehy MH, Kim HY. Lecithin blended polyamide-6 high aspect ratio nanofiber scaffolds via electrospinning for human osteoblast cell culture. Mater Sci Eng, C 2011;31:486–93.
[140] Stephens JS, Chase DB, Rabolt JF. Effect of the electrospinning process on polymer crystallization chain conformation in nylon-6 and nylon-12. Macromolecules 2004;37:877–81.
[141] Pant HR, Nam KT, Oh HJ, Panthi G, Kim HD, Kim B, et al. Effect of polymer molecular weight on the fiber morphology of electrospun mats. J Colloid Interface Sci 2011;364:107–11.
[142] Li L, Bellan LM, Craighead HG, Frey MW. Formation and properties of nylon-6 and nylon-6/montmorillonite composite nanofibers. Polymer 2006;47:6208–17.
[143] Pant HR, Pandeya DR, Nam KT, Baek W, Hong ST, Kim HY. Photocatalytic and antibacterial properties of a TiO_2/nylon-6 electrospun nanocomposite mat containing silver nanoparticles. J Hazard Mater 2011;189:465–71.
[144] McKee MG, Layman JM, Cashion MP, Long TE. Phospholipid nonwoven electrospun membranes. Science 2006;311:353.
[145] Parks J, Bullock B, Rudel L. The reactivity of plasma phospholipids with lecithin: cholesterol acyltransferase is decreased in fish oil-fed monkeys. J Biol Chem 1989;264:2545.
[146] Liang D, Hsiao BS, Chu B. Functional electrospun nanofibrous scaffolds for biomedical applications. Adv Drug Deliv Rev 2007;59:1392–412.
[147] Shen J, Fu X, Ou L, Zhang M, Guan Y, Wang K, et al. Construction of ureteral grafts by seeding urothelial cells and bone marrow mesenchymal stem cells into polycaprolactone-lecithin electrospun fibers. Int J Artif Organs 2010;33:161–70.
[148] Zhu N, Cui F, Hu K, Zhu L. Biomedical modification of poly (L-lactide) by blending with lecithin. J Biomed Mater Res 2007;82:455–61.
[149] Nirmala R, Navamathavan R, Kang HS, El-Newehy MH, Kim HY. Preparation of polyamide-6/chitosan composite nanofibers by a single solvent system via electrospinning for biomedical applications. Colloids Surf, B 2011;83:173–8.
[150] MacDiarmid AG. Synthetic metals: a novel role for organic polymers (Nobel lecture). Angew Chem Int Ed 2001;40:2581–90.
[151] Hoeben FJM, Jonkheijm P, Meijer EW, Schenning APHJ. About supramolecular assemblies of π-conjugated systems. Chem Rev 2005;105:1491–546.
[152] Kang E, Neoh K, Tan K. Polyaniline: a polymer with many interesting intrinsic redox states. Prog Mater Sci 1998;23:277–324.
[153] Attout A, Yunus S, Bertrand P. Electrospinning and alignment of polyaniline-based nanowires and nanotubes. Polym Eng Sci 2008;48:1661–6.
[154] MacDiarmid A, Yang L, Huang W, Humphrey B. Polyaniline: electrochemistry and application to rechargeable batteries. Synth Met 1987;18:393–8.
[155] Virji S, Huang JX, Kaner RB, Weiller BH. Polyaniline nanofiber gas sensors: examination of response mechanisms. Nano Lett 2004;4:491–6.
[156] Parajuli DC, Bajgai MP, Ko JA, Kang HK, Khil MS, Kim HY. Synchronized polymerization and fabrication of poly(acrylic acid) and nylon hybrid mats in electrospinning. ACS Appl Mater Interfaces 2009;1:750–7.
[157] Li L, Hsieh Y. Ultra-fine polyelectrolyte fibers from electrospinning of poly(acrylic acid). Polymer 2005;46:5133–9.
[158] Ding B, Kim J, Miyazaki Y, Shiratori S. Electrospun nanofibrous membranes coated quartz crystal microbalance as gas sensor for NH_3 detection. Sensor Actuat, B 2004;101:373–80.
[159] Chen H, Snyder JD, Elabd YA. Electrospinning and solution properties of nafion and poly (acrylic acid). Macromolecules 2008;41:128–35.
[160] McKee MG. The influence of branching and intermolecular interactions on the formation of electrospun fibers. Virginia Polytechnic Institute and State University; 2005.
[161] Lu Y, Wang DF, Li T, Zhao XQ, Cao YL, Yang HX, et al. Poly(vinyl alcohol)/poly(acrylic acid) hydrogel coatings for improving electrode-neural tissue interface. Biomaterials 2009;30:4143–51.
[162] Stejskal J, Kratochval P, Helmstedt M. Polyaniline dispersions. 5. Poly (vinyl alcohol) and poly (N-vinylpyrrolidone) as steric stabilizers. Langmuir 1996;12:3389–92.
[163] Ding B, Kim H, Lee S, Shao C, Lee D, Park S, et al. Preparation and characterization of a nanoscale poly(vinyl alcohol) fiber aggregate produced by an electrospinning method. J Polym Sci, Part B: Polym Phys 2002;40:1261–8.
[164] Ding B, Ogawa T, Kim J, Fujimoto K, Shiratori S. Fabrication of a super-hydrophobic nanofibrous zinc oxide film surface by electrospinning. Thin Solid Films 2008;516:2495–501.
[165] Pedicini A, Farris RJ. Mechanical behavior of electrospun polyurethane. Polymer 2003;44:6857–62.
[166] Amoroso NJ, D'Amore A, Hong Y, Wagner WR, Sacks MS. Elastomeric electrospun polyurethane scaffolds: the interrelationship between fabrication conditions, fiber topology, and mechanical properties. Adv Mater 2011;23:106–11.
[167] Mieszawska AJ, Jalilian R, Sumanasekera GU, Zamborini FP. The synthesis and fabrication of one-dimensional nanoscale heterojunctions. Small 2007;3:722–56.
[168] Li B, Jiang B, Boyce BM, Lindsey BA. Multilayer polypeptide nanoscale coatings incorporating IL-12 for the prevention of biomedical device-associated infections. Biomaterials 2009;30:2552–8.
[169] Chang G, Shen J. Fabrication of microropes via bi-electrospinning with a rotating needle collector. Macromol Rapid Commun 2010;31:2151–4.
[170] Hunley MT, Pötschke P, Long TE. Melt dispersion and electrospinning of non-functionalized multiwalled carbon nanotubes in thermoplastic polyurethane. Macromol Rapid Commun 2009;30:2102–6.
[171] Demir MM, Yilgor I, Yilgor E, Erman B. Electrospinning of polyurethane fibers. Polymer 2002;43:3303–9.

[172] Sambaer W, Zatloukal M, Kimmer D. 3D modeling of filtration process via polyurethane nanofiber based nonwoven filters prepared by electrospinning process. Chem Eng Sci 2011;66:613–23.
[173] Traub H, Hirt P, Herlinger H. Mechanical properties of fibers made of polytrimethylene terephthalate. Chem Fibers Int 1995;45:110–1.
[174] Wu D, Shi T, Yang T, Sun Y, Zhai L, Zhou W, et al. Electrospinning of poly(trimethylene terephthalate)/carbon nanotube composites. Eur Polym J 2011;47:284–93.
[175] Xu Y, Jia HB, Piao JN, Ye SR, Huang J. Crystallization behavior of poly (trimethylene terephthalate)/multi-walled carbon nanotube composites. J Mater Sci 2008;43:417–21.
[176] Jin HJ, Fridrikh SV, Rutledge GC, Kaplan DL. Electrospinning *Bombyx mori* silk with poly (ethylene oxide). Biomacromolecules 2002;3:1233–9.
[177] Zhou C, Chu R, Wu R, Wu Q. Electrospun polyethylene oxide/cellulose nanocrystal composite nanofibrous mats with homogeneous and heterogeneous microstructures. Biomacromolecules 2011;12:2617–25.
[178] Son WK, Youk JH, Lee TS, Park WH. The effects of solution properties and polyelectrolyte on electrospinning of ultrafine poly (ethylene oxide) fibers. Polymer 2004;45:2959–66.
[179] Deitzel JM, Kleinmeyer JD, Hirvonen JK, Beck Tan N. Controlled deposition of electrospun poly (ethylene oxide) fibers. Polymer 2001;42:8163–70.
[180] Subramanian A, Vu D, Larsen GF, Lin HY. Preparation and evaluation of the electrospun chitosan/PEO fibers for potential applications in cartilage tissue engineering. J Biomater Sci Polym Ed 2005;16:861–73.
[181] Habibi Y, Lucia LA, Rojas OJ. Cellulose nanocrystals: chemistry, self-assembly, and applications. Chem Rev 2010;110:3479–500.
[182] Zoppe JO, Peresin MS, Habibi Y, Venditti RA, Rojas OJ. Reinforcing poly (ε-caprolactone) nanofibers with cellulose nanocrystals. ACS Appl Mater Interfaces 2009;1:1996–2004.
[183] Peresin MS, Habibi Y, Zoppe JO, Pawlak JJ, Rojas OJ. Nanofiber composites of polyvinyl alcohol and cellulose nanocrystals: manufacture and characterization. Biomacromolecules 2010;11:674–81.
[184] Kim SE, Heo DN, Lee JB, Kim JR, Park SH, Jeon SH, et al. Electrospun gelatin/polyurethane blended nanofibers for wound healing. Biomed Mater 2009;4:044106.
[185] Young S, Wong M, Tabata Y, Mikos AG. Gelatin as a delivery vehicle for the controlled release of bioactive molecules. J Control Release 2005;109:256–74.
[186] Zhang Y, Ouyang H, Lim CT, Ramakrishna S, Huang ZM. Electrospinning of gelatin fibers and gelatin/PCL composite fibrous scaffolds. J Biomed Mater Res Part B 2005;72:156–65.
[187] Zhang S, Huang YQ, Yang XP, Mei F, Ma Q, Chen GQ, et al. Gelatin nanofibrous membrane fabricated by electrospinning of aqueous gelatin solution for guided tissue regeneration. J Biomed Mater Res Part A 2009;90A:671–9.
[188] Huang ZM, Zhang YZ, Ramakrishna S, Lim CT. Electrospinning and mechanical characterization of gelatin nanofibers. Polymer 2004;45:5361–8.
[189] Ki CS, Baek DH, Gang KD, Lee KH, Um IC, Park YH. Characterization of gelatin nanofiber prepared from gelatin–formic acid solution. Polymer 2005;46:5094–102.
[190] Sisson K, Zhang C, Farach-Carson MC, Chase DB, Rabolt JF. Evaluation of cross-linking methods for electrospun gelatin on cell growth and viability. Biomacromolecules 2009;10:1675–80.
[191] No H, Meyers S, Prinyawiwatkul W, Xu Z. Applications of chitosan for improvement of quality and shelf life of foods: a review. J Food Sci 2007;72:R87–R100.
[192] Gil G, del Mónaco S, Cerrutti P, Galvagno M. Selective antimicrobial activity of chitosan on beer spoilage bacteria and brewing yeasts. Biotechnol Lett 2004;26:569–74.
[193] Huang XJ, Ge D, Xu ZK. Preparation and characterization of stable chitosan nanofibrous membrane for lipase immobilization. Eur Polym J 2007;43:3710–8.
[194] Nirmala R, Il BW, Navamathavan R, El-Newehy MH, Kim HY. Preparation and characterizations of anisotropic chitosan nanofibers via electrospinning. Macromol Res 2011;19:345–50.
[195] Bhattarai N, Edmondson D, Veiseh O, Matsen FA, Zhang M. Electrospun chitosan-based nanofibers and their cellular compatibility. Biomaterials 2005;26:6176–84.
[196] Ohkawa K, Cha DI, Kim H, Nishida A, Yamamoto H. Electrospinning of chitosan. Macromol Rapid Commun 2004;25:1600–5.
[197] Geng XY, Kwon OH, Jang JH. Electrospinning of chitosan dissolved in concentrated acetic acid solution. Biomaterials 2005;26:5427–32.
[198] Wang XF, Ding B, Sun M, Yu JY, Sun G. Quartz crystal microbalance-based nanofibrous membranes for humidity detection: theoretical model and experimental verification. Int J Nonlinear Sci Numer Simul 2010;11:509–15.
[199] Lam HL. Electrospinning of single wall carbon nanotube reinforced aligned fibrils and yarns. Drexel University; 2004.
[200] Li D, Xia YN. Fabrication of titania nanofibers by electrospinning. Nano Lett 2003;3:555–60.
[201] Ryu YJ, Kim HY, Lee KH, Park HC, Lee DR. Transport properties of electrospun nylon 6 nonwoven mats. Eur Polym J 2003;39:1883–9.
[202] Guo M, Ding B, Li XH, Wang XL, Yu JY, Wang MR. Amphiphobic nanofibrous silica mats with flexible and high-heat-resistant properties. J Phys Chem C 2010;114:916–21.
[203] Lee K, Kim H, Bang H, Jung Y, Lee S. The change of bead morphology formed on electrospun polystyrene fibers. Polymer 2003;44:4029–34.
[204] Friend R, Gymer R, Holmes A, Burroughes J, Marks R, Taliani C, et al. Electroluminescence in conjugated polymers. Nature 1999;397:121–8.
[205] Theron S, Zussman E, Yarin A. Experimental investigation of the governing parameters in the electrospinning of polymer solutions. Polymer 2004;45:2017–30.
[206] Ramakrishna S. An introduction to electrospinning and nanofibers. World Scientific Publ. Co. Inc.; 2005.
[207] Sill TJ, von Recum HA. Electrospinning: applications in drug delivery and tissue engineering. Biomaterials 2008;29:1989–2006.

[208] Zong XH, Kim K, Fang DF, Ran SF, Hsiao BS, Chu B. Structure and process relationship of electrospun bioabsorbable nanofiber membranes. Polymer 2002;43:4403–12.
[209] Kim C, Ngoc BTN, Yang KS, Kojima M, Kim YA, Kim YJ, et al. Self-sustained thin webs consisting of porous carbon nanofibers for supercapacitors via the electrospinning of polyacrylonitrile solutions containing zinc chloride. Adv Mater 2007;19:2341–6.
[210] Patel AC, Li SX, Wang C, Zhang WJ, Wei Y. Electrospinning of porous silica nanofibers containing silver nanoparticles for catalytic applications. Chem Mater 2007;19:1231–8.
[211] Kim B, Park H, Lee SH, Sigmund WM. Poly(acrylic acid) nanofibers by electrospinning. Mater Lett 2005;59:829–32.
[212] Talwar S, Krishnan AS, Hinestroza JP, Pourdeyhimi B, Khan SA. Electrospun nanofibers with associative polymer-surfactant systems. Macromolecules 2010;43:7650–6.
[213] Lin T, Wang HX, Wang HM, Wang XG. The charge effect of cationic surfactants on the elimination of fibre beads in the electrospinning of polystyrene. Nanotechnology 2004;15:1375–81.
[214] Ji LW, Medford AJ, Zhang XW. Electrospun polyacrylonitrile/zinc chloride composite nanofibers and their response to hydrogen sulfide. Polymer 2009;50:605–12.
[215] Theron SA, Zussman E, Yarin AL. Experimental investigation of the governing parameters in the electrospinning of polymer solutions. Polymer 2004;45:2017–30.
[216] Nirmala R, Nam KT, Park SJ, Shin YS, Navamathavan R, Kim HY. Formation of high aspect ratio polyamide-6 nanofibers via electrically induced double layer during electrospinning. Appl Surf Sci 2010;256:6318–23.
[217] Zhang X, Reagan MR, Kaplan DL. Electrospun silk biomaterial scaffolds for regenerative medicine. Adv Drug Deliv Rev 2009;61:988–1006.
[218] Wang N, Wang X, Ding B, Yu J, Sun G. Tunable fabrication of three-dimensional polyamide-66 nano-fiber/nets for high efficiency fine particulate filtration. J Mater Chem 2012;22:1445–52.
[219] Wu H, Sun Y, Lin DD, Zhong R, Zhang C, Pan W. GaN nanofibers based on electrospinning: facile synthesis, controlled assembly, precise doping, and application as high performance UV photodetector. Adv Mater 2009;21:227–31.
[220] Sun M, Li XH, Ding B, Yu JY, Sun G. Mechanical and wettable behavior of polyacrylonitrile reinforced fibrous polystyrene mats. J Colloid Interface Sci 2010;347:147–52.
[221] Du J, Che PL, Aich U, Tan E, Kim HJ, Sampathkumar SG, et al. Deciphering glycan linkages involved in Jurkat cell interactions with gold-coated nanofibers via sugar-displayed thiols. Bioorg Med Chem Lett 2011;21:4980–4.
[222] Sutherland K. Developments in filtration: what is nanofiltration? Filtr Separat 2008;45:32–5.
[223] Ma HY, Yoon K, Rong LX, Mao YM, Mo ZR, Fang DF, et al. High-flux thin-film nanofibrous composite ultrafiltration membranes containing cellulose barrier layer. J Mater Chem 2010;20:4692–704.
[224] Suthat A, Chase G. Nanofibres in filter media. Chem Eng 2001;726:26–8.
[225] Hung CH, Leung WWF. Filtration of nano-aerosol using nanofiber filter under low Peclet number and transitional flow regime. Sep Purif Technol 2011;79:34–42.
[226] Ma HY, Hsiao BS, Chu B. Thin-film nanofibrous composite membranes containing cellulose or chitin barrier layers fabricated by ionic liquids. Polymer 2011;52:2594–9.
[227] Li BJ, Cao HQ. ZnO@graphene composite with enhanced performance for the removal of dye from water. J Mater Chem 2011;21:3346–9.
[228] Yoon K, Kim K, Wang X, Fang D, Hsiao BS, Chu B. High flux ultrafiltration membranes based on electrospun nanofibrous PAN scaffolds and chitosan coating. Polymer 2006;47:2434–41.
[229] Gopal R, Kaur S, Ma Z, Chan C, Ramakrishna S, Matsuura T. Electrospun nanofibrous filtration membrane. J Membr Sci 2006;281:581–6.
[230] Wang MR. Structure effects on electro-osmosis in microporous media. J Heat Transfer-Trans ASME 2012. 134.
[231] Grafe TH, Graham KM. Nanofiber webs from electrospinning. Nonwovens in Filtration-Fifth International Conference. Stuttgart, Germany2003. p. 1-5.
[232] Yang DJ, Kamienchick I, Youn DY, Rothschild A, Kim ID. Ultrasensitive and highly selective gas sensors based on electrospun SnO_2 nanofibers modified by Pd loading. Adv Funct Mater 2010;20:4258–64.
[233] Noy A, Artyukhin AB, Misra N. Bionanoelectronics with 1D materials. Mater Today 2009;12:22–31.
[234] Wang M. The physical chemistry of materials. Mater Today 2010;13:67.
[235] Kim J, Kim F, Huang JX. Seeing graphene-based sheets. Mater Today 2010;13:28–38.
[236] Grate JW. Acoustic wave microsensor arrays for vapor sensing. Chem Rev 2000;100:2627–47.
[237] Dahlin AB, Jonsson P, Jonsson MP, Schmid E, Zhou Y, Hook F. Synchronized quartz crystal microbalance and nanoplasmonic sensing of biomolecular recognition reactions. ACS Nano 2008;2:2174–82.
[238] Ariga K, Vinu A, Ji Q, Ohmori O, Hill JP, Acharya S, et al. A layered mesoporous carbon sensor based on nanopore-filling cooperative adsorption in the liquid phase. Angew Chem Int Ed 2008;120:7364–7.
[239] Sauerbrey G. The use of quartz oscillators for weighing thin layers and for microweighing. Z Phys 1959;155:206–22.
[240] Ricco AJ, Crooks RM, Osbourn GC. Surface acoustic wave chemical sensor arrays: New chemically sensitive interfaces combined with novel cluster analysis to detect volatile organic compounds and mixtures. Acc Chem Res 1998;31:289–96.
[241] Palaniappan A, Li X, Tay FEH, Li J, Su XD. Cyclodextrin functionalized mesoporous silica films on quartz crystal microbalance for enhanced gas sensing. Sensor Actuat, B 2006;119:220–6.
[242] Chen HW, Wu RJ, Chan KH, Sun YL, Su PG. The application of CNT/Nafion composite material to low humidity sensing measurement. Sensor Actuat, B 2005;104:80–4.
[243] Ayad MM, Abu El-Nasr A. Adsorption of cationic dye (methylene blue) from water using polyaniline nanotubes base. J Phys Chem C 2010;114:14377–83.
[244] Zhang CY, Wang XF, Lin JY, Ding B, Yu JY, Pan N. Nanoporous polystyrene fibers functionalized by polyethyleneimine for enhanced formaldehyde sensing. Sensor Actuat, B 2011;152:316–23.
[245] Korposh S, Selyanchyn R, Lee SW. Nano-assembled thin film gas sensors. IV. Mass-sensitive monitoring of humidity using quartz crystal microbalance (QCM) electrodes. Sensor Actuat, B 2010;147:599–606.
[246] Lu WS, Lin L, Jiang L. Nanogold hollow balls with dendritic surface for hybridization of DNA. Biosensors Bioelectron 2007;22:1101–5.

[247] Yamazoe N, Shimizu Y. Humidity sensors: principles and applications. Sensor Actuat 1986;10:379–98.
[248] Li Y, Yang M, She Y. Humidity sensitive properties of crosslinked and quaternized poly (4-vinylpyridine-co-butyl methacrylate). Sensor Actuat, B 2005;107:252–7.
[249] Gong M, Joo S, Choi B. Humidity sensor using mutually reactive copolymers containing quaternary ammonium salt and reactive function. Sensor Actuat, B 2002;86:81–7.
[250] Wang XF, Ding B, Sun M, Yu JY, Sun G. Nanofibrous polyethyleneimine membranes as sensitive coatings for quartz crystal microbalance-based formaldehyde sensors. Sensor Actuat, B 2010;144:11–7.
[251] Kuang Q, Lao C, Wang Z, Xie Z, Zheng L. High-sensitivity humidity sensor based on a single SnO_2 nanowire. J Am Chem Soc 2007;129:6070–1.
[252] Huang X, Sun Y, Wang L, Meng F, Liu J. Carboxylation multi-walled carbon nanotubes modified with $LiClO_4$ for water vapour detection. Nanotechnology 2004;15:1284.
[253] Li ZY, Zhang HN, Zheng W, Wang W, Huang HM, Wang C, et al. Highly sensitive and stable humidity nanosensors based on LiCl doped TiO_2 electrospun nanofibers. J Am Chem Soc 2008;130:5036–7.
[254] Yao W, Chen XJ, Zhang J. A capacitive humidity sensor based on gold–PVA core–shell nanocomposites. Sensor Actuat, B 2010;145:327–33.
[255] Estella J, de Vicente P, Echeverria JC, Garrido JJ. A fibre-optic humidity sensor based on a porous silica xerogel film as the sensing element. Sensor Actuat, B 2010;149:122–8.
[256] Verma D, Dutta V. Nano-polyaniline thin films as humidity sensors prepared using spin coating technique. Sensor Lett 2009;7:143–7.
[257] Bae JS, Gong MS. Electrical properties of low-temperature polymeric humidity sensor prepared by dip coating method. Polym Soc Korea 1996;20:996–1003.
[258] Su PG, Cheng KH. Self-assembly of polyelectrolytic multilayer thin films of polyelectrolytes on quartz crystal microbalance for detecting low humidity. Sensor Actuat, B 2009;142:123–9.
[259] Cho NB, Lim TH, Jeon YM, Gong MS. Humidity sensors fabricated with photo-curable electrolyte inks using an ink-jet printing technique and their properties. Sensor Actuat, B 2008;130:594–8.
[260] Suska A, Ibanez AB, Lundstrom I, Berghard A. G protein-coupled receptor mediated trimethylamine sensing. Biosensors Bioelectron 2009;25:715–20.
[261] Zheng JB, Li G, Ma XF, Wang YM, Wu G, Cheng YN. Polyaniline–TiO_2 nano-composite-based trimethylamine QCM sensor and its thermal behavior studies. Sensor Actuat, B 2008;133:374–80.
[262] Ayad MM, Torad NL. Quartz crystal microbalance sensor for detection of aliphatic amines vapours. Sensor Actuat, B 2010;147:481–7.
[263] Bouchard M, Noisel N, Carrier G. Evaluation of the health impact of lowering the formaldehyde occupational exposure limit for Quebec workers. Regul Toxicol Pharmacol 2007;48:118–27.
[264] Bunkoed O, Davis F, Kanatharana P, Thavarungkul P, Higson SPJ. Sol–gel based sensor for selective formaldehyde determination. Anal Chim Acta 2010;659:251–7.
[265] Ma Q, Cui HL, Su XG. Highly sensitive gaseous formaldehyde sensor with CdTe quantum dots multilayer films. Biosensors Bioelectron 2009;25:839–44.
[266] Tanaka H, Sugimoto H, Kanno Y. Mist sensing of formaldehyde and toluene with quartz crystal microbalance coated with lipid film using ultrasonic atomizer. Jpn J Appl Phys 2008;47:671–5.
[267] Bunde RL, Jarvi EJ, Rosentreter JJ. A piezoelectric method for monitoring formaldehyde induced crosslink formation between poly-lysine and poly-deoxyguanosine. Talanta 2000;51:159–71.
[268] Feng L, Liu YJ, Zhou XD, Hu JM. The fabrication and characterization of a formaldehyde odor sensor using molecularly imprinted polymers. J Colloid Interface Sci 2005;284:378–82.
[269] Hu WL, Chen SY, Liu LT, Ding B, Wang HP. Formaldehyde sensors based on nanofibrous polyethyleneimine/bacterial cellulose membranes coated quartz crystal microbalance. Sensor Actuat, B 2011;157:554–9.
[270] Rakow NA, Suslick KS. A colorimetric sensor array for odour visualization. Nature 2000;406:710–3.
[271] Zhang C, Suslick KS. A colorimetric sensor array for organics in water. J Am Chem Soc 2005;127:11548–9.
[272] O'Donnell JL, Paske AC, Earl LD. Interfacially polymerized metalloporphyrin thin films for colorimetric sensing of organic vapors. Sensor Actuat, B 2011;155:687–91.
[273] Dunbar ADF, Brittle S, Richardson TH, Hutchinson J, Hunter CA. Detection of volatile organic compounds using porphyrin derivatives. J Phys Chem B 2010;114:11697–702.
[274] Feng L, Musto CJ, Suslick KS. A simple and highly sensitive colorimetric detection method for gaseous formaldehyde. J Am Chem Soc 2010;132:4046–7.
[275] Nakano N, Nagashima K. An automatic monitor of formaldehyde in air by a monitoring tape method. J Environ Monitor 1999;1:255–8.
[276] Nakano N, Ishikawa M, Koabayashi Y, Nagashima K. Development of a monitoring tape for formaldehyde using hydroxylamine sulfate and methyl yellow. Anal Sci 1994;10:641–5.
[277] Pretto A, Milani MR, Cardoso AA. Colorimetric determination of formaldehyde in air using a hanging drop of chromotropic acid. J Environ Monitor 2000;2:566–70.
[278] Feng L, Musto CJ, Kemling JW, Lim SH, Suslick KS. A colorimetric sensor array for identification of toxic gases below permissible exposure limits. Chem Commun 2010;46:2037.
[279] Suslick KS, Feng LA, Musto CJ, Kemling JW, Lim SH, Zhong WX. Colorimetric sensor array for determination and identification of toxic industrial chemicals. Anal Chem 2010;82:9433–40.
[280] Maruo YY, Nakamura J, Uchiyama M, Higuchi M, Izunli K. Development of formaldehyde sensing element using porous glass impregnated with Schiff's reagent. Sensor Actuat, B 2008;129:544–50.
[281] Wang X, Si Y, Wang JL, Ding B, Yu JY, Sun G. A facile and highly sensitive colorimetric sensor for the detection of formaldehyde based on electro-spinning/netting nano-fiber/nets. Sensor Actuat, B 2012;163:186–93.
[282] Tan S, Huang X, Wu B. Some fascinating phenomena in electrospinning processes and applications of electrospun nanofibers. Polym Int 2007;56:1330–9.

[283] Kang YK, Park CH, Kim J, Kang TJ. Application of electrospun polyurethane web to breathable water-proof fabrics. Fibers Polym 2007;8:564–70.
[284] Lee S, Kay Obendorf S. Developing protective textile materials as barriers to liquid penetration using melt-electrospinning. J Appl Polym Sci 2006;102:3430–7.
[285] Schreuder-Gibson H, Gibson P, Senecal K, Sennett M, Walker J, Yeomans W, et al. Protective textile materials based on electrospun nanofibers. J Adv Mater 2002;34:44–55.
[286] Lee S, Obendorf SK. Use of electrospun nanofiber web for protective textile materials as barriers to liquid penetration. Text Res J 2007;77:696–702.
[287] Thandavamoorthy S, Gopinath N, Ramkumar SS. Self-assembled honeycomb polyurethane nanofibers. J Appl Polym Sci 2006;101:3121–4.
[288] Wang M, Kang QJ, Pan N. Thermal conductivity enhancement of carbon fiber composites. Appl Thermal Eng 2009;29:418–21.
[289] Wang MR, He JH, Yu JY, Pan N. Lattice Boltzmann modeling of the effective thermal conductivity for fibrous materials. Int J Thermal Sci 2007;46:848–55.
[290] Wong SC, Baji A, Leng SW. Effect of fiber diameter on tensile properties of electrospun poly(epsilon-caprolactone). Polymer 2008;49:4713–22.
[291] Pham QP, Sharma U, Mikos AG. Electrospinning of polymeric nanofibers for tissue engineering applications: a review. Tissue Eng 2006;12:1197–211.
[292] Du J, Yarema KJ. Carbohydrate engineered cells for regenerative medicine. Adv Drug Deliv Rev 2010;62:671–82.
[293] Du J, Che PL, Wang ZY, Aich U, Yarema KJ. Designing a binding interface for control of cancer cell adhesion via 3D topography and metabolic oligosaccharide engineering. Biomaterials 2011;32:5427–37.
[294] Du J, Meledeo MA, Wang ZY, Khanna HS, Paruchuri VDP, Yarema KJ. Metabolic glycoengineering: sialic acid and beyond. Glycobiology 2009;19:1382–401.
[295] Li YP, Xiao K, Luo JT, Lee J, Pan SR, Lam KS. A novel size-tunable nanocarrier system for targeted anticancer drug delivery. J Control Release 2010;144:314–23.
[296] Li YP, Xiao K, Luo JT, Xiao WW, Lee JS, Gonik AM, et al. Well-defined, reversible disulfide cross-linked micelles for on-demand paclitaxel delivery. Biomaterials 2011;32:6633–45.
[297] Boudriot U, Dersch R, Greiner A, Wendorff JH. Electrospinning approaches toward scaffold engineering: a brief overview. Artif Organs 2006;30:785–92.
[298] Kuijpers AJ, van Wachem PB, van Luyn MJA, Plantinga JA, Engbers GHM, Krijgsveld J, et al. In vivo compatibility and degradation of crosslinked gelatin gels incorporated in knitted Dacron. J Biomed Mater Res 2000;51:136–45.
[299] Li MY, Mondrinos MJ, Gandhi MR, Ko FK, Weiss AS, Lelkes PI. Electrospun protein fibers as matrices for tissue engineering. Biomaterials 2005;26:5999–6008.
[300] Yang F, Murugan R, Wang S, Ramakrishna S. Electrospinning of nano/micro scale poly (L-lactic acid) aligned fibers and their potential in neural tissue engineering. Biomaterials 2005;26:2603–10.
[301] Nirmala R, Kang HS, El-Newehy MH, Navamathavan R, Park HM, Kim HY. Human osteoblast cytotoxicity study of electrospun polyurethane/calcium chloride ultrafine nanofibers. J Nanosci Nanotechnol 2011;11:4749–56.